Breakdown Conduction in Thin Films of SiO, MgF_2, CaF_2, CeF_3, CeO_2 and Teflon

Submitted by Paul P. Budenstein
Physics Department
Auburn University
Auburn, Alabama

NAL REPORT

GRANT NGR-01-003-011

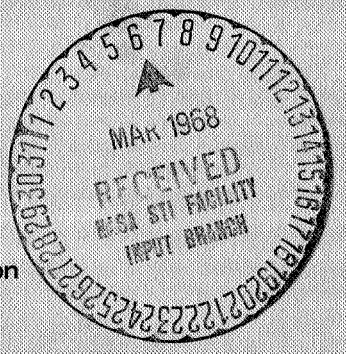

Submitted to

National Aeronautics and Space Administration
Office of Grants and Contracts
Washington, D.C. 20546

February, 1968

BREAKDOWN CONDUCTION IN THIN FILMS OF

SiO, MgF_2, CaF_2, CeF_3, CeO_2 and Teflon

Submitted by Paul P. Budenstein
Physics Department
Auburn University
Auburn, Alabama

Final Report

Grant NGR-01-003-011

Submitted to

National Aeronautics and Space Administration
Office of Grants and Contracts
Washington, D.C. 20546

February, 1968

Breakdown Conduction in Thin Films of SiO, MgF_2, CaF_2, CeF_3, CeO_2, and Teflon

Paul P. Budenstein
Physics Department, Auburn University

ABSTRACT

Breakdown studies on thin film dielectrics are reported covering the materials SiO, MgF_2, CaF_2, CeF_3, CeO_2, and Teflon. Experimental data includes prebreakdown V-I-T characteristics, impedance-temperature characteristics at 1000 cycles/sec, voltage threshold for the onset of breakdown vs temperature and dielectric thickness, voltage threshold for the cessation of breakdown vs temperature and thickness, time-resolved spectroscopy of the light emitted during breakdown, photomicrography of breakdown sites, and some additional observations. The data are evaluated using the theoretical treatments of Forlani and Minnaja, O'Dwyer, and Klein and Gafni. A critique of the theoretical treatments is given pointing out that none of them is completely successful in describing both the thickness and temperature dependence of the average field for the onset of breakdown. None of the theories attempt to describe conduction during the breakdown period. It is found that

breakdown behavior is not predictable from prebreakdown conduction properties, neither dc nor ac. The threshold field for the onset of breakdown varies approximately as $w^{-\frac{1}{2}}$, where w is the dielectric thickness, in accordance with the prediction of Forlani and Minnaja. The magnitudes of the breakdown fields are about 10^6 V/cm for all of the materials and the temperature dependence is nil or a slight monotonic decrease in field with increasing temperature. All of the materials are found to have a voltage threshold for the cessation of breakdown that is temperature and thickness independent. For most capacitors regardless of the dielectric, this voltage is between 10 and 20 volts. Time-resolved spectroscopy of the light emitted during breakdown shows that the light is made up of line spectra from atoms of both of the electrodes and from the dielectric. The light emission starts at the same time that the voltage waveforms indicate breakdown conduction is starting. Both the light and the voltage waveforms indicate that the transition from prebreakdown to breakdown conduction occurs in less than 10 nanoseconds. Once breakdown conduction has started the resistance remains nearly constant, at about 30 ohms, until the approach of the voltage for the cessation of breakdown. A theoretical analysis is given of prebreakdown conduction that indicates the field within the dielectric is inhomogeneous. A model is offered to explain the general features of the onset of breakdown, conduction during breakdown, and the cessation. The central feature of this is the generation of a plasma at the onset of breakdown. This plasma serves as the principal conducting path during breakdown. When the applied voltage can no longer sustain the plasma, breakdown conduction ceases.

CONTENTS

FIGURES

TABLES

I. INTRODUCTION

This is a study of the electrical properties of dielectric thin films in the thickness range from 1000 Å to 15000 Å. Materials studied include SiO, MgF_2, CaF_2, CeF_3, CeO_2, and Teflon. The emphasis is on the description of the processes of destructive breakdown.

The effort is a continuation of work initiated in the summer of 1964 (Contract NAS8 11279, National Aeronautics and Space Administration) to study the causes of failure in Al-SiO-Al thin film capacitors. Final reports on this original study[1,2] were completed in August, 1966 and an article was submitted to the Journal of Applied Physics in October, 1966 (publication date was June, 1967).[3] The proposal on which this current project is based was submitted in November, 1965, which was close to a year before submission of the journal article. Most of the interpretation of the work done from 1964 to 1966 occurred during this period. Hence, partly by conscious choice and partially under the weight of unforeseen circumstances, the study performed differs from that outlined in the proposal. We shall first trace briefly the events from November, 1965 to the present time indicating the main features of the proposal, how our perspective changed, and the rationale in the program actually pursued (which forms the main body of this report).

The study plan was divided into four parts: preparation of thin film capacitors using crystalline dielectrics, study of the electrical and structural properties of these capacitors while observing them in the electron microscope, x-ray studies of the film structures, and electrical measurements outside the electron microscope. The goals for the study were:

1. To obtain a microscopic view of the conduction properties of these systems.
2. To correlate conduction properties to grain size, grain orientation, and any other structural characteristics measureable.

3. To compare thin film conduction properties with those of the bulk materials.

4. To be alert for possible utilization of any special properties observed, such as non-linearity of capacitance, very high dielectric constants, marked photosensitivity, etc.

The study plan and the goals have turned out to be too much for us to accomplish in the allotted time. They were optimistically described to be for three graduate students and a faculty member, each working only part time, for a period of one year. It now appears that the program outlined can provide the thesis work of at least three physics doctoral candidates and a number of M.S. candidates for a period of three to five years.

Between November, 1965 and October, 1966 a large mass of data on Al-SiO-Al capacitors were analyzed and the results interpreted in terms of a qualitative model of destructive breakdown. Several features not previously reported were described.[1-3] These include the existence of breakdown centers clearly identifiable in the electron microscope, the triggering of breakdown at these centers using the beam of the electron microscope, measurement of the threshold for the onset of breakdown from 80°K to 380°K, the discovery of a threshold voltage for the cessation of breakdown and the observation that this threshold is temperature and thickness independent, and the discovery of the presence of crystalline silicon as an end product of breakdown. It was hypothesized that breakdown conduction started with the field dissociation of the dielectric.

However, we could only suggest a qualitative model describing breakdown conduction. Also we did not know which of the observed features were unique to the Al-SiO-Al system and which were general features characteristic of all thin film, or even of bulk, dielectrics. The most distinctive feature, perhaps, was the identification of a threshold for the cessation of breakdown. Hence, during the past year, much of our efforts have been devoted to the measurement of this threshold for different systems. To date it has been found in each of the

capacitor systems studied, regardless of the dielectric or the electrode material.

The need for further information that might indicate the proper mechanisms of breakdown caused us to pursue the suggestion of H. E. Carr that we analyze the light emitted during breakdown. This has been done during the past year and it provides new insights on the breakdown mechanism.

A. PROGRAM OUTLINE

The study during the past year has dealt with the properties of SiO, MgF_2, CaF_2, CeF_3, CeO_2 and Teflon thin film dielectrics. More specifically, the work has included the following aspects:

1. Preparation of capacitors.
2. Measurement of capacitance, dissipation factor, and dc voltage-current characterisitcs as a function of temperature.
3. Measurement of the threshold for the onset of breakdown and the cessation of breakdown as a function of temperature.[4,5]
4. Miscellaneous electrical measurements not pursued extensively.
5. Time-resolved spectroscopy of the light emitted during breakdowns.[6]
6. X-ray diffraction of films.
7. Optical microscopy.
8. Electron microprobe scan of capacitors with breakdown areas.
9. Study of the theory of prebreakdown and breakdown conduction. Analysis of experimental data in terms of some of the theoretical models. Study of mechanisms that lead to a non-uniform field within the dielectric.

Virtually no electron microscopy has been done during the past year in spite of our intentions to pursue the microscopy. The prime reason for this was the fact that the graduate student scheduled to do the microscopy left Auburn because of family responsibilities. He was already a trained microscopist

and we could not replace him. Fortunately, however, we now have some new graduate students who will pursue this aspect during the next few years. They will have the use of a new Philips electron microscope EM300 which has just been installed on the Auburn campus.

B. SURVEY OF RECENT WORK ON BREAKDOWN

N. Klein and his co-workers[8,9,10,11] have made extensive studies on breakdown in Al-SiO-Al capacitors that have paralleled our studies in many respects. Most measurements were made on capacitors having an area of 0.2 cm^2 and a capacitance of about 10^{-9}f. They have measured dc voltage-current-temperature characteristics, studied voltage waveforms during breakdown, studied the physical appearance of breakdowns, and have made extensive measurements of the voltages for the onset of breakdown. These they correlate with the series resistance in their charging circuit, with the specimen's past breakdown history, and with the changing capacitance of the material as the breakdowns reduce the capacitor size. Both dc and ac breakdown studies have been made. They note the existence of the voltage threshold at the end of breakdown and point out its similarity to the extinction voltage of an electric arc. The following[9] is a quotation describing single breakdowns and then several "modes" of breakdown.

> "Hole diameters from a few microns to nearly 100 microns were observed, and the heat of evaporation of the material removed in a single hole breakdown is found to equal roughly the electrostatic energy stored in the capacitor. These facts were interpreted that single hole breakdown is due to the discharge of the capacitor into a flaw in the dielectric. The discharge is produced when current through the flaw causes thermal instability and increase in conductance by many orders of magnitude. The Joule heat causes evaporation and eruption at high mechanical pressure and formation of the hole.
>
> At high voltages and when the series resistor is 10 kilohms or less in these experiments a second type of breakdown, the propagating breakdown occurs. Figure 2 shows typical destruction, which is large compared with that of a single hole breakdown. Oscillograms show that energy for the propagation is supplied from the external source. Propagating breakdown is triggered by a single hole breakdown and there are several modes of propagation. In one, an arc destroys the upper electrode, the

> arc burning as long as the supply can maintain it. In a second mode, single hole breakdowns occur at adjacent sites. The temperature increase and possible mechanical damage at the previous site aid the breakdown at the new site when energy is supplied at a sufficient rate from the supply.
>
> In the investigation described here, a further mode of breakdown propagation was observed in relatively thick dielectrics, when the single hole is produced at voltages above 350 volts. This propagation seems to be caused by the breakdown of the air in the hole through the dielectric."

Klein and Gafni go on to describe capacitors as being "soft" or "hard". "Soft" capacitors experience a range of breakdown threshold values in a fairly continuous fashion, while "hard" capacitors, after a few preliminary breakdowns, sustain a rather large applied voltage until they breakdown in one grand burst where the entire unit (area 0.2 cm^2) is destroyed. In this latter case, the leakage current typically changes from about 5×10^{-9} amps at 10 volts to about 10^{-3} amps at 240 volts, the breakdown voltage. Klein and Gafni continue by developing a theory of thermal breakdown. They assume that the equilibrium temperature of the capacitor prior to breakdown can be determined by equating the Joule heat with that lost by heat transfer to the surroundings

$$\sigma \frac{A}{h} V^2 = \Gamma (T - T_o) , \qquad (1)$$

where σ is the electrical conductivity, A the effective capacitor area, h the dielectric thickness, T_o the ambient temperature and Γ the thermal conductance. Using the temperature variation in σ found experimentally, values of the breakdown field for capacitors of different thickness are predicted and compared with experiment. The agreement is surprisingly good.

Sze[12] applied the method of Klein and Gafni to breakdown in SiN capacitor structures. Whereas Klein and Gafni used their theory for the desription of breakdown in "hard" capacitors, Sze applied the theory to "soft" capacitors. He used a different current-voltage-temperature relation and several approximations and obtained good agreement between theory and experiment at temperatures above $200^{o}K$.

The agreement mentioned above between the phenomenological theory and experiment seems to us to be fortuitous. Measurements we have made on systems other than SiO or SiN where there is virtually no temperature dependence of the prebreakdown conductivity yield virtually the same breakdown behavior as in SiO. This is not to be expected on the Klein-Gafni theory. In the original development of Klein and Gafni, the capacitors used to test the theory were "hard" capacitors that had extremely high leakage currents immediately prior to breakdown. Their dc voltage-current-temperature curves are quite different from the ones we have obtained on measurements covering many capacitors. Hence, the breakdown described may well be more nearly like that of a resistor than of a capacitor. Finally, the theory gives no insight on the time history of the breakdown, on the reason for the existence of a threshold voltage for the cessation of breakdown, and on the size and configuration of the breakdown areas. Since breakdown is regarded as a smooth continuation of prebreakdown behavior, no special mechanisms are invoked to explain breakdown. Yet the very rapid transition from prebreakdown to breakdown conduction (in less than 10 nanoseconds) in all materials tested suggests strongly that special mechanisms are operative. The similarity in breakdown fields in thin films with those of bulk materials suggest these conduction mechanisms are distinct, for the leakage currents in bulk dielectrics prior to breakdown can be small compared to the leakage currents in thin films.

An important way in which our breakdown studies vary from those of Klein and his co-workers is in the nature of the applied voltage used in making the breakdown tests. In our breakdown threshold measurements, we apply a slowly rising ramp voltage to the capacitor under test and continue the ramp until breakdown occurs. The ramp is terminated by a silicon controlled rectifier activated by the breakdown pulse. If the ramp is continued without removal of the applied voltage, succeeding breakdowns generally occur at a voltage higher than that of the first breakdown. Thus, our work is on the "single-hole" breakdowns, to use the terminology of Klein, while his studies concentrate on the

"maximum voltage" breakdowns. His maximum-voltage breakdowns are preceded by currents far larger than those that we have observed in SiO prior to breakdown. It is not clear why his ac breakdown studies give results resembling his dc studies rather than our ramp studies.

O'Dwyer[13] has recently pointed out some difficulties in the theory of avalanche breakdown as described by Seitz[14] for bulk dielectrics. He points out that Seitz' theory would require the build up of fields of the order of 10^{11} volts/cm, values that are orders of magnitude too high. The reason for these large fields is the lack of a continuity condition on the current in the dielectric. On imposing such a condition, O'Dwyer finds that the field inside the dielectric must be inhomogeneous and larger at the cathode than elsewhere. Time is required to set up the inhomogeneous field, thus explaining why the breakdown voltage depends on the rate at which voltage is applied to the capacitor. The large field at the cathode causes field emission from the cathode into the dielectric. For thin dielectrics, there is no temperature dependence. The thickness dependence seems to fit the observations of several observers for NaCl and Al_2O_3 and is similar to that obtained in Forlani and Minnaja[15].

O'Dwyer's approach seems to be more satisfying than that of Klein and Gafni. However, it gives no time scale for the breakdown, it gives little insight into conduction during breakdown and it tells nothing of the termination of breakdown. Further, it gives no insight to the size of the breakdown or to the varied nature of the appearance of breakdown patterns. However, the generality of O'Dwyer's approach gives his theory credibility, since breakdown behavior seems to be so similar for materials that are otherwise very different.

II. EXPERIMENTAL METHODS

A. SPECIMEN PREPARATION

Capacitors were prepared by vacuum evaporation using resistance-type sources. All three layers of the capacitor could be deposited without breaking vacuum. Unless otherwise indicated, the substrate material was soft glass (microscope slides). A variety of mask arrangements was employed, depending upon the type of test envisaged. Most of the electrical measurements were made on structures having areas of 5.4 cm^2 or 8.4 cm^2. Thickness and rate of deposition were monitored during deposition using crystal monitors. Dielectric thickness was subsequently measured by multiple-beam interferometry (Tolansky method). Deposition conditions for the various capacitor structures are summarized in Table 1.

Table 1 shows the several different evaporation systems that were used in preparing capacitors. All were bell jar systems with oil diffusion pumps, optical baffles that could be cooled with liquid nitrogen (liquid nitrogen was not normally used, however), and source to substrate distances from 9 to 18 inches. The substrates could be heated by radiant heaters mounted just above the substrates. Shields were used to prevent depositing large amounts of material on the bell jars or on the fittings. In those cases where the substrate was heated prior to deposition of the dielectric, the preheating time was deliberately kept to 10 or 15 minutes to avoid crazing of the initial aluminum layer.[7]

Electrical connections from the capacitors to the external circuitry were made either in the form of pressure contacts or solder connections. Generally silver contacts were fired onto the substrates prior to the final cleaning operations and external leads were soldered to these or pressure contacts were made to them. However, it was found possible to make reliable contacts directly to aluminum electrodes by using a silver pressure contact.

The procedure for cleaning substrates was varied slightly during the course of these experiments. The procedure currently used starts with a ten-minute wash with a detergent (Tide) using deionized water and ultrasonic agitation, then three

Table 1. Deposition conditions

Dielectric	Deposition System	Source Type	Substrate Temperature	Rate of Evaporation (Å/sec)
SiO	1,2,3,5	Baffled boat (Ta)	Ambient	1-80
MgF_2	1	Open and baffled boats (Ta)	~250°C	5-30
CeF_2	2	Open and baffled boats (Ta)	Ambient	~30
CeO_2	1,5	Open Tungsten boat	Ambient or greater	3-5
CeF_3	1	Open boat (Ta)	~250°C	~5
Teflon	4	RF - sputtering	Ambient (substrate holder water-cooled)	~2

Systems

1. CVC-18
2. NRC
3. Shop fabricated
4. RF - Sputtering
5. Denton 10-in. system

rinses in deionized water, then three more rinses in deionized water each with at least ten minutes of ultrasonic agitation, and finally a half hour or more in a vapor degreaser using isopropyl alcohol. The silver contact tabs are then painted on and the system heated to 550°C. To avoid contamination from the oven, a layer of aluminum foil is wrapped about the glass rack containing the substrates. After cooling, the substrates are stored in a dessicator. Immediately before evaporation, the entire washing procedure is repeated. The substrates are transferred from the vapor degreaser, loaded onto the substrate holder in a clean bench, and carried to the adjacent evaporator with the substrate downward.

The first washing procedure is a somewhat recent addition to the cleaning procedure. By washing prior to firing, any dirt on the substrates is subjected to the cleaning process. The additional wash also seems to improve the adhesion of the silver and to provide a cleaner final surface.

The above procedure seems to yield clean surfaces judging by the adhesion of evaporated films, the uniformity of breath condensation and evaporation patterns, and microscopic examination. However, microscopic examination of the substrates after cleaning reveals, using dark field illumination, a distribution of tiny irregularities in the glass surface. These are in the micron to submicron range and are randomly distributed. They are of about the same density and size as the point irregularities generally seen in the deposited films. It has been found that the blunt tweezers used in transferring the substrates cause micro-chipping of the glass surface. Probably some of the "scum" occasionally observed is really an array of these microchips. Thus, it is desirable to avoid contact by tweezers over the region of the substrate that is ultimately to be covered with the films.

B. ELECTRICAL MEASUREMENTS

1. Prebreakdown Measurements

a. Capacitance and Dissipation Factor

Capacitance and dissipation factor were measured as a function of

temperature at a frequency of 1000 cycles using an ESI Model 250 DA impedance bridge. These measurements were usually started at room temperature and made as the system was cooled in vacuum to liquid nitrogen temperature (see Fig. 1 for the arrangement of the cryostat). Frequently, the capacitors had to be formed before any measurements of capacitance were possible. This need was more pronounced with the crystalline dielectrics than for the SiO.

b. Dc Voltage-Current-Temperature Characteristics

Measurement of the dc voltage-current-temperature characteristics were made as the capacitor was warmed from 78°K up to about 380°K. The measuring circuit employed is shown in Fig. 2. The applied voltage was obtained from a Hewlett-Packard function generator, Model 3000A with Model 3302A Plug-in. This provided a triangular wave of controllable period and amplitude that could be applied in single pulses or repetitively. Normally, the negative half of the pulse was bypassed by a diode instead of being applied to the capacitor. The voltage was not allowed to rise more than a few tenths of a volt above ten volts. The rise rate of the applied voltage was usually about 1 volt/sec. At very low currents an electrometer (GR Model 1230A) could be used to measure the current. This instrument has a recorder output which could be displayed on the same xy-recorder, Moseley Model 7000A, as was used otherwise.

The current going to the capacitor (displacement plus leakage) was determined by measuring the voltage across a standard resistance, usually 1000 ohms (see Fig. 2). In any event, care was taken to keep this resistance small compared to the input impedance of the recorder (1 megohm). In cases where the leakage currents through the capacitors were very small (less than 0.1 uA) it was necessary to subtract the charging current from the total current if the leakage was to be measured. Thus $I_{total} = I_{charging} + I_{leakage}$. If the applied voltage increases linearly and the time constant of the circuit is very small, then $I_{charging}$ is a constant. The value of $I_{charging}$ can be determined by measuring

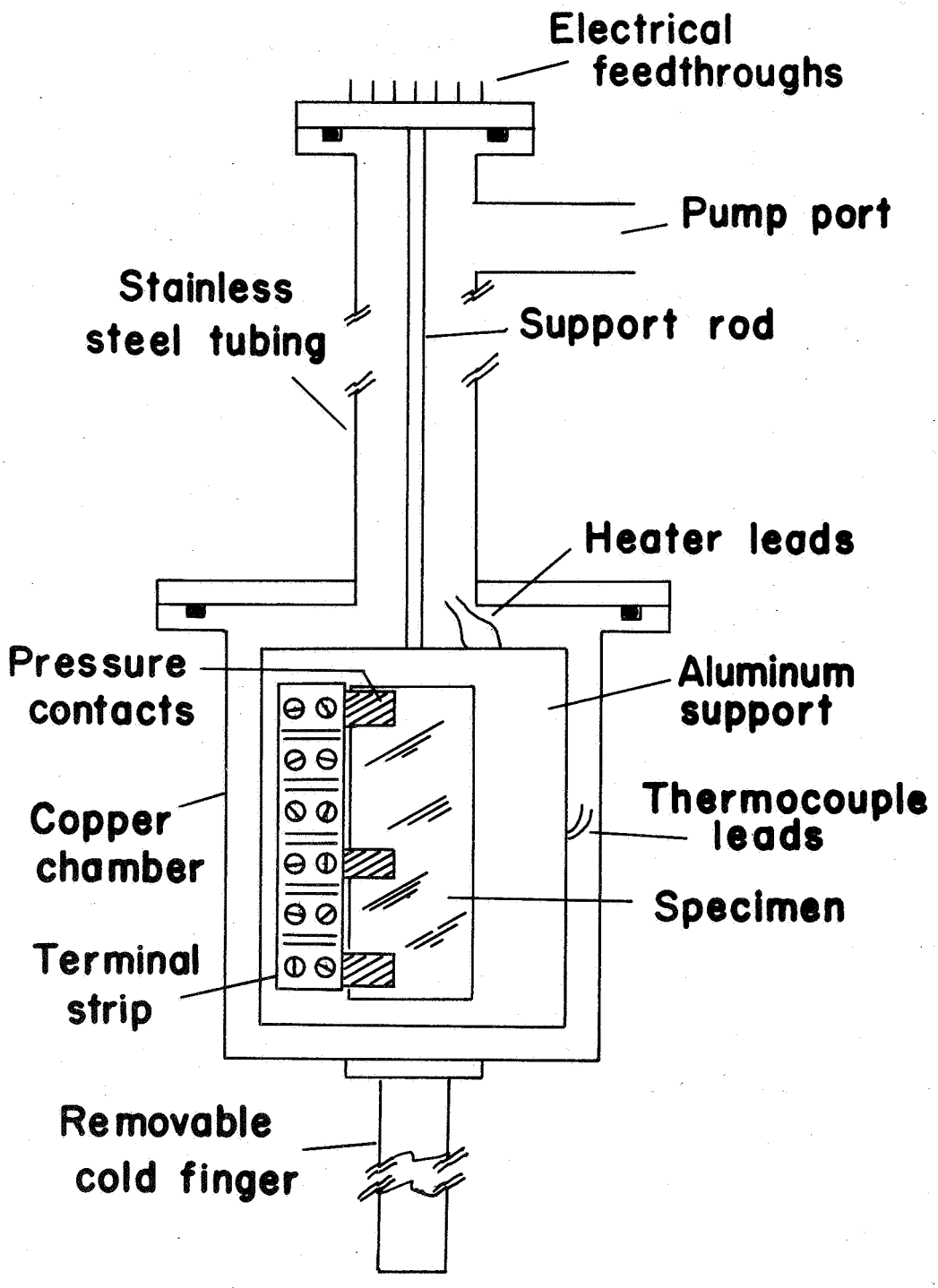

Fig. 1. Cryostat for electrical measurements of capacitors in vacuua.

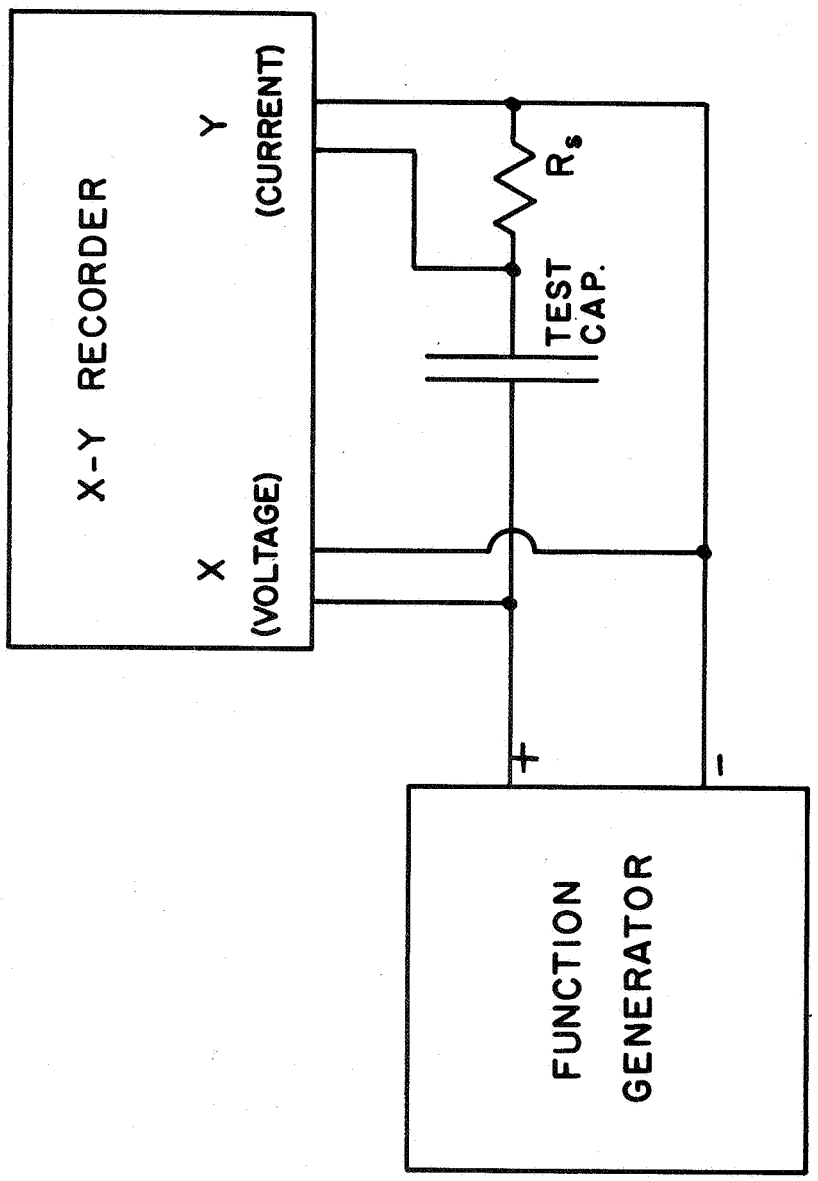

Fig. 2. Measuring circuit used in obtaining dc V-I-T characteristics and impedance-temperature data.

the current at very low voltage when $I_{leakage}$ is negligible, assuming that the charging rate is constant.[1]

c. Carrier Type

In order to distinguish ionic conduction from electron or hole conduction, a steady voltage was applied for a long period and the current measured at regular intervals. If the current did not vary with time after the first few seconds, it was assumed that the current was electronic in nature. On the other hand, if the current gradually fell to zero, then the current was taken to be ionic. The circuit employed in this is shown in Fig. 3.

d. Local Conductance

An attempt has been made to measure the microscopic variations in conductivity by a probe method (see Fig. 4). An electropolished tungsten point was moved over the surface of a dielectric film deposited on top of a base film of aluminum. The current was observed when the voltage between probe and base was maintained constant. The purpose was to describe the electrical variations found and to correlate them to topographical pecularities, to the forming process, to prebreakdown conduction, and to breakdown conduction.

2. Breakdown Measurements

The method used in the breakdown measurements is the same as that previously described[1-3] with only minor changes in the circuitry (see Fig. 5). The applied voltage was in the form of a ramp whose rise time could be controlled. The rise time was chosen so that it was typically more than 100 times the RC time constant of the charging circuit. Thus, the voltage across the capacitor was essentially that of the applied ramp. The ramp voltage was supplied from the sweep circuit of a Tektronix oscilloscope or a Hewlett-Packard function generator (Model 3000A) and an external amplifier when necessary. The amplifier was essential both to attain sufficiently high voltages and to preserve the ramp waveform if the test capacitor became extremely leaky prior to breakdown.

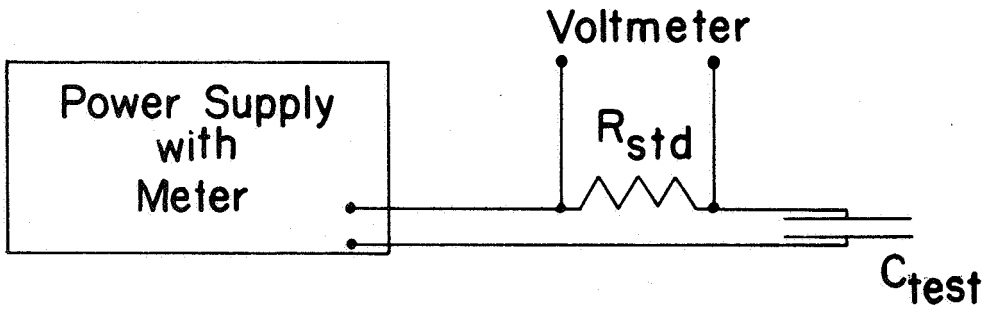

Fig. 3. Circuit employed to detect ionic conductivity.

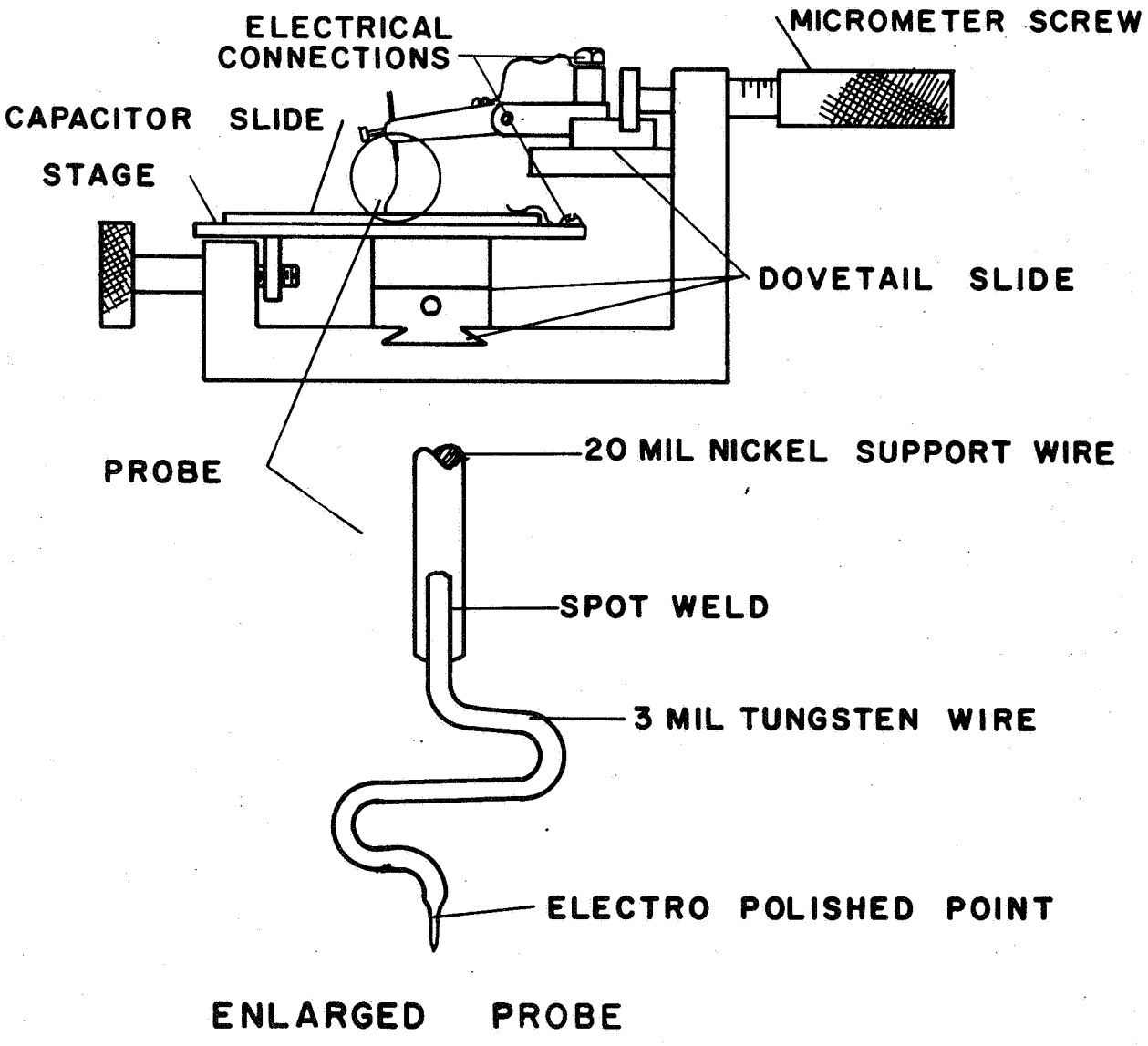

Fig. 4. Probe arrangement for local conductance study.

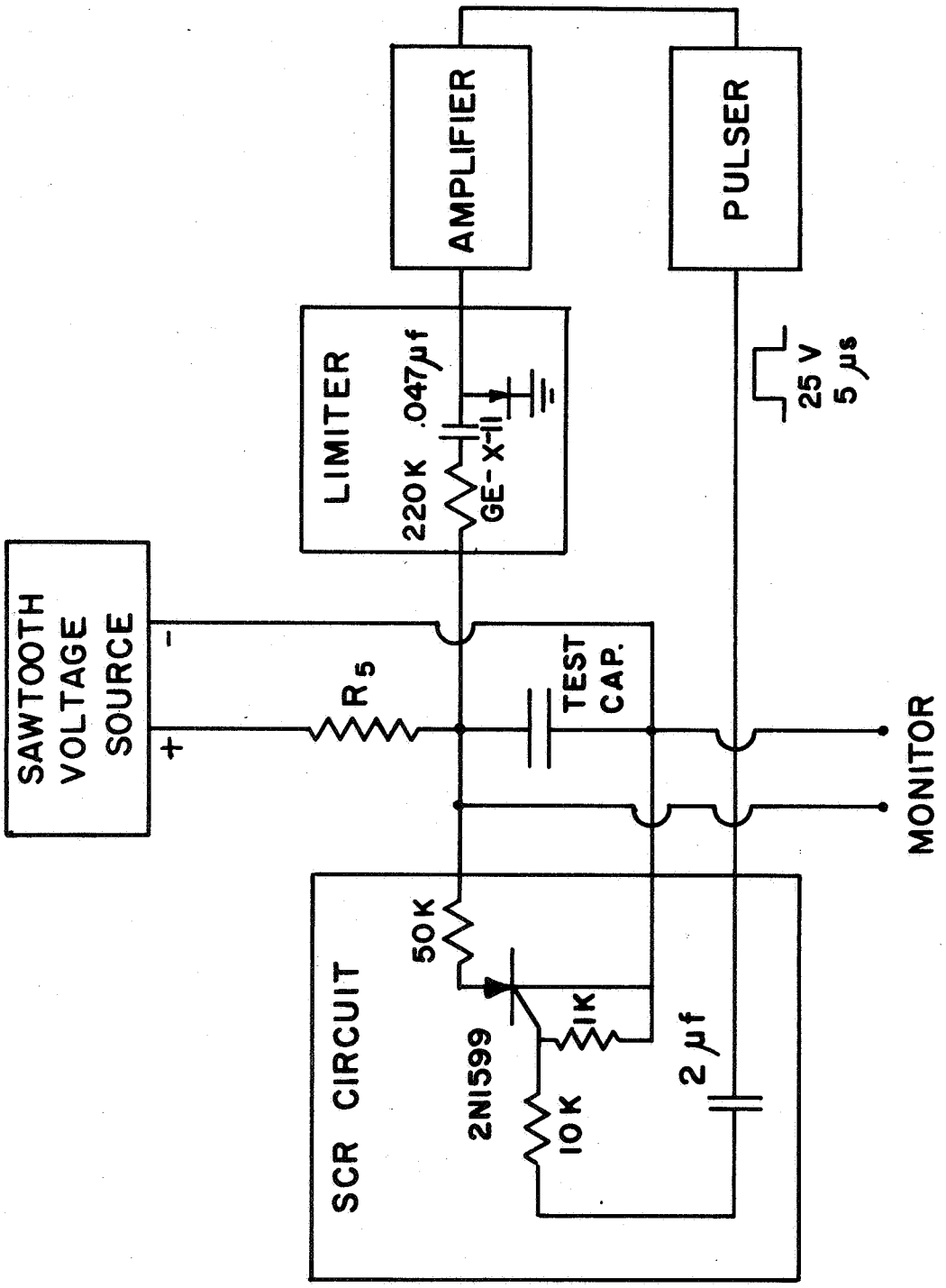

Fig. 5. Circuit for measuring breakdown voltages by the ramp method. The silicon-controlled rectifier removes the ramp within a few microseconds of the occurrence of the breakdown.

a. Threshold for the Onset of Breakdown

In measuring the voltage for the onset of breakdown, an attempt was made to limit the capacitor to only one breakdown for each ramp. This was accomplished by shorting out the supply voltage with a silicon controlled rectifier activated by the voltage pulse accompanying the breakdown. The circuit containing the silicon-controlled rectifier could be removed to be sure that it was not influencing the measurement of the breakdown voltage. The ramp rise time to the breakdown voltage was generally several seconds. The value of the ramp voltage was recorded on a Bausch and Lomb Model VOM 7 recorder as the ramp rose to the breakdown voltage and then dropped abruptly on the occurrence of the breakdown.

Measurements of the voltage for the onset of breakdown were made as a function of temperature and of ramp speed. Where necessary, the waveform was recorded oscillographically instead of with the slow chart recorder. In one series of measurements, a group of six capacitors of differing areas were simultaneously deposited. These were subsequently broken down and the breakdown voltages, waveforms, capacitor sizes, and the dimensions of the breakdowns were correlated. The capacitor configurations are shown in Fig. 6.

b. Threshold for the Cessation of Breakdown

The voltage at the termination of breakdown was determined from the voltage waveforms of breakdowns. The ramp voltage was not cut off immediately after the first breakdown, rather it was continued until ten or more breakdowns had occurred in succession. A characteristic cutoff value was obtained for each capacitor. This threshold for the cessation of breakdown was measured as a function of temperature and capacitor area.

c. Breakdown Voltage Waveforms

The waveforms of single breakdowns were studied to determine the presence of precursors to breakdowns, the nature of the onset of breakdown conduction, the conductance during breakdown, and the conditions terminating the breakdown.

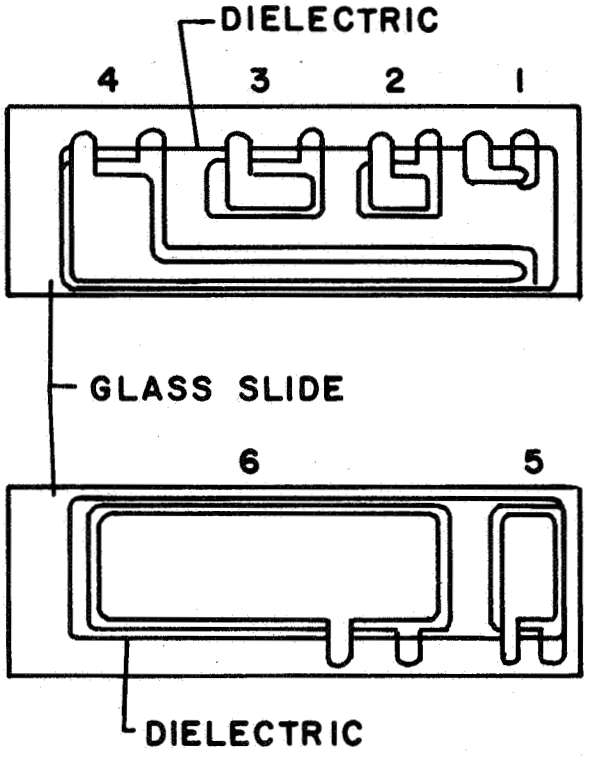

Fig. 6. Capacitor configuration for areal studies. Capacitor areas are: 1. 0.064 cm^2; 2. 0.45 cm^2; 3. 0.65 cm^2; 4. 1.11 cm^2; 5. 3.23 cm^2; 6. 6.68 cm^2.

C. OPTICAL SPECTROSCOPY OF BREAKDOWNS

Destructive breakdown is accompanied by a flash of light. Experiments were performed to determine the nature of the emitted light and to try to relate the emitted light to other aspects of the breakdown process. First the spectrum of a breakdown was determined, then the individual spectral lines were studied to determine how their intensities varied with time.

1. Spectra

The spectrum of the emitted light was found using a Bausch and Lomb quartz prism spectrograph having a range of 2100 Å to 6500 Å. In the ordinary use of the spectrograph a broad, continuously emitting light source is placed about two feet from the entry slit (see Fig. 7). Light is focused on the slit by a quartz lens located between the source and the slit. Since the spectrometer has an effective aperture of f/12, not all of the light entering the slit passes through the system onto the photographic plate.

It should be appreciated that a capacitor breakdown is not a typical spectrometer source. The capacitor undergoing breakdown does not continuously emit from a constant location. Each breakdown lasts only about a microsecond, each is localized to a region less than a tenth of a millimeter in diameter, and each occurs at a different spot on the capacitor. The location of a breakdown site cannot be predicted prior to the occurrence of the breakdown. If a capacitor of large area were positioned at the location of the conventional illuminating source of the spectrograph, the probability of breakdowns occurring so that their light would enter the slit and be recorded on the photographic plate is small. No spectrum was obtained when this method was tried.

A method that did provide spectra is illustrated in Figs. 7, 8, and 9. A capacitor 3 mm wide and 8 mm long is positioned as shown in Fig. 7 in front of the spectrometer slit using the special mounting jig of Fig. 8. Electrical contacts

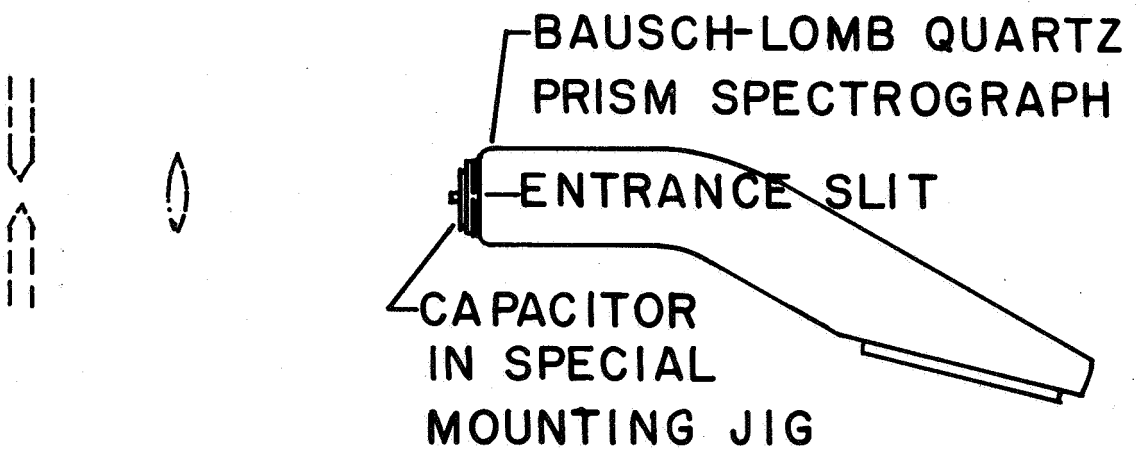

Fig. 7. Spectrographic arrangement.

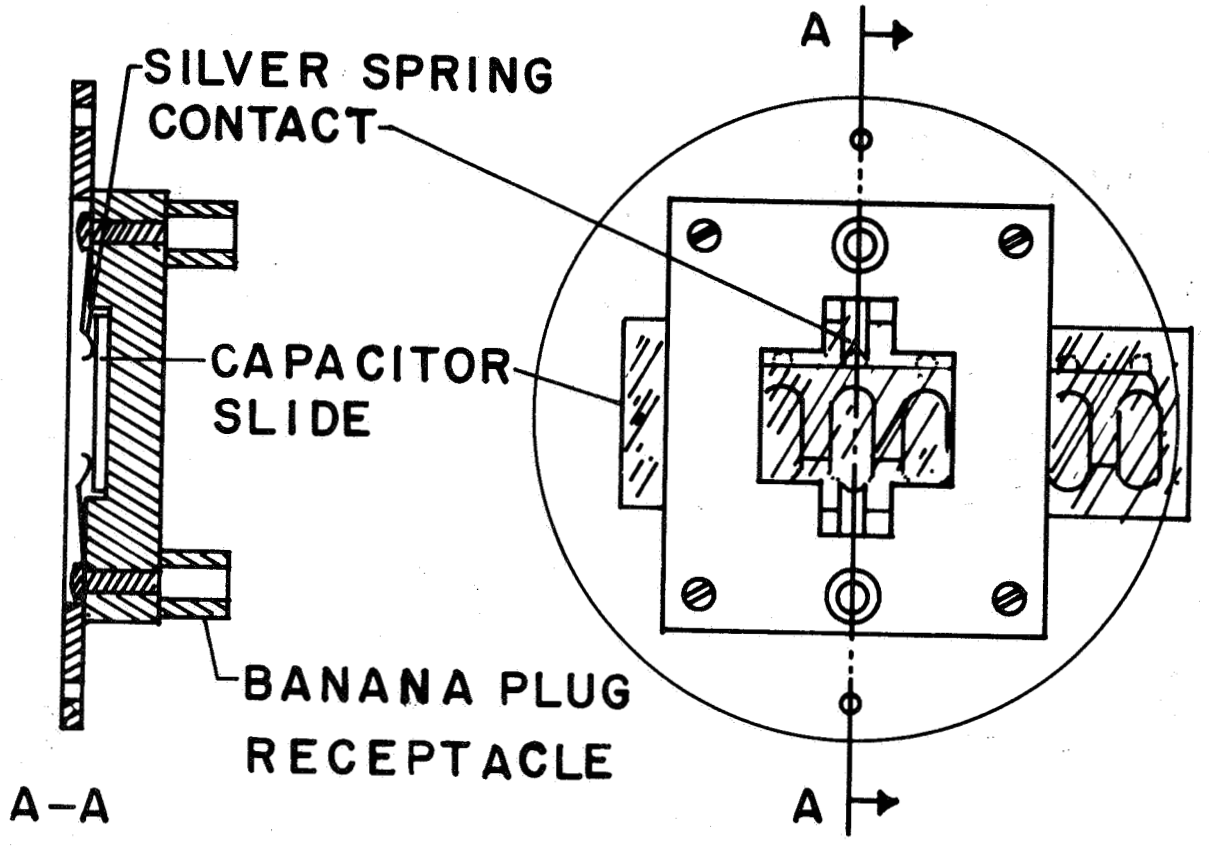

Fig. 8. Spectrometer jig.

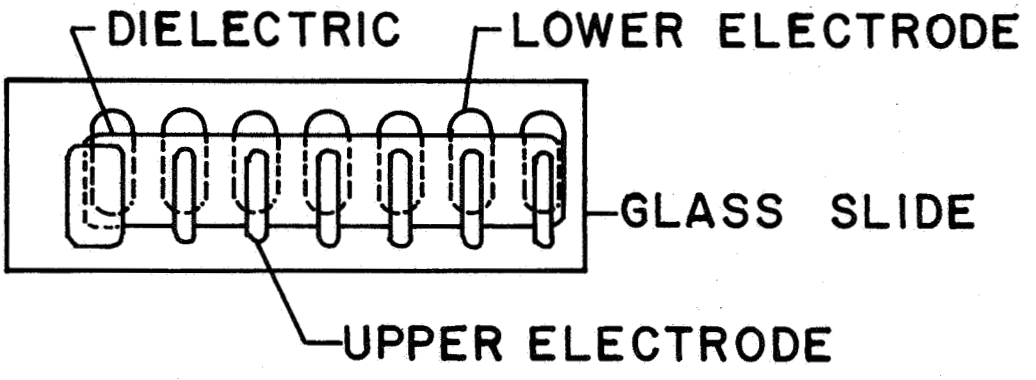

Fig. 9. Capacitor configuration for spectrometer jig.

were made using pressure contacts directly to the aluminum electrodes. The capacitor faced directly into the slit with no intervening layer of glass. Seven of the small capacitors, each with independent electrodes, were fabricated on a single 1" x 3" microscope slide (see Fig. 9). Upon application of a ramp voltage of sufficient amplitude, destructive breakdown occurred.

Ordinary spectrographic plates were too insensitive to obtain spectra, so Kodak Royal-X Pan film (speed ASA1600) was used. Since the emulsion on this film was not available in 2" x 10" plates, the size required by the spectrometer, 120 film was trimmed and taped to 2" x 10" plates. The film was developed for seven minutes in Kodak DK-60A developer at 68°F.

Since each breakdown is very nearly a point source of light, the spectrum that it produces is a single dot at each wavelength present. The position of the dot vertically (the spectrograph disperses horizontally) is determined by the vertical location of the breakdown with respect to the spectrometer slit. A series of breakdowns along the length of the slit is needed in order to clearly map out a line. It was felt desirable to do this (even though the dots of a single breakdown really determined the spectrum) so that there would be no confusion between possible electrode arcing effects and genuine breakdowns.

Line spectra were obtained. These were identified by making comparison arc spectra of pure samples of the major constituents of the capacitors. A tracing of a capacitor breakdown spectrum is shown in Fig. 10. The lines are identified and are listed in Table 2.

2. Time-Resolved Spectroscopy

After discovering that line spectra were emitted during breakdown, an experiment was performed to relate the voltage waveform and the light output at each wavelength as a function of time. A spectrometer for time-resolved spectroscopy was assembled as shown in Fig. 11. The test capacitor is held in the same jig as in Fig. 8 which is mounted at the entry slit of a monochromator (component part of a Bausch and Lomb Spectronic 505 spectrophotometer) that has

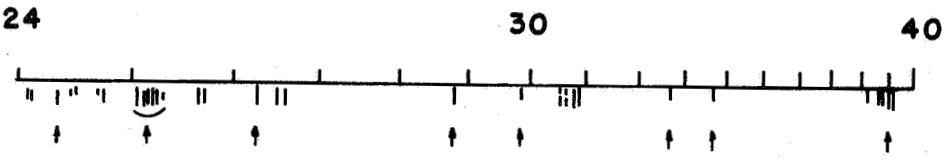

Fig. 10. Breakdown spectrum from an Al-SiO-Al capacitor.

Table 2. Spectral lines observed in the breakdown of Al-Sio-Al capacitors.

Material	Wavelength (Å)	Ionization State	Relative Intensity
Silicon	2435	I	4
	2506	I	5
	2514	I	5
	2516	I	5
	2519	I	5
	2524	I	5
	2528	I	5
	2631	I	4
	2881	I	6
	2987	I	3
	3905	I	2
Aluminum	2567	neutral	3
	2575	neutral	3
	2652	I	2
	2660	I	3
	3041	II	1
	3074	II	1
	3082	I	6
	3092	I	6
	3944	I	10
	3961	I	10

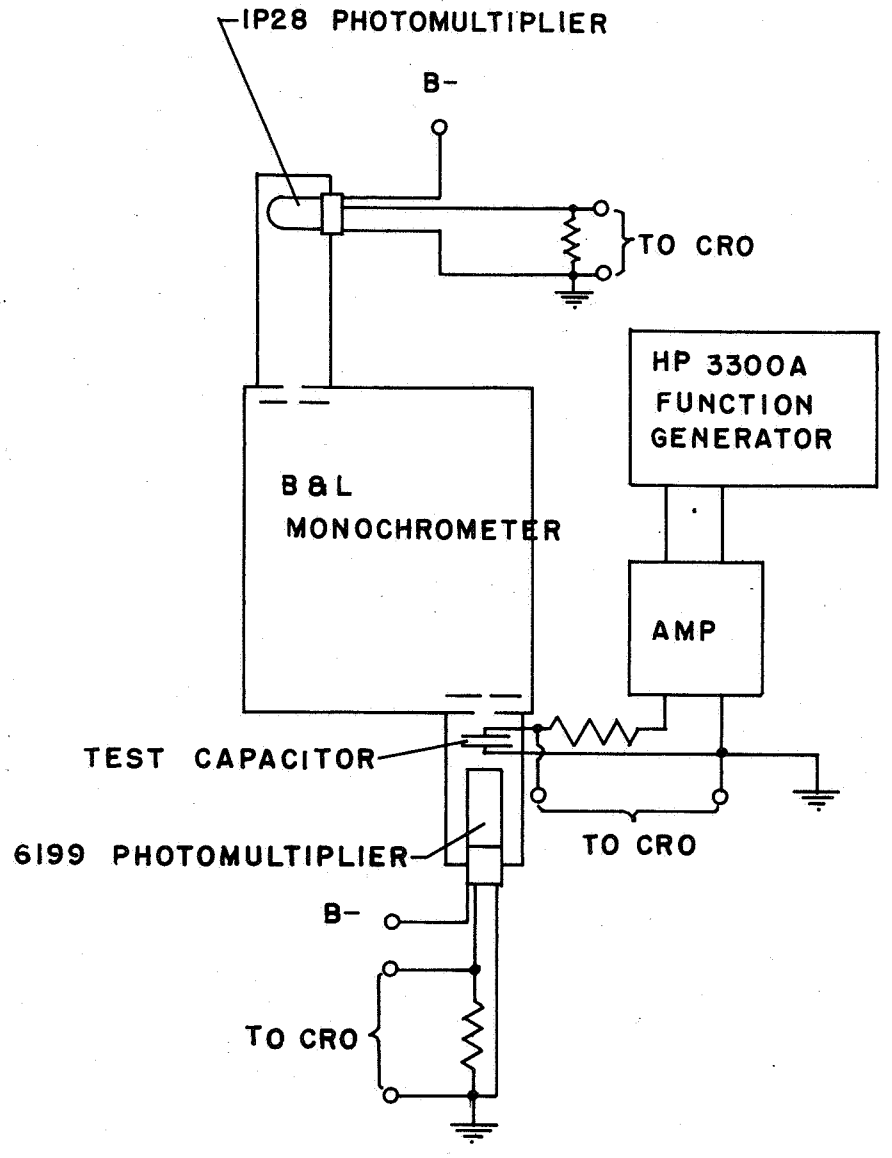

Fig. 11. Arrangement for time-resolved spectroscopy.

a resolution of 5 Å or 50 Å, depending upon the slit settings. The wider slit width was used during most of the experiments on lines that were well-isolated so that the location of the breakdown with respect to the spectrometer slit would not be quite so critical.

The light passing through the monochromator was detected by a RCA 1P28 photomultiplier tube (ultraviolet sensitive). The tube was operated with 1000 volts from anode to cathode and with 100 volts per dynode stage. A metal shield placed in contact with the tube envelope and maintained at the cathode potential reduced the noise level markedly. The voltage signal from the photomultiplier was displayed on a Tektronix dual beam oscilloscope, Model 551. Typical waveforms are shown in Fig. 12.

A second photomultiplier tube, RCA 6199, was positioned over the capacitor mounting jig as shown in Fig. 11. This gave the integrated intensity of the light over the visible range of the spectrum and was useful as a monitor. It also operated at 1000 volts.

The voltage waveform across the capacitor could be displayed and recorded with either one of the above, or with both if a second oscilloscope was used.

In performing the experiments the Hewlett-Packard function generator was used to supply the ramp. The ramp amplitude was normally chosen so that only one or two breakdowns occurred during a single ramp. The oscilloscope could be triggered by the capacitor voltage pulse accompanying breakdown, by the integrated light signal, or by the output of the monochromator. There was always a one-to-one correspondence between the breakdown voltage waveform and the integrated light signal. However, not every breakdown occurred at a position that would allow light to get through the monochromator. Tests were made to determine the amplitude of the continuous spectral background. In the region between 2000 and 4000 Å, this background (measured with the 50 Å slit) was less than 1% of the peak intensity of the strong spectral lines.

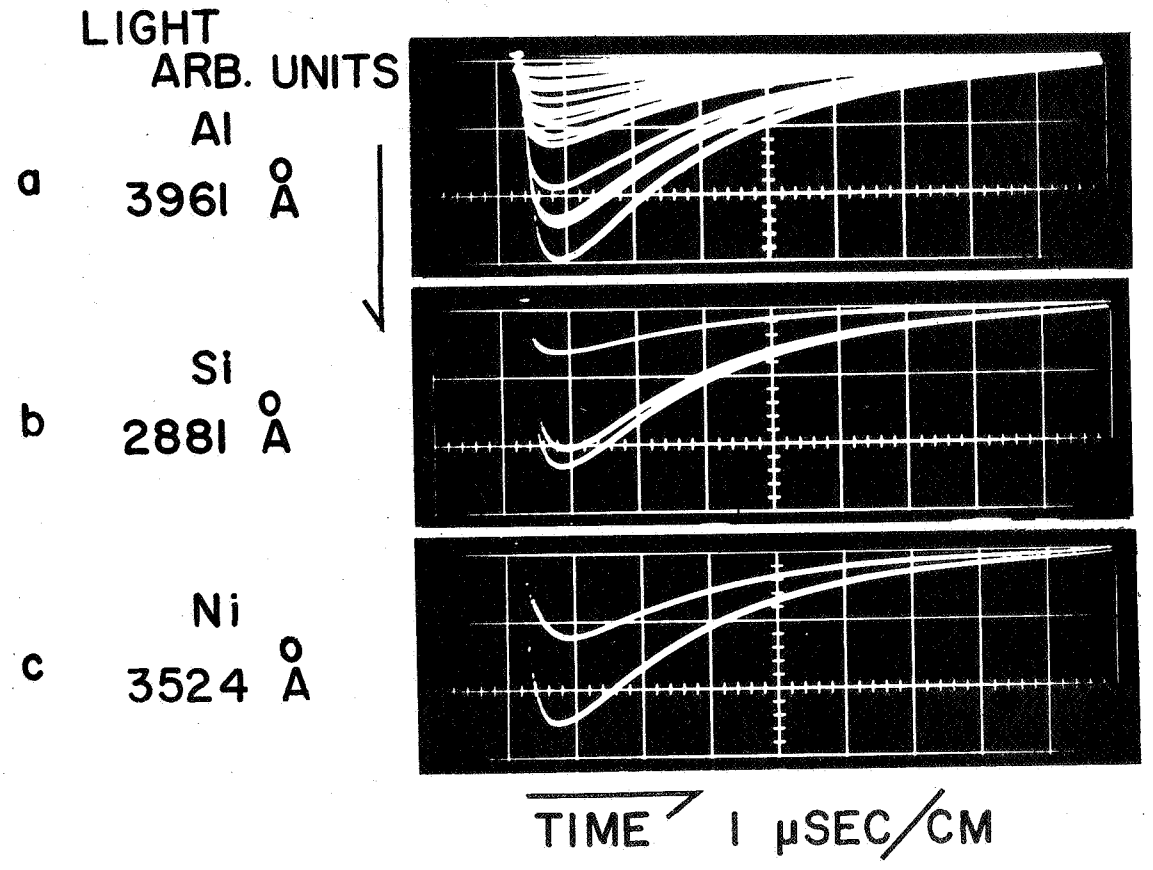

Fig. 12. Light intensity and voltage waveforms from individual spectral lines. Each oscillogram is due to several individual breakdowns. (a) Aluminum electrode, λ = 3961 Å. (b) Silicon (from the dielectric SiO), λ = 2881 Å. (c) Nickel electrode, λ = 3524 Å.

D. OPTICAL MICROSCOPY AND OTHER OBSERVATIONS

1. Optical Microscopy

Capacitors, individual films, and substrates were examined at different stages of their history using an optical microscope with transmitted, illumination reflected, bright and dark field illumination, and reflected-polarized illumination.

2. X-ray Diffraction

X-ray diffraction data were obtained comparing the structures of the films prior to deposition, after deposition, and after breakdown.

3. X-ray Microprobe

Specimens were examined using x-ray microprobes by Roy Bicklehaupt of the Southern Research Institute and by R. A. Parr and Gordon Marsh of the Marshall Space Flight Center. They sought to determine concentrations of elements before and subsequent to breakdown.

III. RESULTS

A. ELECTRICAL MEASUREMENTS

1. Prebreakdown

a. Capacitance and Dissipation Factor

The temperature dependence of the capacitance per unit area, C/A, and of the dissipation factor are shown in Fig. 13 for typical capacitors of each of the materials of this study. Peaks are found in the dissipation factor at 5°C in CeF_3, at -60°C in CaF_2, and at -100°C in CeO_2. Accompanying these peaks are changes (with increasing temperature) in the real part ε' of the relative dielectric constant by a factor of 16 in CeF_3, of 1.2 in CaF_2, and of 10 in CeO_2. Such behavior is typical of a system with a single relaxation time in the range of measurement.[16] Both CeF_3 and CeO_2 have large dissipation factors, but not appreciably larger than that of MgF_2. The capacitance per unit area of CeF_3 and CeO_2 is close to two orders of magnitude greater than that of the other materials. The temperature dependence exhibited by C/A and D is quite similar in SiO and MgF_2. This is to be noted because the dc current-voltage-temperature characteristics of these two materials (see Figs. 18 and 19) differ markedly.

Figures 14 and 15 show the values of ε' and ε'', the real and imaginary parts of the relative dielectric constant, for each of the materials studied. The data are plotted as a function of dielectric thickness and the measurements were taken in vacuua at room temperature at 1000 Hz. It is seen that there is considerable scatter in all materials in the value of ε''. The value of ε' in SiO and in MgF_2 is found to be essentially independent of thickness and each is fairly well-defined. This is in contrast to the wide scatter in ε' in the other materials.

CeO_2 seems to display a systematic thickness dependence in both ε' and ε''. There is a monotonic increase in both up to about 3500A°, then an abrupt drop.

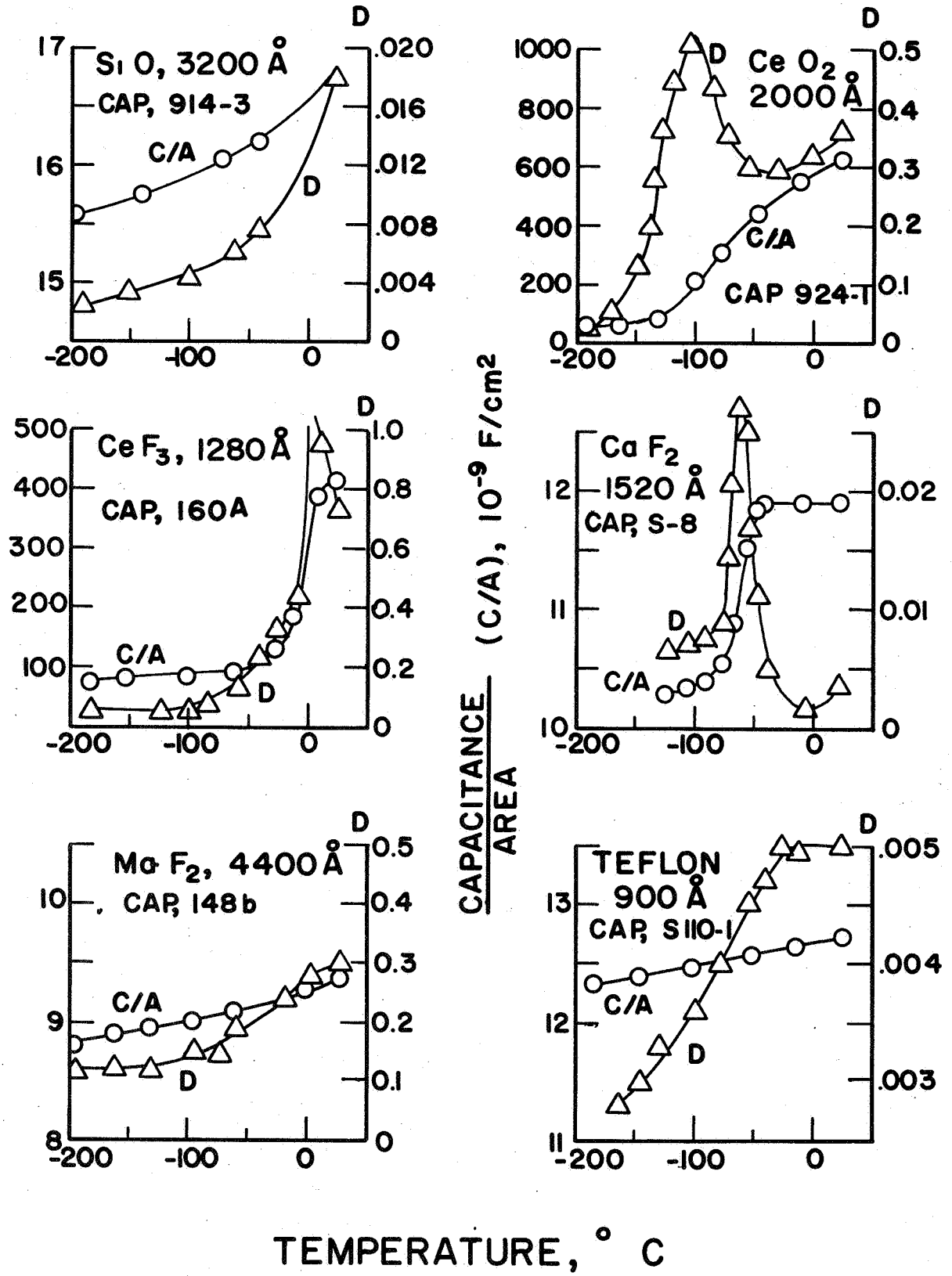

Fig. 13. Capacitance/area and dissipation factor vs temperature. (a) SiO. (b) CeF_3. (c) MgF_2. (d) CeO_2. (e) CaF_2. (f) Teflon.

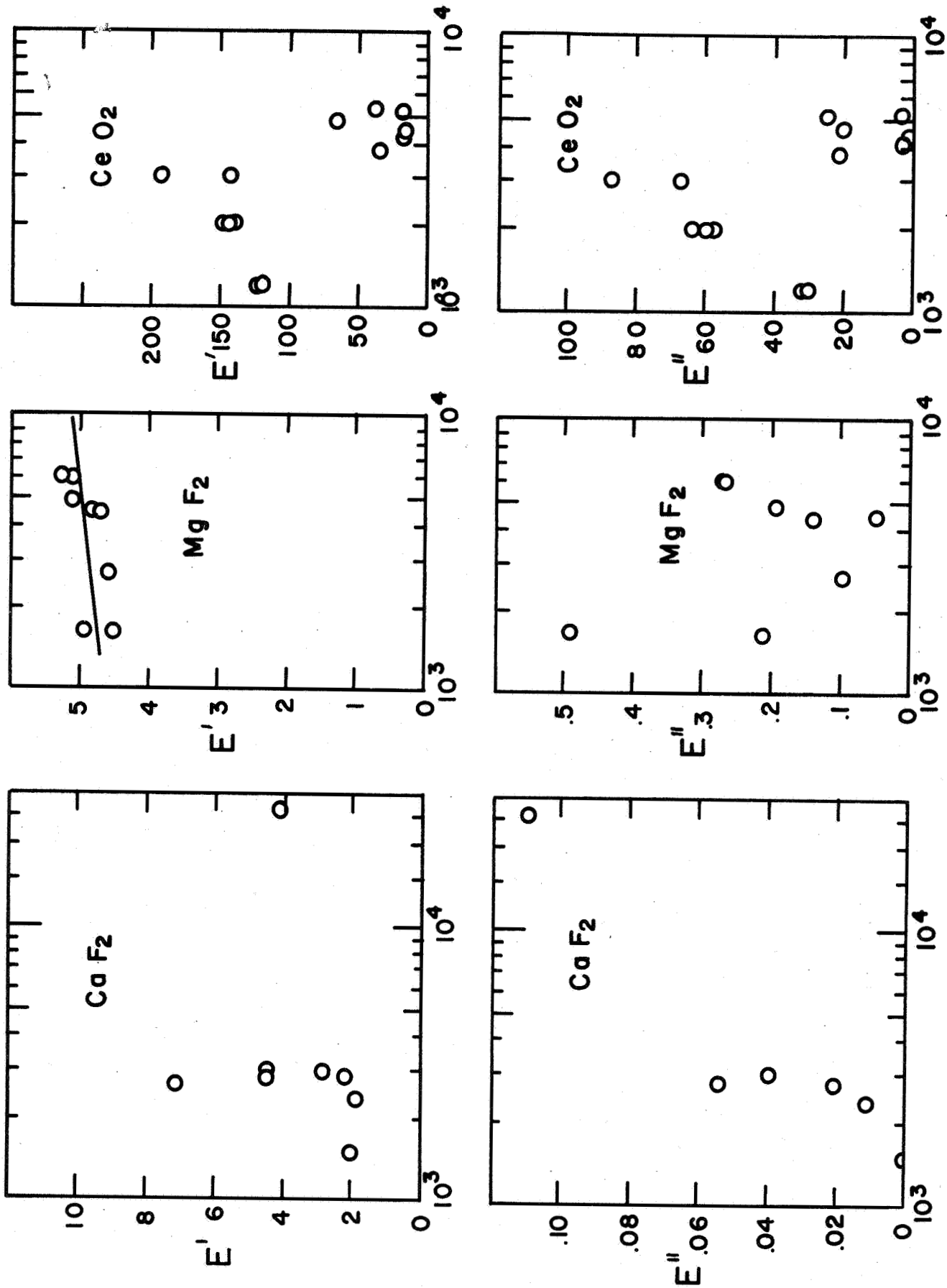

Fig. 14. ϵ' and ϵ'' vs dielectric thickness for CaF_2, MgF_2, and CeO_2 at room temperature and 1000 Hz.

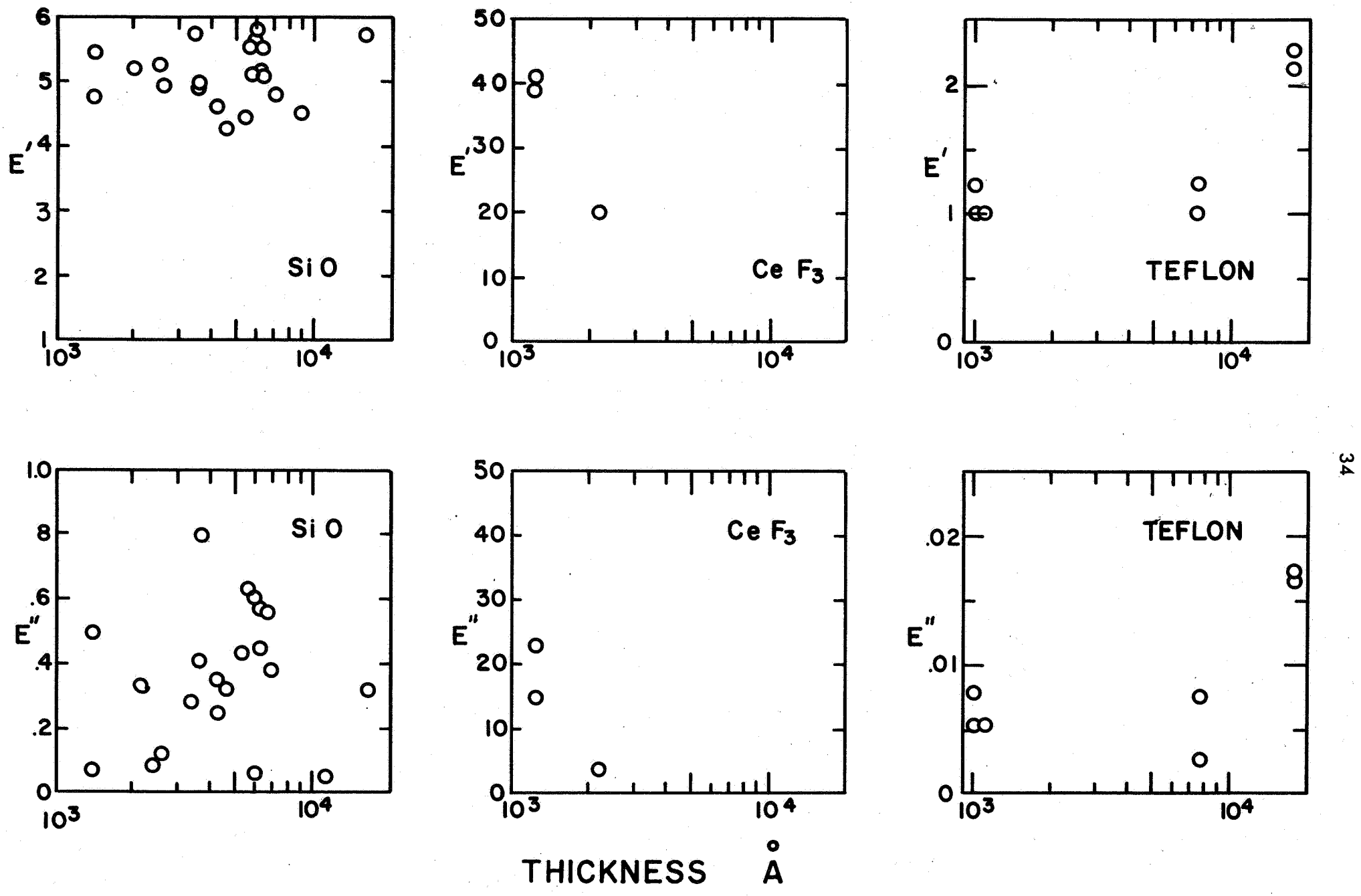

Fig. 15. ϵ' and ϵ'' vs dielectric thickness for SiO, CeF_3, and Teflon at room temperature and 1000 Hz.

In room air the dielectric constant ε' (and correspondingly ε'') was very high and somewhat unpredictable (100 to 600).

When the capacitors were placed in vacuum ε' typically decreased. For dielectric thickness greater than 3500A° this decrease was considerable (50% to 95%), while for dielectric thicknesses less than 3500A° the decrease was slight. The change in ε' is attributed to a decrease in humidity rather than pressure. The dielectric constant did not increase again when air was let into the crybstat through a drying agent but did increase when the capacitor was removed from the cryostat and placed in open air. The sudden change in ε' and ε'' at a thickness of 3500A° could possibly be related to a thickness dependent humidity sensitivity. No indication of different oxide structures resulted from x-ray diffraction of dielectrics in the two thickness ranges.

Table 3 contains average values of ε' and ε'' and compares these with values from bulk specimens.

It should be pointed out that a meaningful correlation has been found in the SiO data between rate of deposition and both ε' and ε''. This is generally attributed to the higher percentage of SiO_2 at the lower deposition rates.[17] A comparison of ε' and ε'' with deposition rate is not made for all of the materials since this parameter has generally been held constant to reduce deposition variables. However, deposition rate is an important parameter.[18] Probably the widest range in deposition rates in these experiments occurred in SiO and in MgF_2. In the case of SiO the rate of deposition was intentionally varied, while with the MgF_2 there were large differences accompanying experiments to determine the best type of evaporation boat. If the boat is a baffled type and is not heated uniformly, then the material condenses on the cooler parts near the current leads and the evaporation rate from the source is generally less than 10 Å/sec. More typically deposition rates for MgF_2 were about 30 Å/sec.

Table 3. Average values of ϵ' and ϵ'' for thin films compared to bulk materials (at room temperature and 1000 Hz).

Material	Thin Film Average Values at Room Temperature ϵ'	ϵ''	Bulk Values ϵ'	ϵ''
SiO	$5.4 \pm .1$ a $5.0 \pm .1$ b	$.49 \pm .05$ a $.30 \pm .04$ b	c	c
CeO_2	$(1.4 \pm .1)\ 10^2$ d $(.3 \pm .1)\ 10^2$ e	$(6 \pm 1)\ 10^1$ d (12 ± 4) e	26 f	c
MgF_2	$4.84 \pm .07$	$.2 \pm .1$	c	c
CaF_2	3 ± 1	$.04 \pm .02$	6.78 g	10^{-3} g
CeF_3	33 ± 7	14 ± 5	c	c
Teflon	$1.6 \pm .3$	$.009 \pm .002$	2.00 (10^6 Hz)	.001

a Rate of deposition greater than 30 Å/sec.
b Rate of deposition less than 30 Å/sec.
c Bulk values are not available.
d Thickness less than 3200 Å.
e Thickness greater than 3200 Å.
f H. Graenecher, Helvetica Physica Acta 24, 619 (1951).
g K. V. Rao and A. Smakula, J. Appl Phys. 37, 319 (1966).
h R. C. Weast, Editor, Handbook of Chemistry and Physics, 47th Edition, The Chemical Rubber Company, Cleveland, Ohio, E58 (1966).

b. Dc voltage-current-temperature characteristics.

Figure 16 shows the current density as a function of the applied voltage for each of the materials at low and high temperatures (no low temperature data has yet been obtained on Teflon). Strong temperature dependencies are exhibited by SiO, CeO_2 and CeF_3, whereas MgF_2 and CaF_2 are only mildly temperature dependent. The magnitude of the current density in MgF_2 among different capacitors, at a given voltage, has varied by about four orders of magnitude. Yet the temperature insensitivity is always the same. Sometimes the current at a given voltage decreases slightly with increasing temperature, which is different from the curves of Fig. 16c.

Figure 17 contains curves of current density vs. inverse absolute temperature at constant voltage (10 volts for all curves except that of CeF_3, which is at 5 volts). The SiO and CeO_2 curves each can be described by two straight-line segments. Figure 18 contains the SiO curves for different values of the voltage. It is seen that the slopes are essentially independent of the voltage.[1] The values of the slopes at each region and for each voltage are given in Table 4. Also shown in Table 4 are slopes computed from CeO_2 data. The voltage dependence of these slopes is slight and it is not systematic.

Figure 19 contains the current density temperature curves of MgF_2 for three voltages. Note that the current density scale is linear and that centigrade temperature is plotted rather than inverse absolute temperature as in Fig. 17. Up to about $-20^{o}C$ there is virtually no temperature effect. The data do not go to a sufficiently high temperature to determine the activation energy at the high temperature region.

It is important to note the widely different prebreakdown dc conduction in SiO and MgF_2 in comparison to the similarities in the breakdown conduction of the two materials. It has previously been pointed out[3] that widely different

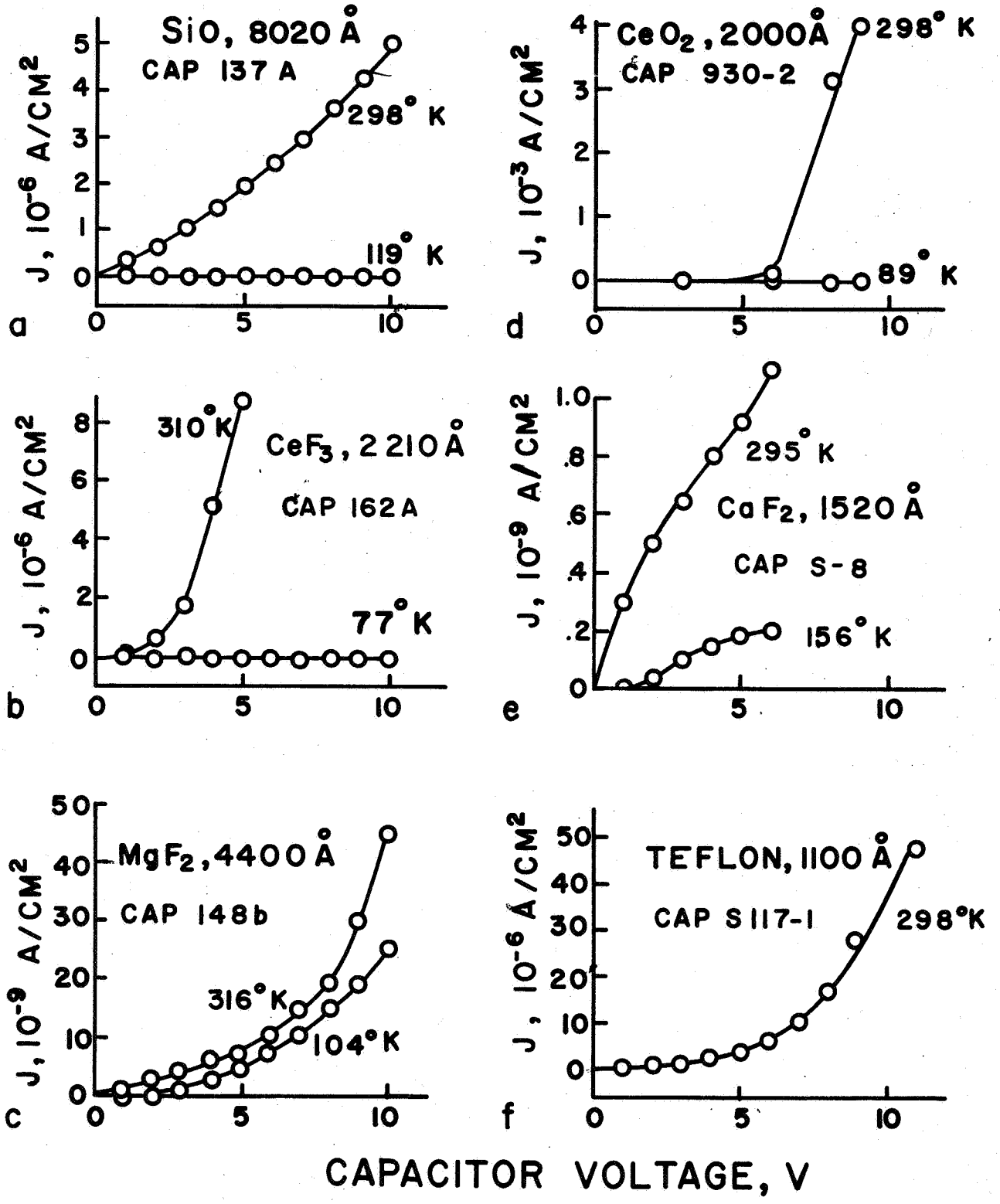

Fig. 16. Dc voltage-current curves at low and high temperatures. (a) SiO. (b) CeF_3. (c) MgF_2. (d) CeO_2. (e) CaF_2. (f) Teflon.

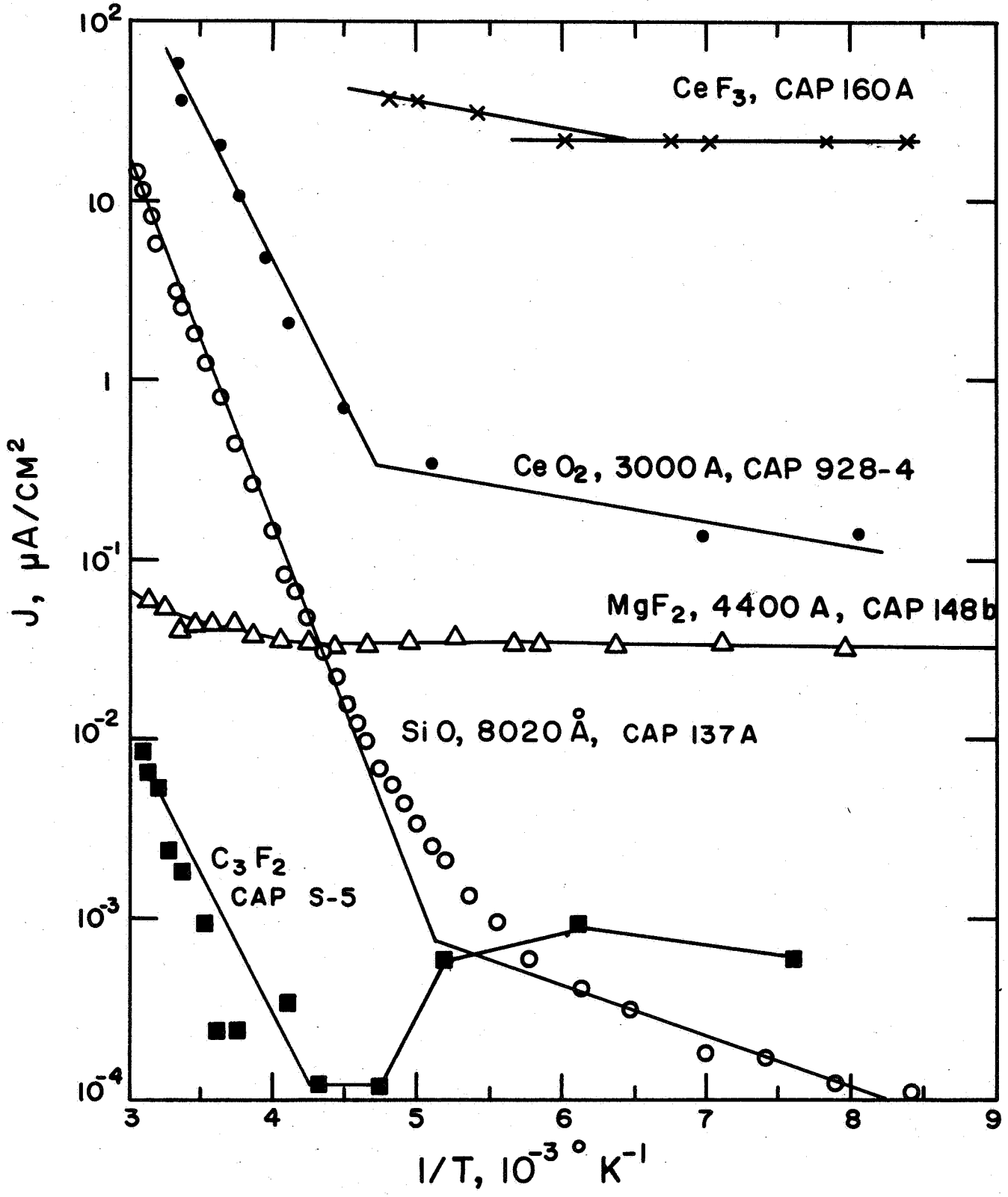

Fig. 17. Temperature dependence of dc current for dielectrics SiO, CeO_2, CaF_2, MgF_2, and CeF_3 when the voltage is held constant. (All curves are at 10 V except the CeF_3 curve which is at 5 V.)

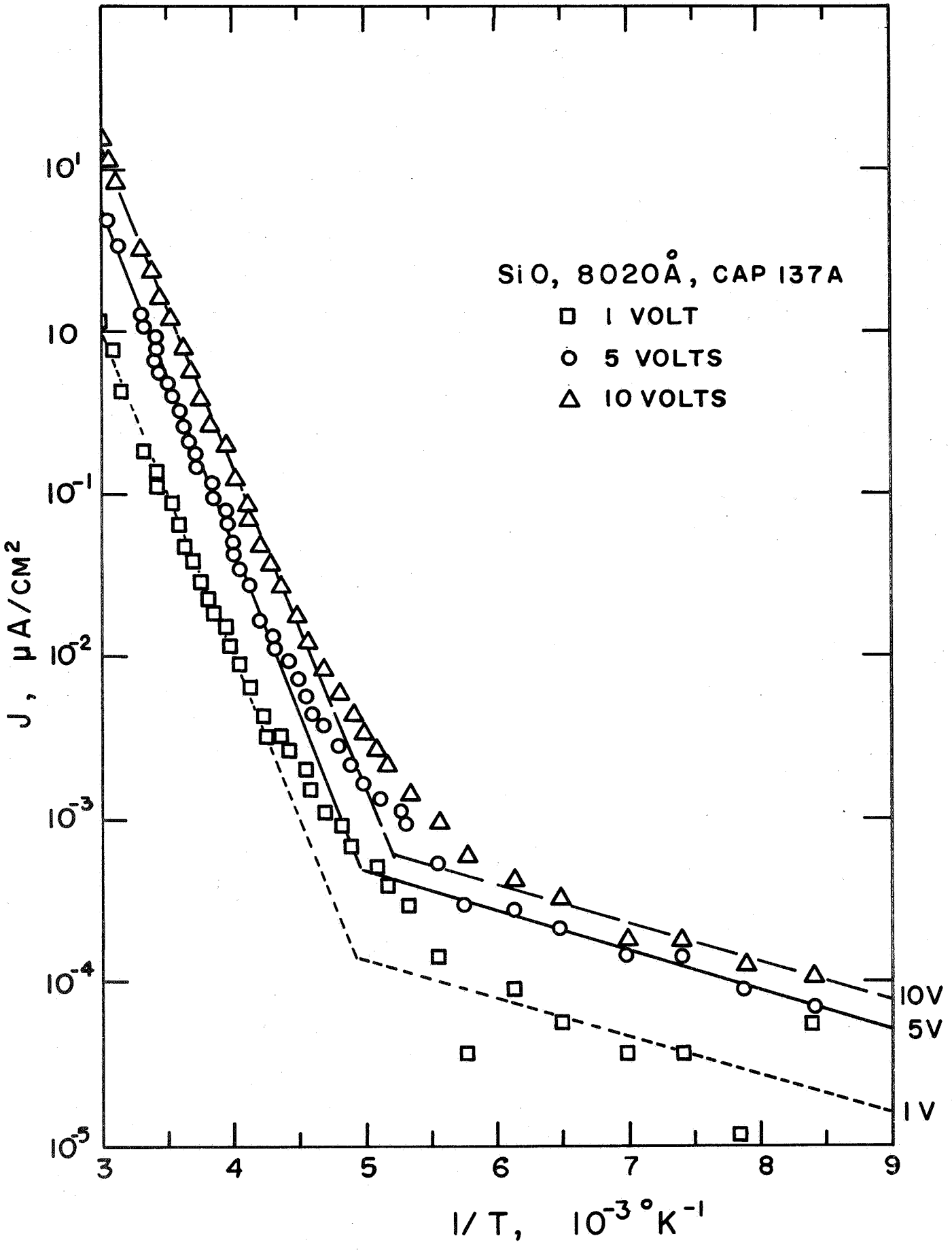

Fig. 18. Current density vs 1/T curves at constant voltage for Al-SiO-Al capacitor 137a. See Table 4 for slopes.

Table 4. Slopes of the constant voltage characteristics of the Al-SiO-Al capacitor of Fig. 18 and of similar characteristics of an Al-CeO_2-Al capacitor.

Capacitor	Voltage (V)	Slope in high temperature region (eV)	Slope in low temperature region (eV)	Transition temperature (^{o}C)
Al-SiO-Al	1	.370	.05	-80
	5	.396	.052	-80
	10	.407	.027	-80
Al-CeO_2-Al	3	.12	---	---
	6	.13	.0012	-100
	8	.14	.0033	-100
	9	.19	.0052	-100

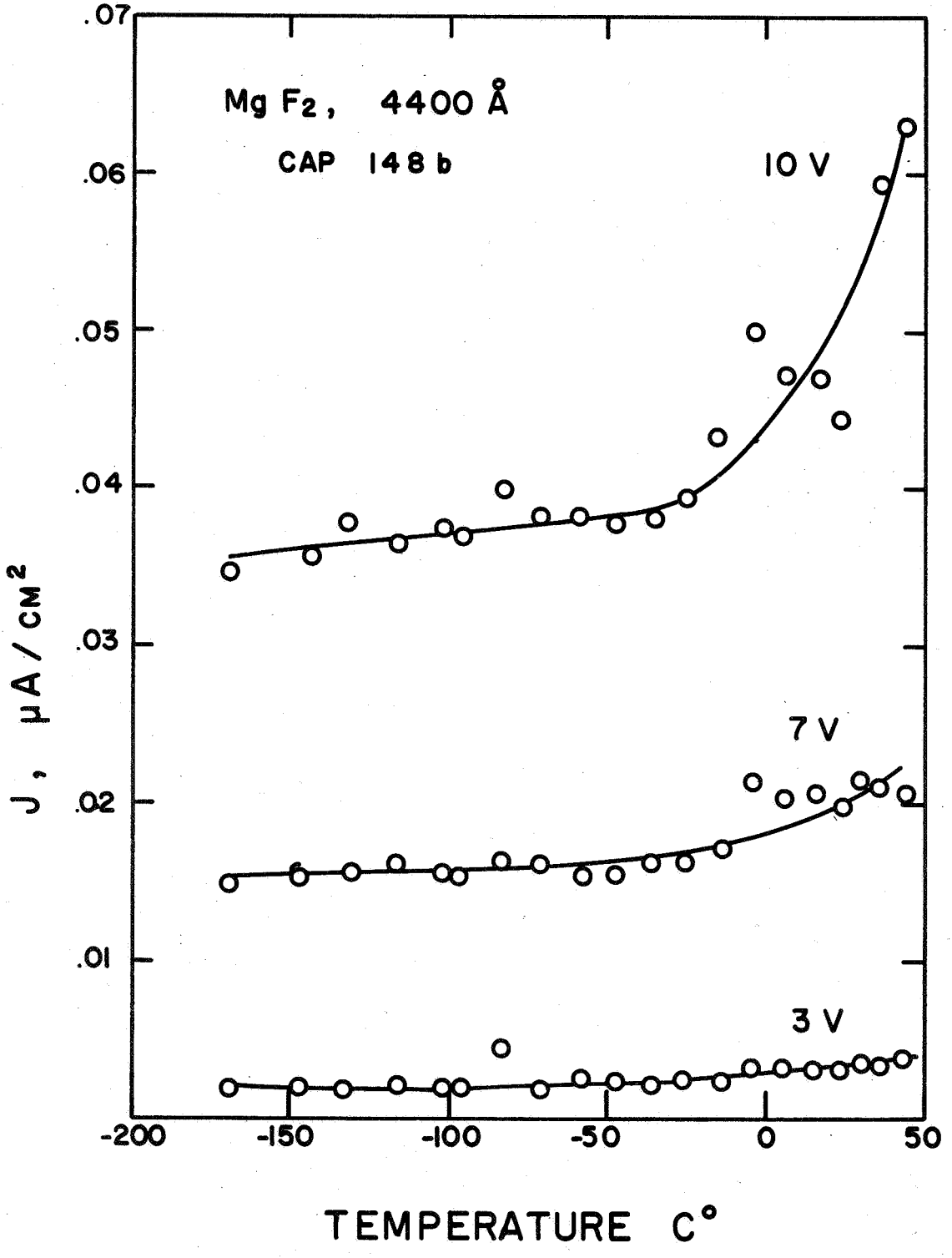

Fig. 19. Current density vs temperature curves at constant voltage for Al-MgF_2-Al capacitor 148b.

prebreakdown conductances in SiO capacitors could not be correlated to breakdown thresholds. Further, the strong temperature dependence of prebreakdown conductivity occurs with breakdown thresholds that are almost temperature independent.

c. Carrier type.

When dc voltages were applied for long periods to an SiO capacitor (7 volts) and to an MgF_2 capacitor (10 volts), the former showed no appreciable change in the current even after a week. The latter, however, changed as shown in Fig. 20. After an initial rise, the current dropped and then rose for a brief period, and then decreased monotonically (but not exponentially) with time. After 8 days the current reading was determined by the resistance of the shunting voltmeter rather than by the capacitor. Neither the SiO nor the MgF_2 capacitor seemed to be damaged by its long electrical stress. From these measurements it is concluded that the conductivity in SiO is electronic in nature, while the conductivity in MgF_2 is of an ionic nature. The conductivity in MgF_2 probably becomes very small because the system ceases to conduct as the ions are swept to one side of the dielectric.

d. Local Conductance.

In preliminary measurements, it has been found that there are local current fluctuations of great magnitude when a biased probe is dragged across a dielectric backed by a counter electrode. Subsequent microscopic examination of the regions of high conductance showed them to be the sites of small imperfections in the films, having diameters of about one micron. No details could be resolved within these small imperfections, so it is not known whether the probe was making direct metallic contact with the lower electrode. It is planned to refine these experiments to obtain an adequate description of the conducting channels and to determine whether these may be correlated to forming or to breakdown.

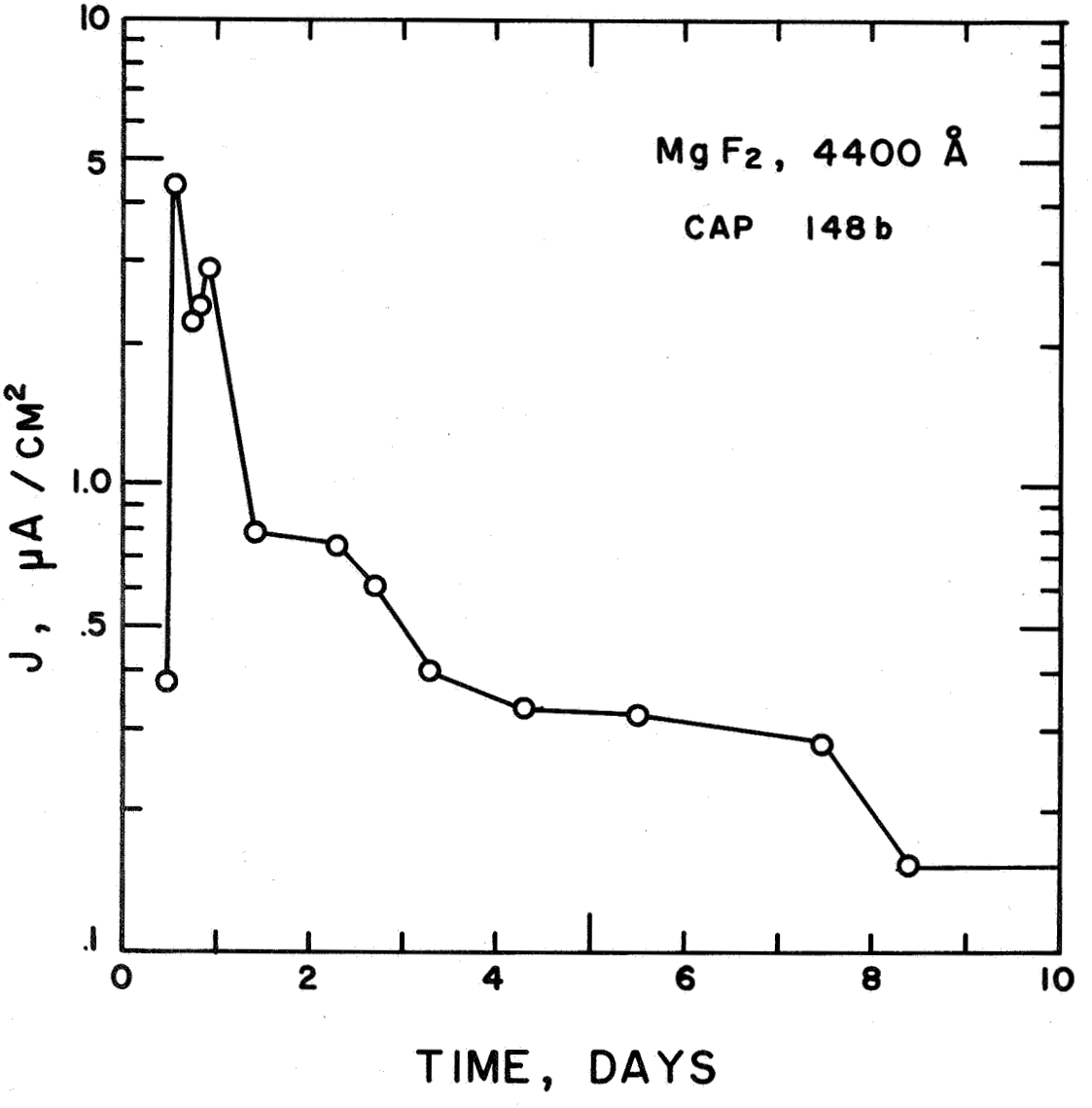

Fig. 20. Dc current-time characteristic at constant voltage for Al-MgF_2-Al capacitor 148b.

2. Breakdown.

a. Threshold for the onset of breakdown.

Figure 21 shows the voltage waveforms when ramps are applied to capacitors of each of the materials studied. The ramps are continued after the occurrence of the first breakdown so that many breakdowns occur. All of the figures illustrate the existence of a threshold for the cessation of breakdown V_{min}. However, in the SiO and the CaF_2 waveforms, the voltage for the onset of breakdown for successive breakdowns usually increases with time. In the other waveforms, successive breakdowns occur at essentially the same voltage as the initial breakdown.

In measuring the threshold for the onset of breakdown V_{max}, the voltage of the first breakdown in a given ramp is used. This has been found to be reproducible for a wide range of ramp speeds even in SiO and CaF_2. Figure 22 shows the temperature dependence of F_{max} (F_{max} is the ratio of V_{max} to the dielectric thickness w) for each of the materials. Temperature data has not yet been obtained on Teflon.

Figure 22 indicates there is virtually no temperature dependence in F_{max} in SiO and in MgF_2, in contrast to their widely different prebreakdown I-V-T characteristics (see Figs. 18 and 19). The temperature dependence of F_{max} found in each of the other materials (Teflon was not measured) is small and does not seem to correlate in any way with the dc I-V-T curves or the impedance data. Thus, the conclusion formed in the SiO study[3] of the independence of F_{max} and prebreakdown conduction seems to be true in all of the materials studied.

Figures 23-25 show the thickness dependence of F_{max}. Figures 26-28 show the thickness dependence of V_{max}. Figures 23-25 also contain lines of slope $-\frac{1}{2}$ representing the fit of the data to the theory of Forlani and Minnaja.[15]

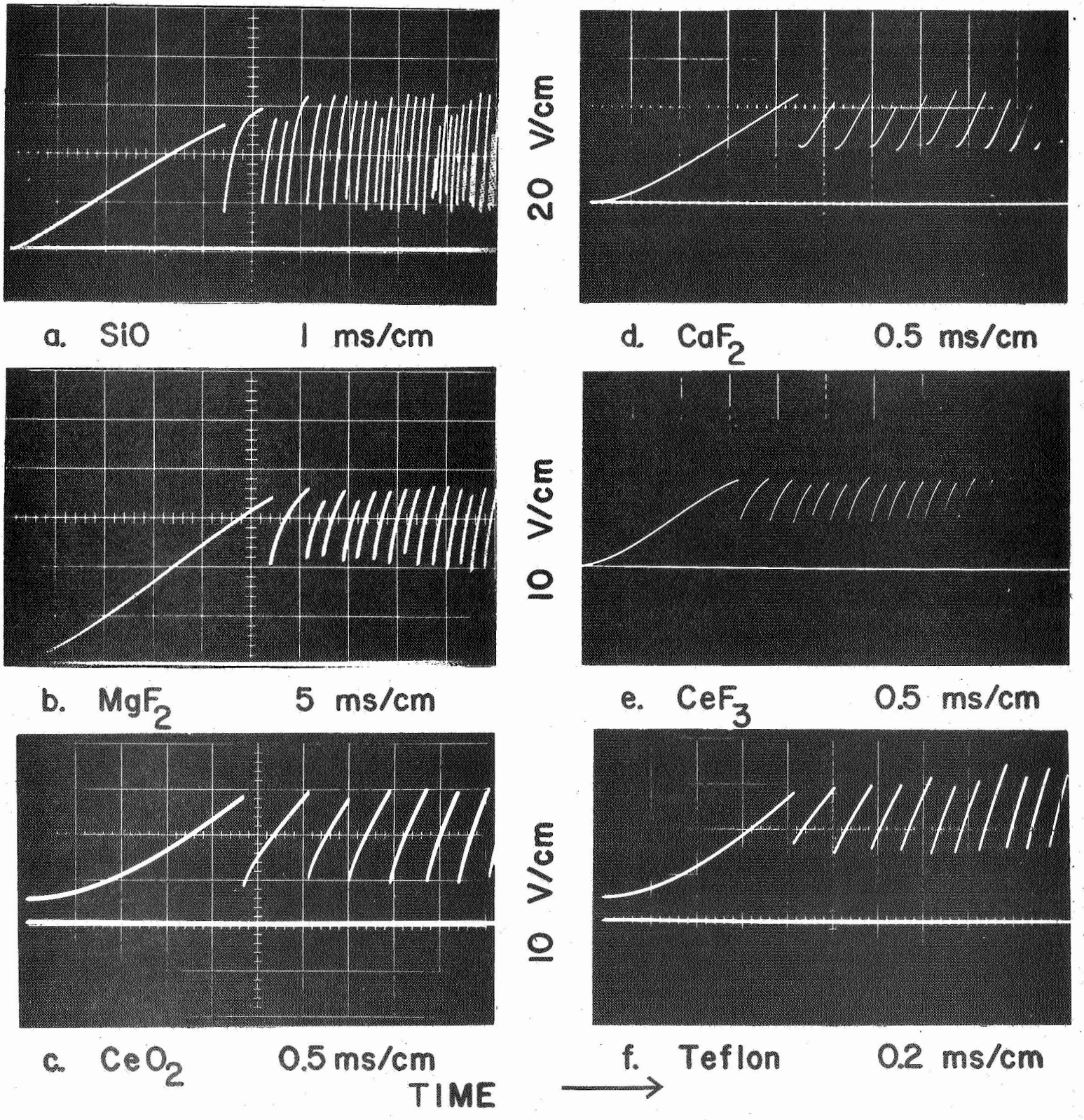

Fig. 21. Breakdown waveforms showing the applied ramp voltage and repeated breakdowns. The voltages V_{max} and V_{min} are indicated. (a) SiO. (b) MgF_2. (c) CeO_2. (d) CaF_2. (e) CeF_3. (f) Teflon.

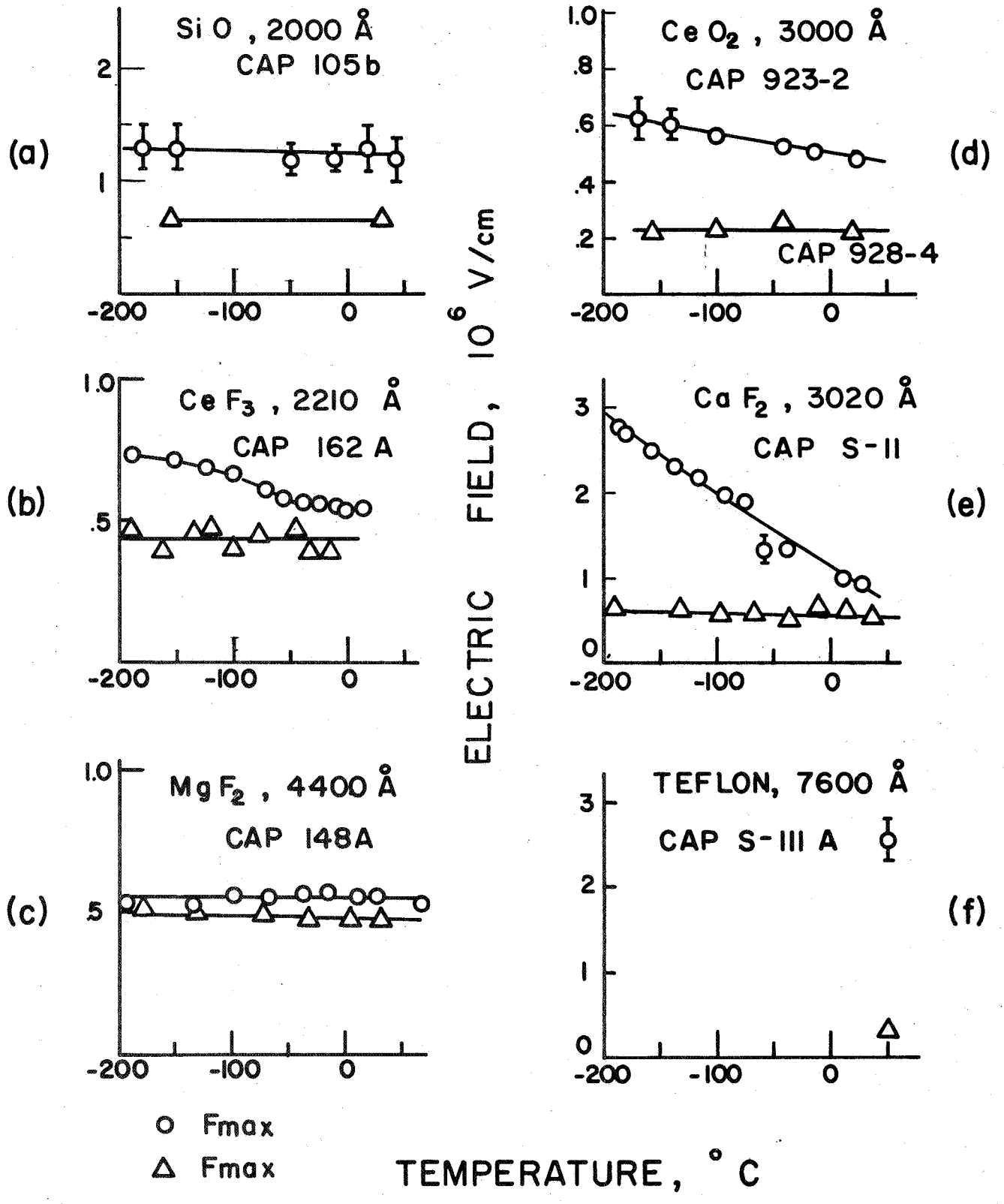

Fig. 22. F_{max} vs temperature. (a) SiO. (b) CeF_3. (c) MgF_2. (d) CeO_2. (e) CaF_2. (f) Teflon.

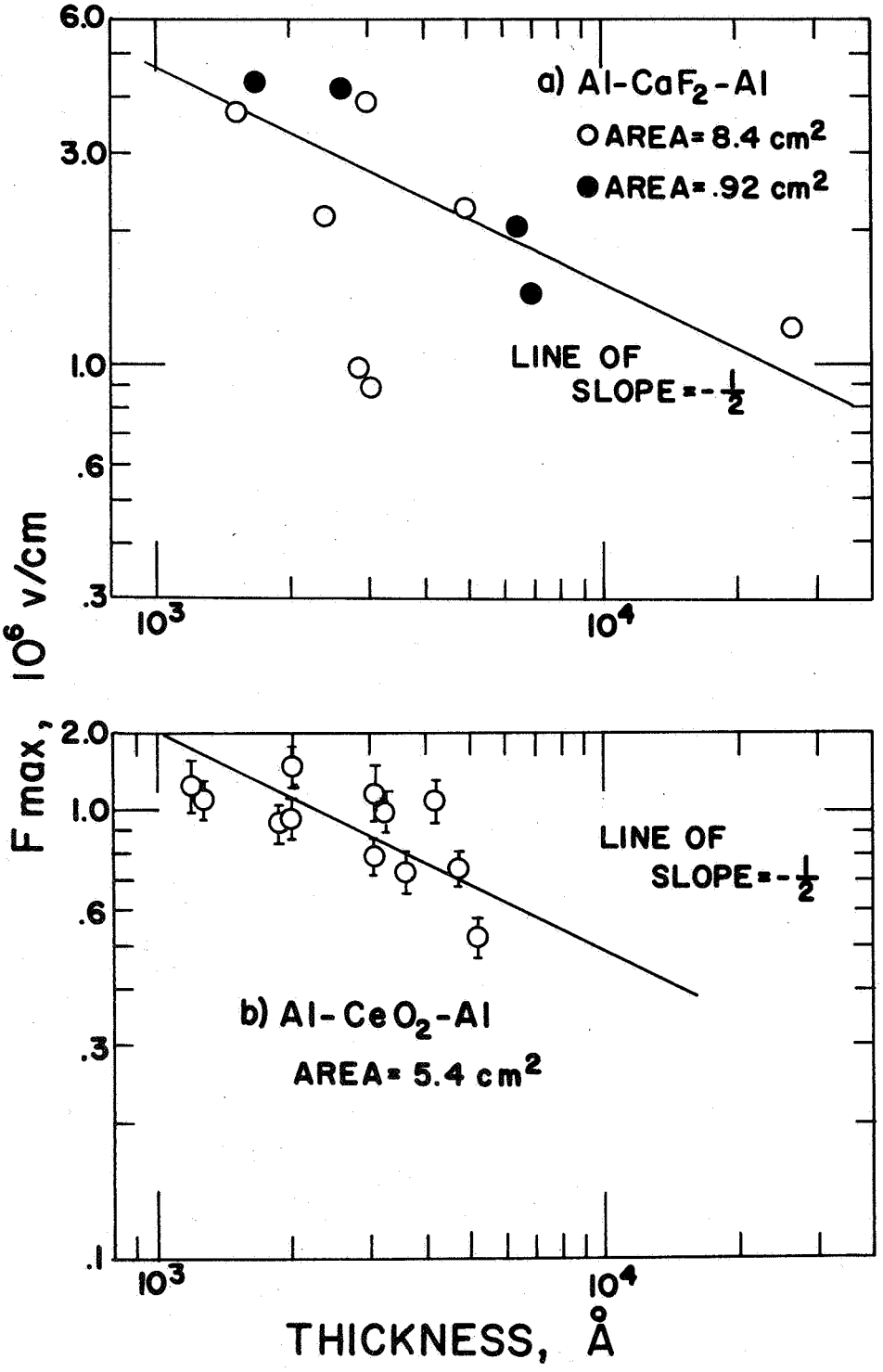

Fig. 23. F_{max} vs dielectric thickness for CaF_2 and CeO_2 capacitors.

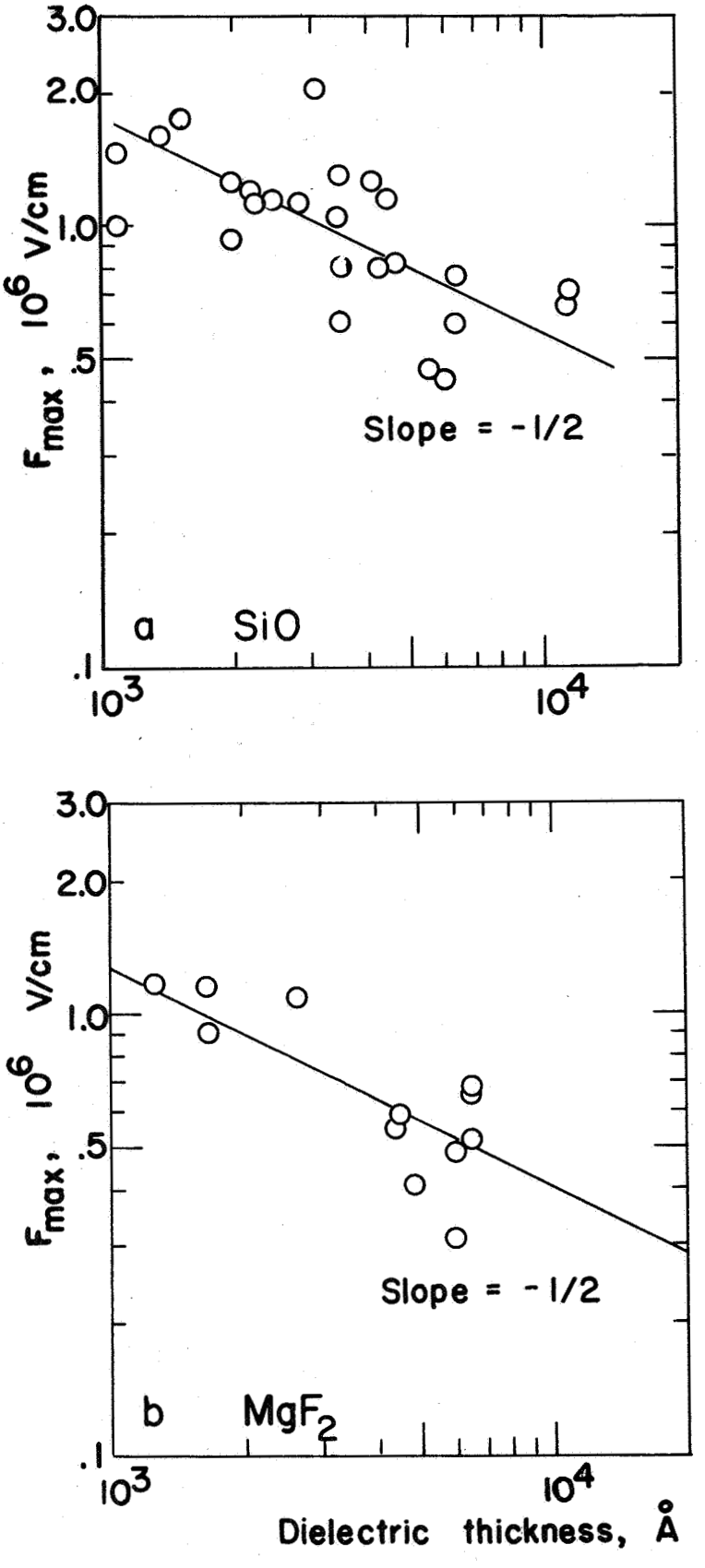

Fig. 24. F_{max} vs dielectric thickness for SiO and MgF_2 capacitors.

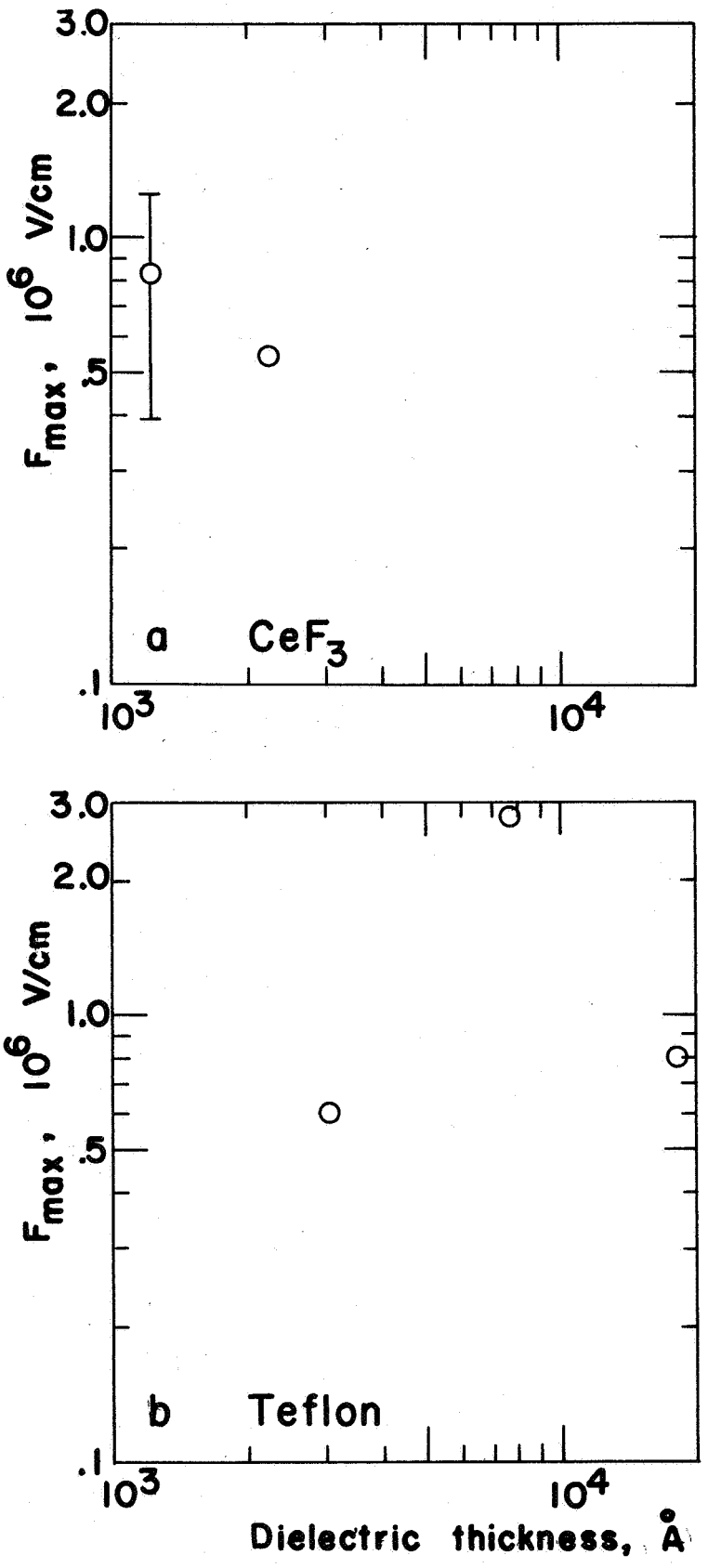

Fig. 25. F_{max} vs dielectric thickness for CeF_3 and Teflon capacitors.

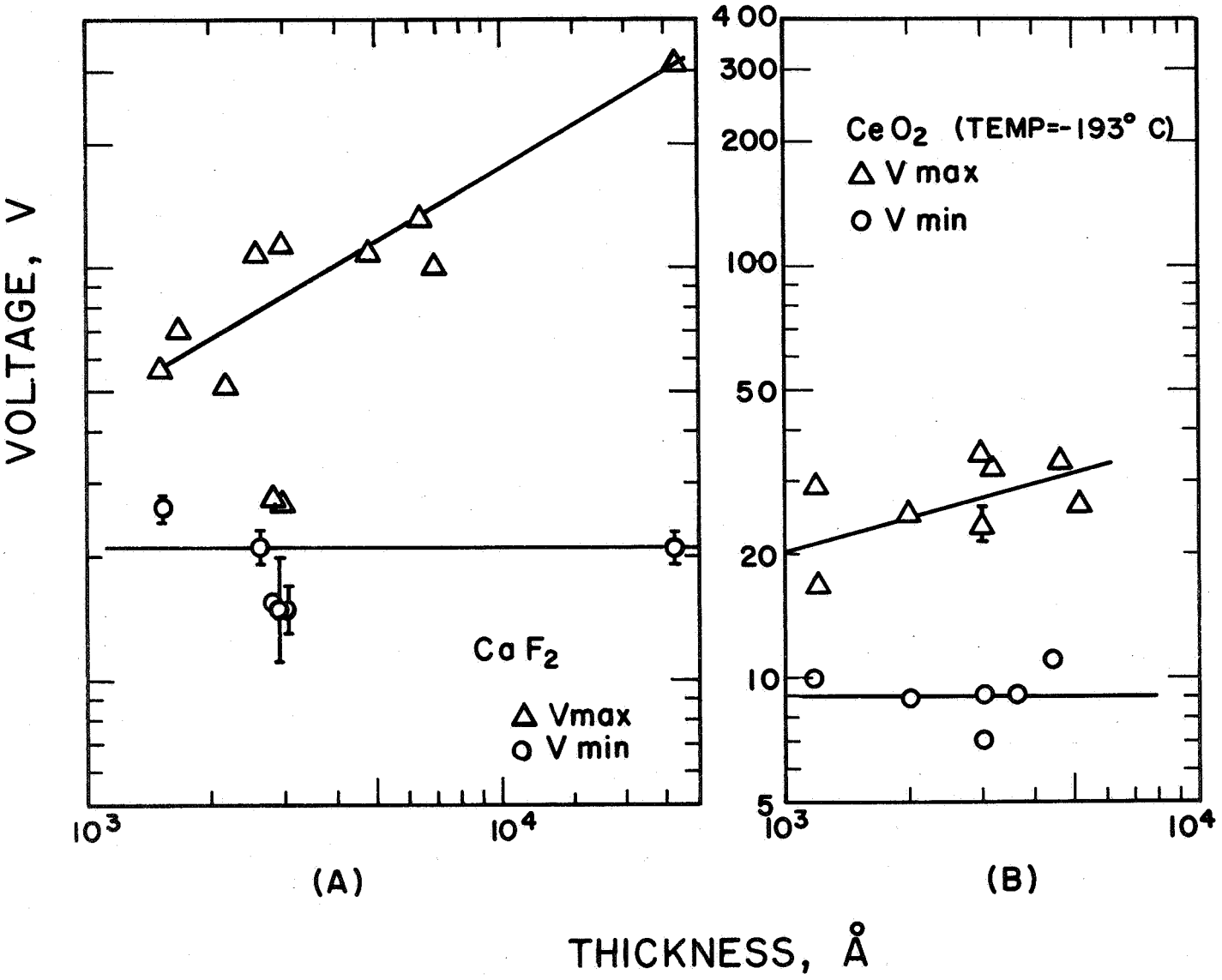

Fig. 26. V_{max} and V_{min} vs dielectric thickness for CaF_2 and CeO_2 capacitors.

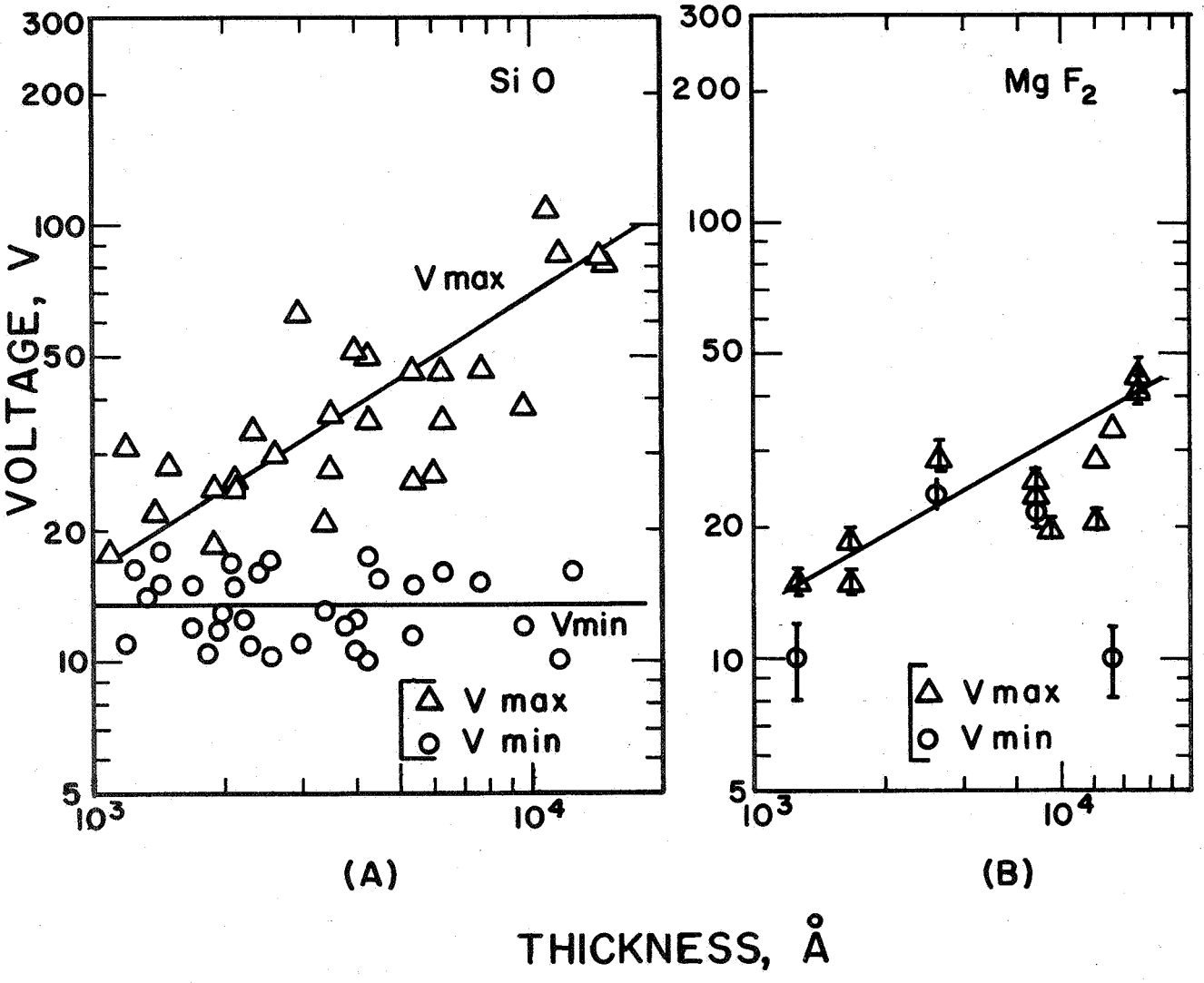

Fig. 27. V_{max} and V_{min} vs dielectric thickness for SiO and MgF_2 capacitors.

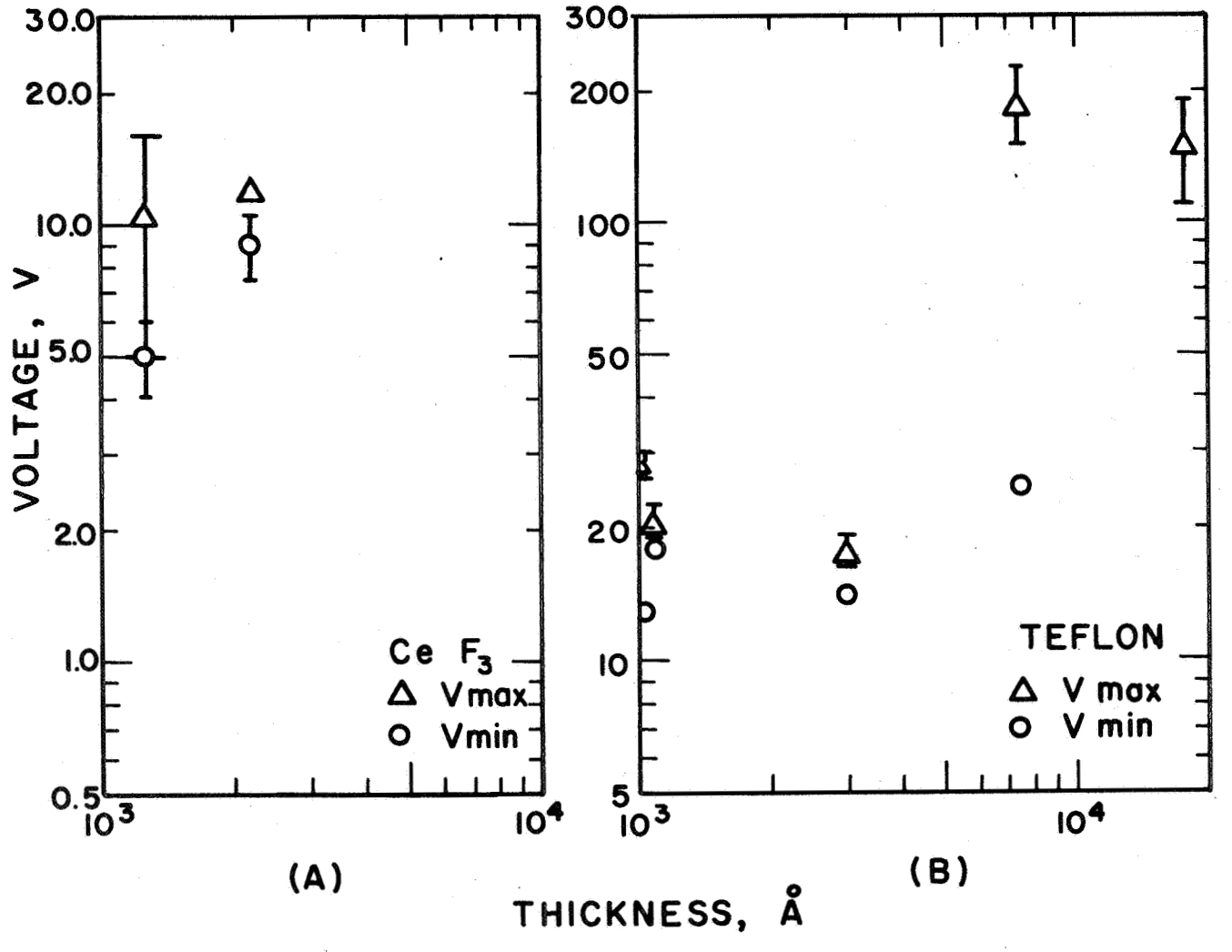

Fig. 28. V_{max} and V_{min} vs dielectric thickness for CeF_3 and Teflon capacitors.

O'Dwyer's theory[13] contains several parameters which are chosen to give a "best" fit to the thickness data (see Table 6).

b. Threshold for the cessation of breakdown.

The existence of the threshold for the cessation of breakdown V_{min} for each of the materials studied has been shown in Fig. 21. In Figs. 26, 27, and 28, where V_{min} is plotted for different capacitors as a function of thickness, it is seen that V_{min} does not vary with thickness of the dielectric. For a given capacitor, it is found that V_{min} and, hence, F_{min} (F_{min} is the ratio of V_{min} to the dielectric thickness w) are independent of the temperature. This is shown in Fig. 22. The fact that V_{min}, and <u>not</u> F_{min}, is thickness independent has been interpreted to mean that the field must be inhomogeneous in the conducting portion at the end of breakdown.[3] Thus the data on a variety of materials has again given essentially the same result as was found in SiO.

c. Effect of ramp speed on V_{max} at different temperatures.

The threshold for the onset of breakdown gradually increases as the rate of rise of the applied voltage increases. As is discussed further in Section IV, this is believed to arise from the build-up of a space charge in the dielectric. The space charge causes the field in the dielectric to be inhomogeneous.

One mechanism for producing a space charge in ionic crystalline materials is through the motion of ions in the presence of the applied electrid field (see Section IV.B). Since ionic motion is thermally activated, with an activation energy of about 0.1 eV, this motion should be greatly reduced at 80°K compared to its magnitude at 300°K. Hence the breakdown threshold was measured at about 80°K and at room temperature for ramps having different rise rates. Results for CaF_2 are shown in Fig. 29. If the field inhomogeniety were due to ionic motion, then at the lower temperature, where there would be virtually no ionic motion regardless of the ramp rise rate, the breakdown voltage would be

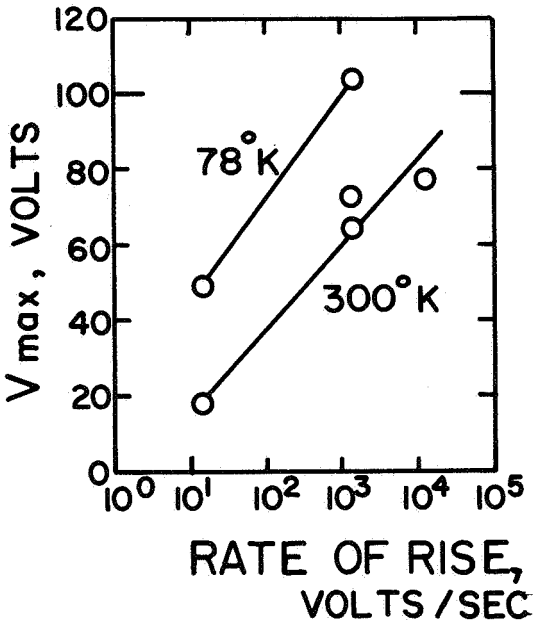

Fig. 29. Breakdown voltage V_{max} vs ramp rise rate for CaF_2 capacitors at 78°K and 300°K.

independent of the ramp rise rate. At the upper temperature, where the ionic motion could occur, there would be a rise in breakdown voltage with increasing rise rate. Figure 29 shows there is no significant difference in the shapes of the curves at low and high temperatures. Hence, it appears the field inhomogeneity is not connected with thermally activated ionic charges or other thermal processes.

d. Voltage waveforms during breakdown.

The start of breakdown conduction is very abrupt according to oscillograms of the voltage waveform (see fig. 30). In a time that may be less than 10 nanoseconds, the limit of resolution of the recording equipment, the conductance in the breakdown site probably changes by a factor around 10^{10} and remains at this value until the voltage falls to, or nearly to V_{min}. Sometimes there is a break in the waveform close to V_{min} indicating a decrease by a factor of 10 to 100 in the conductance. If the time constant of the external circuit is sufficiently small, then appreciable energy can be fed into the capacitor during the interval of breakdown conduction. In our experiments, this was avoided. The end of breakdown is believed to occur when the capacitor begins to charge up with a time constant determined by the capacitance of the capacitor (which is virtually unchanged by a single breakdown) and the external load resistance of the charging circuit (the leakage resistance of the capacitor prior to breakdown is usually large compared to the external load resistance).

Breakdown voltage waveforms have been studied in several series of Al-SiO-Al capacitors deposited simultaneously, but of different areas (see Fig. 7 for the capacitor configurations). From these waveforms the time constant during the breakdown is computed. If the capacitance is measured, then the resistance during breakdown can be computed. The waveform determines the value of V_{max} and V_{min}. Hence the energy dissipated during the breakdown can be evaluated

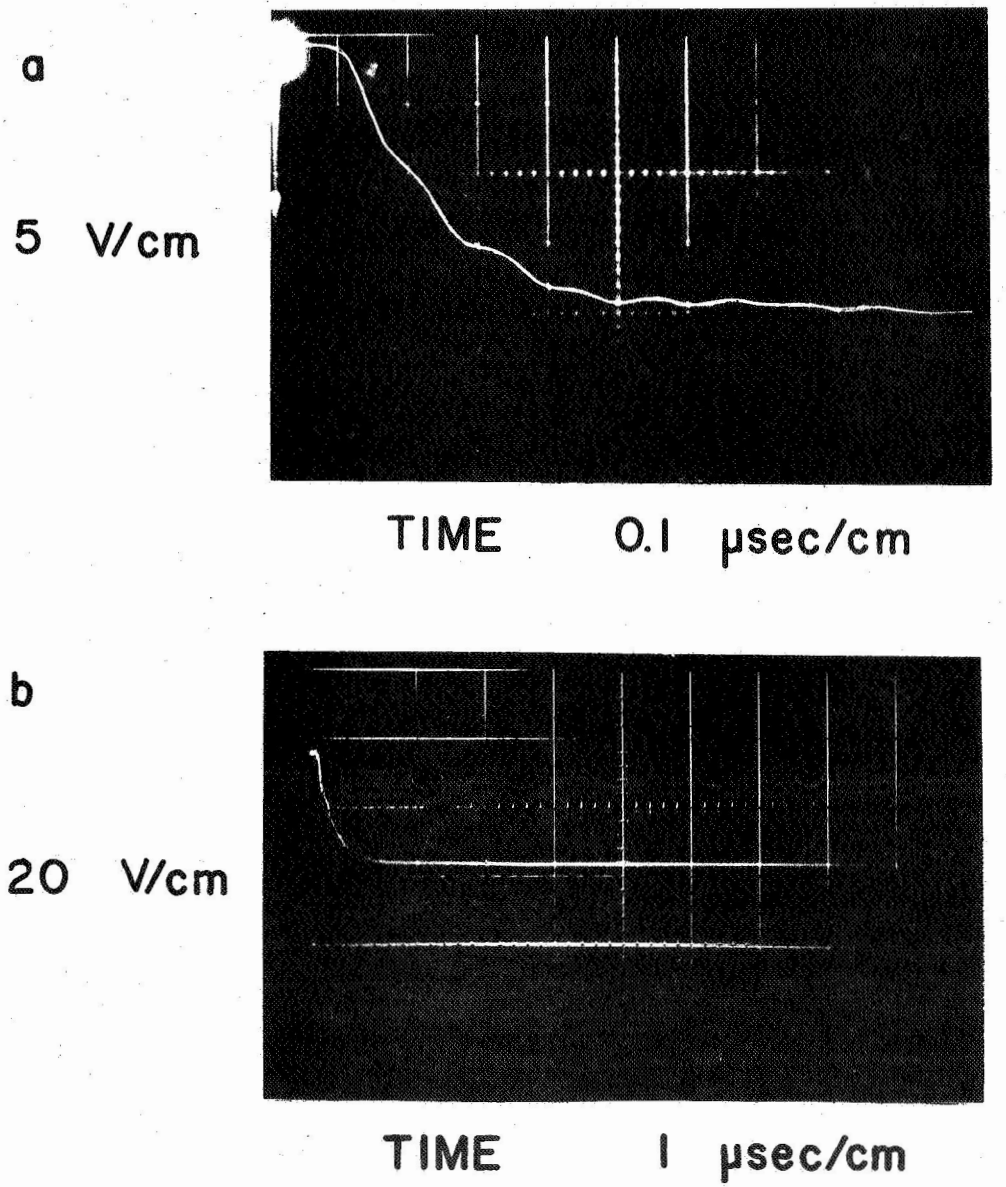

Fig. 30. Oscillograms showing voltage waveforms of breakdowns in Al-SiO-Al capacitors. (a) Sweep rate 0.1 μsec/cm. (b) Sweep rate 1 μsec/cm.

from the relation

$$\Delta W = \tfrac{1}{2} C (V_{max}^2 - V_{min}^2) .$$

This assumes there is no energy added from the external circuit during the breakdown. Microscopic examination of the breakdown sites have been made (see Fig. 31) wherein both the outer diameter and the size of the central area of destruction have been measured.

Measurements on a set of capacitors simultaneously deposited are summarized in Table 5. The capacitors are Al-SiO-Al with a dielectric thickness of $4.08 \pm .02) \times 10^3$ Å. Ac measurements were at 1000 Hz and breakdown measurements were taken with a ramp rise rate of 3×10^4 V/sec. Column 1 identifies each capacitor with a number, Column 2 gives the plate area A, Column 3 the capacitance C, Column 4 the dissipation factor D, Column 5 the capacitance per unit area C/A, Column 6 the resistance in the charging circuit R_{ex}, Column 7 the time constant of the charging circuit prior to the onset of breakdown τ_p, Column 8 the time Δt for the voltage to fall from V_{max} to V_{min}, Column 9 the value of V_{max}, Column 10 the value of V_{min}, Column 11 the time constant during breakdown conduction τ_b, Column 12 the resistance of the capacitor during breakdown R_b, Column 13 the outside diameter OD of individual breakdown sites, Column 14 the diameter of the central CD region of complete destruction of a breakdown, Column 15 the ratio of the area of the central region of complete destruction to the entire area of a single breakdown A_C/A_B, and Column 16 the average energy ΔW dissipated in a single breakdown.

Figure 32 displays data from Table 5 in a graphical form. Where error bars are not shown, the experimental uncertainty is within the circle or triangle about the plotted point. Figure 32a shows that the capacitance varies linearly with area A, thus indicating that the average dielectric thickness and the average of the real part of the dielectric constant is the same for all of the

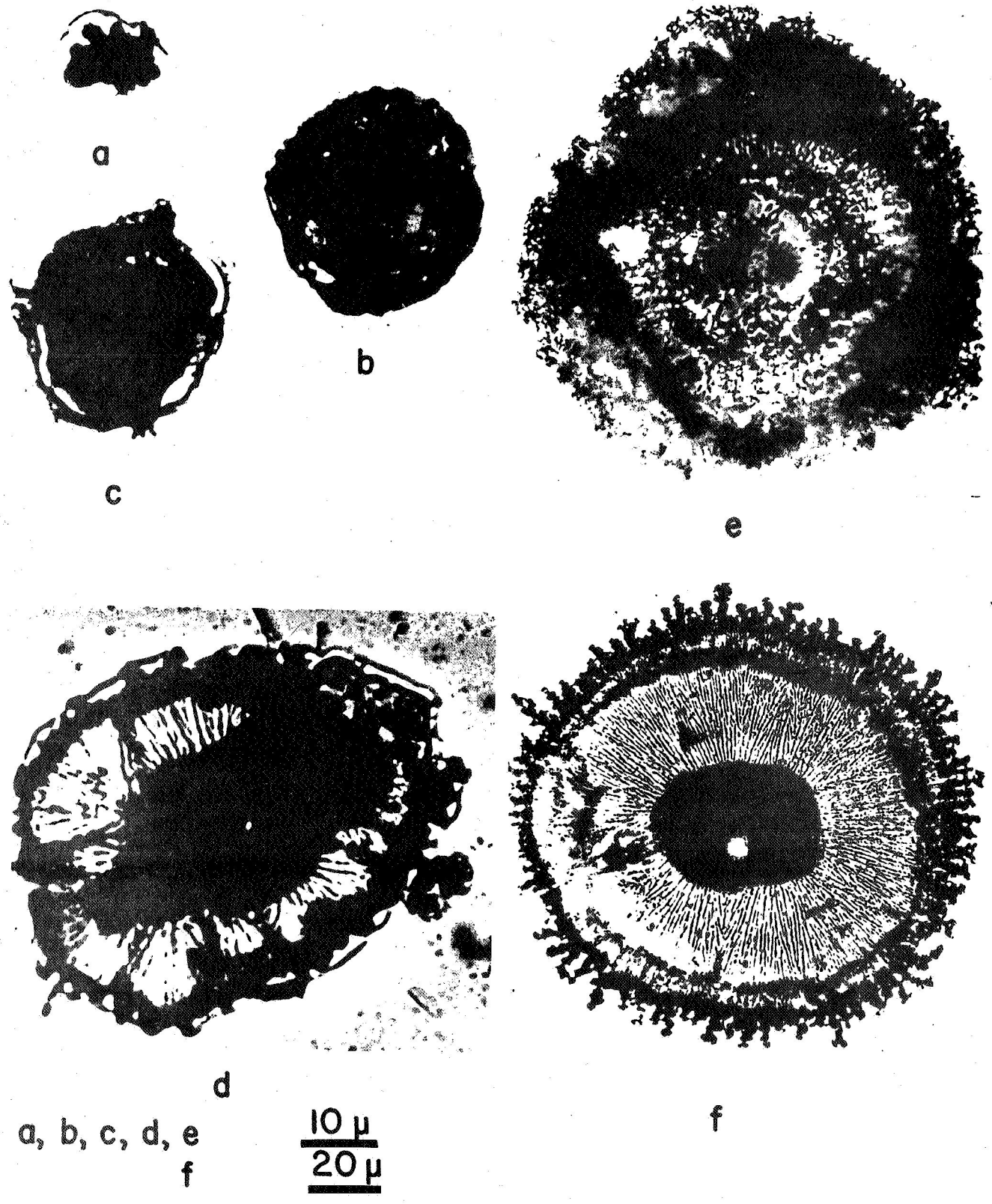

Fig. 31. Photographs of breakdowns of capacitors simultaneously deposited, but of different electrode areas. The central region of destruction remains about the same in size as the plate area increases. However, the outer diameter of the breakdown increases as the plate area increases. The photographs are ordered according to increasing plate areas in going from a to f. Relevant numerical data are given in Table 5.

Table 5. Breakdown characteristics as a function of capacitor area in simultaneously deposited Al-SiO-Al capacitors (Thickness: $(4.08 \pm .02)\ 10^3$ Å, Ramp rise rate: 3×10^4 V/sec).

1 Cap. No.	2 Area (cm^2)	3 C (F)	4 D	5 C/A F/cm^2	6 R_{ex} (Ohms)
1	.064	0.773×10^{-9}	.068	12.1×10^{-9}	2×10^4
2	.45	5.920	.044	13.1	2
3	.65	8.163	.036	12.6	2
4	1.11	14.50	.060	13.1	.5
5	3.23	40.91	.051	12.7	.5
6	6.68	85.90	.050	12.8	.5

Cap. No.	7 τ_p (sec)	8 Δt (sec)	9 V_{max} (Volts)	10 V_{min} (Volts)	11 τ_b (sec)
1	16×10^{-6}	$(.046 \pm .002) \times 10^{-6}$	81 ± 1	15 ± 2	$(1.2 \pm .1) \times 10^{-7}$
2	119	$(.06 \pm .01)$	51 ± 1	14 ± 2	$(2.4 \pm .7)$
3	161	$(.05 \pm .01)$	$49.5 \pm .4$	14 ± 2	$(2.3 \pm .6)$
4	73	$(.10 \pm .02)$	53 ± 1	14 ± 2	$(3.3 \pm .9)$
5	205	$(.80 \pm .02$	$38.2 \pm .3$	15 ± 2	(21 ± 3)
6	428	$(1.10 \pm .04)$	$38.1 \pm .6$	15 ± 2	(35 ± 5)

Cap. No.	12 R_b (ohms)	13 O.D. (Microns)	14 C.D. (Microns)	15 A_C/A_B	16 ΔW (J)
1	$(1.6 \pm .2) \times 10^2$	20 ± 3	13 ± 1	$.4 \pm .1$	2.4×10^{-6}
2	$(.4 \pm .1) \times 10^2$	42 ± 6	27 ± 1	$.4 \pm .1$	7.1
3	$(28 \pm 8) \times 10^0$	41 ± 1	27 ± 2	$.45 \pm .08$	9.4
4	$(23 \pm 6) \times 10^0$	41 ± 2	20 ± 3	$.25 \pm .08$	20
5	$(51 \pm 6) \times 10^0$	95 ± 4	43 ± 4	$.21 \pm .07$	26
6	$(41 \pm 6) \times 10^0$	108 ± 1	34 ± 2	$.098 \pm .003$	54

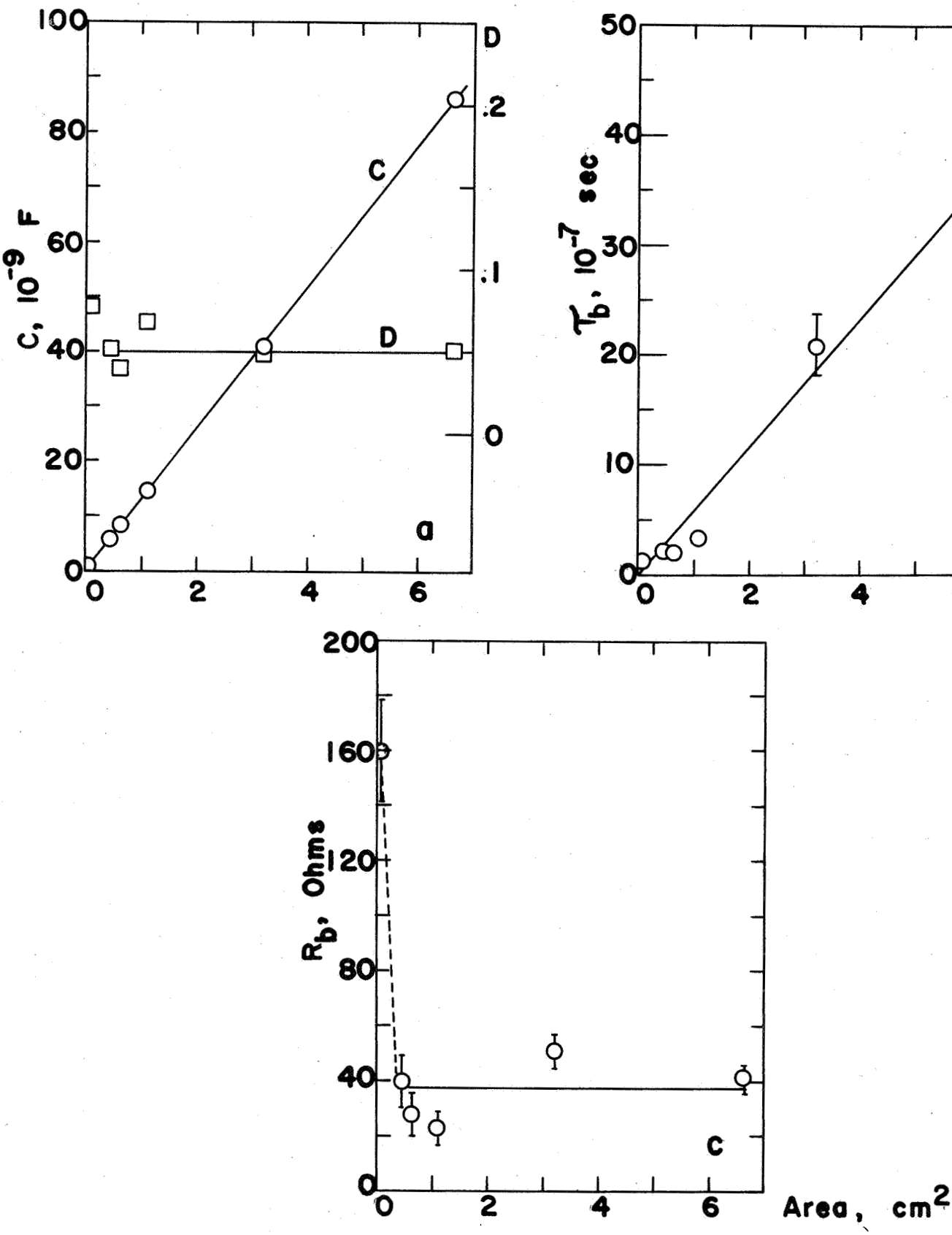

Fig. 32. Comparison of breakdowns in Al-SiO-Al capacitors simultaneously deposited but of different plate areas. Dielectric thickness is (4.08 ± .02) 10^3 Å. (a) Capacitance C and dissipation factor D vs area A. (b) Time constant τ_b during breakdown vs A. (c) Resistance during breakdown R_b vs A.

capacitors. The dissipation factor is very nearly the same for all six capacitors. Figure 32b shows that the time constant during breakdown (computed from the relation $\tau_b = \frac{\Delta t}{\ln \frac{V_{max}}{V_{min}}}$ varies linearly with A. Figure 32c indicates that the resistance during breakdown R_b (R_b is defined as τ_b/C) is about 40 ohms for all capacitors but the smallest one. The smallest one, which also has a very high value of V_{max}, has a resistance of about 160 ohms.

Figure 33 continues the analysis of the areal comparison. In Fig. 33a there is a significant rise in V_{max} as the area becomes smaller. The values of V_{min}, however, are independent of capacitor area. Figure 33b shows that the size of a breakdown tends to increase with area, but the region of high destruction in the center increases in size more slowly than does the outer region. Figure 33c indicates the energy dissipated in a breakdown increases approximately as the capacitor area, but there are deviations for small capacitors because of the high value of V_{max} for these. Finally in Fig. 33d the areal ratio A_C/A_B indicates that the central region of destruction becomes a smaller and smaller part of the average breakdown site as capacitor area (and capacitor energy) increases.

It is concluded from the above that the central region of a breakdown plays a more basic role in breakdown conduction than does the outer region. It is very tempting to associate the major aspects of breakdown conduction with this central region, i.e., the rapid onset of breakdown conduction, the constancy of the resistance during breakdown and the constant value of V_{min}. This interpretation is strengthened by the results of the spectrographic study and of the topography of breakdowns (see Sections III.B and III.C).

The higher values of V_{max} for the very small capacitors is not understood. The obvious explanation that there are few weak spots because the area is small

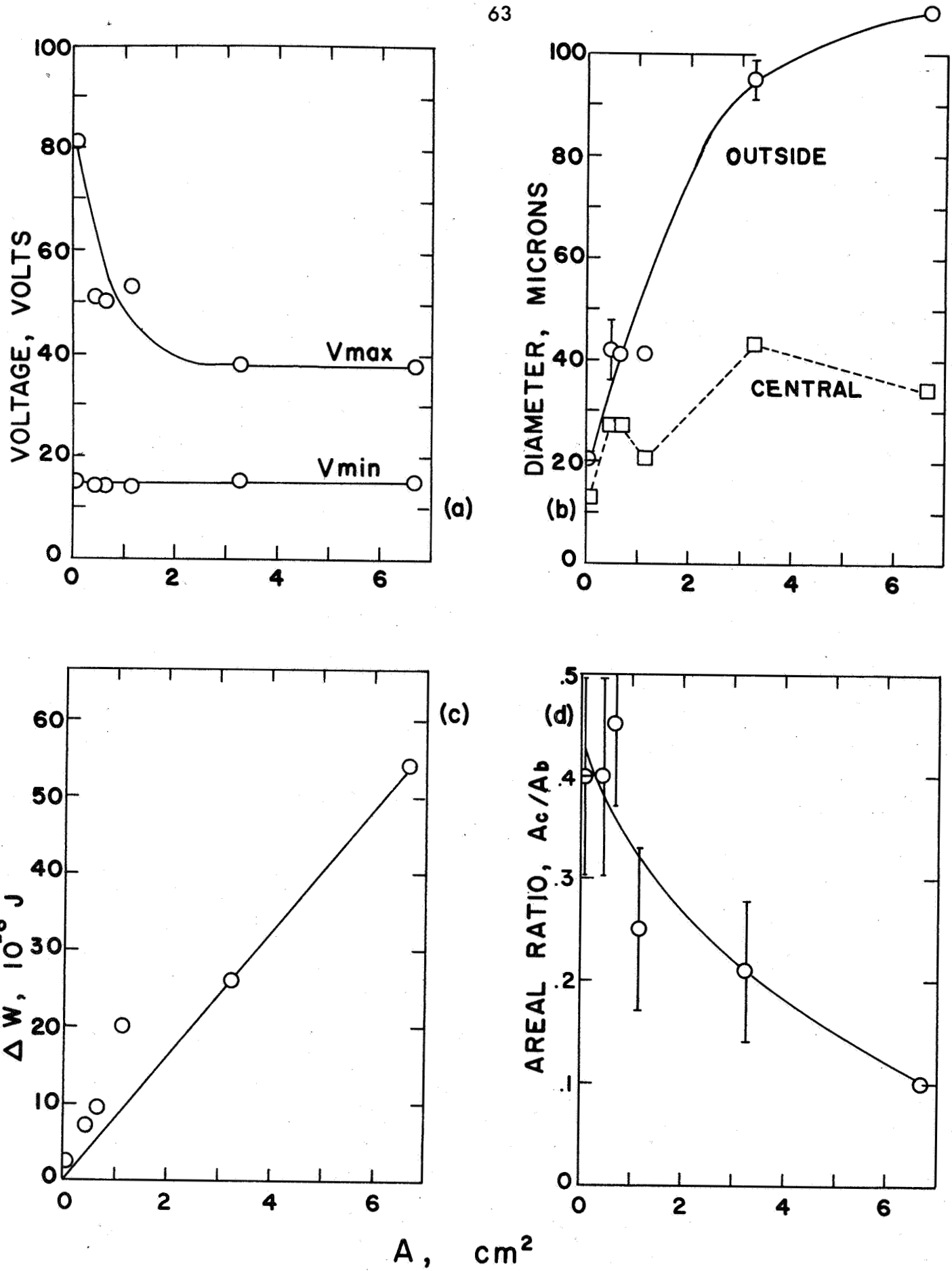

Fig. 33. Continuation of the areal comparisons started in Fig. 32. (a) V_{max} and V_{min} vs A. (b) Outside and central diameters of breakdown sites vs A. (c) Energy dissipated per breakdown vs A. (d) Areal ratio of the central region to the total breakdown area A_c/A_b vs A.

does not seem to hold up to close examination. In larger capacitors, where V_{max} is consistent in value, there are breakdowns spaced much closer than the linear dimensions of the smallest capacitor of the areal study. Hence, it is difficult to understand the absence of the low threshold breakdowns in small area capacitors. It should be noted, however, that the higher values of V_{max} for capacitors of small plate area has been observed repeatedly.

B. OPTICAL SPECTROSCOPY OF BREAKDOWNS

1. Spectra.

Spectrographic studies have been concentrated on Al-SiO-Al capacitors, but some tests have been made with Al-SiO-Cu and Al-SiO-Ni capacitors. The capacitor area was 0.24 cm^2. In every case, line spectra are observed with the same set of lines as are found in the arc spectra of the materials involved. Thus lines of Al and Si, of Al, Si and Cu, and of Al, Si, and Ni are found in the cases mentioned above. (No lines of oxygen were observed, but this is probably because oxygen has no strong lines in the region between 2000 Å and 4500 Å where our measurements were made.) Figure 10 is a tracing of the spectrum observed from breakdowns in Al-SiO-Al capacitors. Table 2 lists the wavelengths, the element emitting each line, and the ionization state of the emitting atom or ion. Most of the lines arise from singly ionized atoms, but some originate from both neutrals and doubly ionized atoms. In those cases where different electrode materials were used in a single capacitor, the spectra of both materials were obtained in every breakdown regardless of the polarity.

It is significant to recall that there is very little continuous spectral background. The presence of the line spectra and the lack of the continuous background indicate the emitting atoms were in a gaseous or plasma state during emission. Further, they were highly excited since the radiation is strong in the ultraviolet.

2. Time-resolved spectroscopy.

Waveforms of the light emitted by electrode atoms and by dielectric atoms in various stages of ionization were examined and related to the voltage waveform. Waveforms are shown in Figs. 12, 34 and 35. The conclusions reached upon study of the light and voltage waveforms are here listed.

i. Prior to the onset of breakdown, as indicated by the voltage waveform, there is no light emission. Thus the light emission is not an ordinary electroluminescent effect. Electroluminescence is normally characterized by a relatively continuous spectrum.[19, 20] Destruction does not accompany electroluminescence.

ii. The waveforms of all the spectral lines are about the same. No distinguishing characteristics have been found to identify the origin of a line from its waveform. (The rise times of the Si lines appear to be very slightly faster than the rise times of the Al lines.)

iii. Light output, for all lines, starts when the voltage waveform indicates breakdown conduction has started.

iv. The light output rises rapidly during the time that the voltage is falling rapidly. However, there are indications that the light occurs in bursts during this rise (see Fig. 34 and the discussion below). The rise time is about 30 nanoseconds.

v. The light intensity falls off gradually, reaching a value about 0.1 of its peak intensity after about 5 μsec from the start of the breakdown. The intensity does not fall to zero for perhaps another 50 μsec. This pattern corresponds roughly to that of the voltage waveform. The abrupt drop in the voltage initially to a value several volts away from V_{min} is followed by a relatively slow approach to V_{min}.

vi. The light output has the same spectral distribution and intensity

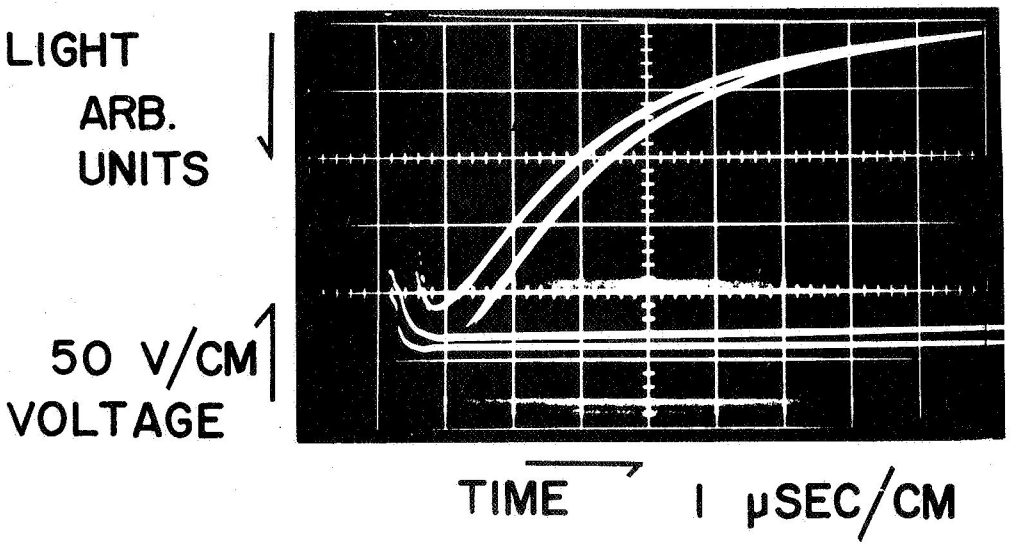

Fig. 34. Light intensity and voltage waveforms from breakdown in Al-SiO-Al capacitors showing the bursts of light during the rapidly rising portion of the light intensity signal (Al line, λ = 3961 Å).

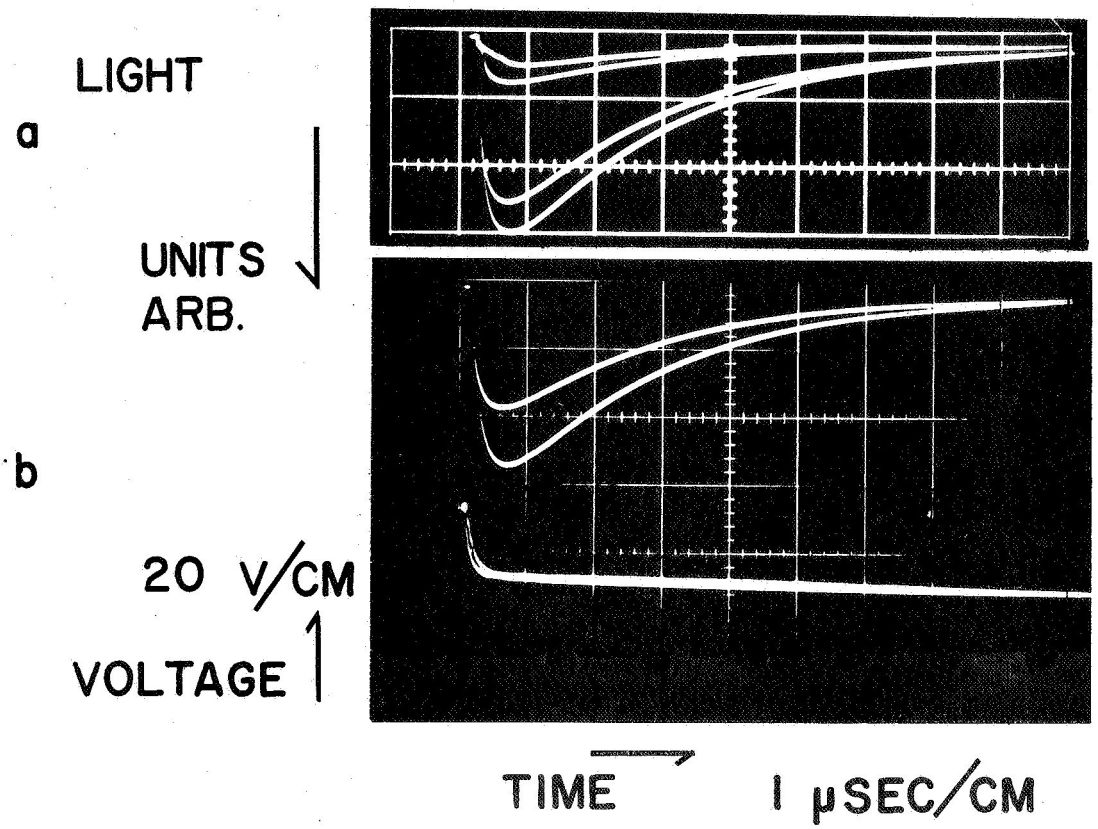

Fig. 35. Light intensity and voltage waveforms emitted by aluminum atoms in two states of ionization. (a) Neutral atoms, λ = 2570 Å. (b) Singly ionized atoms, λ = 3961 Å.

distribution when the polarity is reversed. Thus light from both electrodes and from the dielectric appears from the very beginning of the breakdown regardless of the polarity.

vii. By measuring the area under the light waveforms and using the known geometry of the system, it is estimated that about 10^7 decays of excitation are needed to account for the total light output at a single wavelength during the first 5 μsec of a breakdown. This corresponds to an average decay rate of about 2×10^{12} decays per second and a peak decay rate of about 2×10^{13} decays per second. With the assumption that the central area of destruction is completely converted into a plasma, it is estimated that light emission occurs from about 0.1% of the atoms in the plasma.

Examination of the light waveforms reveals, for some breakdowns, a modulation in the intensity during the initial rising portion (see Fig. 34). This means there has been a burst of light followed by short period where the excitation decays, then another burst and another decay period, and so forth. (The decay time is of the order of 10^{-9} to 10^{-8} sec for strong spectral lines in the ultraviolet.[21]) In a given rise there may be as many as half a dozen bursts.

The relatively slow fall off of the light intensity after its peak seems somewhat in contradiction to the abrupt change in slope seen in the voltage waveform at the end of the initial rapid drop in voltage. This slow fall off cannot be explained by the time required for decay from an excited state because such decay occurs about two order of magnitudes too rapidly. A possible explanation of the long tail is that it is due to the time it takes for recombination of an electron and an ion to form an excited neutral or an excited ion having less ionization. From Table 2 it is seen that most of the observed lines are from singly ionized atoms, and just a few are from doubly ionized or neutral

atoms. If recombination time is significant, then the waveforms of the lines of the neutral atoms rise relatively slowly and fall relatively slowly compared with the waveforms of the ionic spectral lines. Figure 35 shows waveforms for the two cases. It is seen that the shapes are about the same and, hence, recombination is not the limiting process. Thus, there must be a continuous generation of excited neutrals and ions throughout the interval that light is emitted.

The spectroscopic studies indicate there is a plasma phase that starts at the very beginning of breakdown conduction. This is believed to be the most important aspect of breakdown conduction. Thus, theories for the onset of breakdown should explain how the plasma state is initiated. Conduction during the first part of breakdown (while the voltage is falling rapidly) is believed to be primarily through this plasma. Hence, the conductance is that of the rapidly expanding plasma. A number of secondary effects influence this conductance. These will be discussed further in Section VI.

C. OPTICAL MICROSCOPY AND OTHER MEASUREMENTS.

1. Optical Microscopy.

Optical examination of breakdowns reveals a variety of patterns[1,3,6,9] that seem to depend on the dielectric material and its thickness, the conductance of the electrodes, the electrical behavior of the dielectric-electrode interface, the mechanical bond between the dielectric and the electrodes, the energy available for breakdown (which is a function of the stored energy of the capacitor at the time of breakdown and of the ability of the external circuit to supply energy during the time of breakdown conduction), and the polarity of the applied voltage.

Most breakdowns have three fairly distinct topographic features: a central region where there is complete destruction of the dielectric and of

the electrodes (except when the electrodes are made abnormally thick); a concentric region where the electrode damage is severe, but the dielectric is essentially intact; and a terminating outer edge where there may be damage to the electrodes and the dielectric. The central and outer edge are further distinguished if the substrate is examined after scraping the capacitor away with a well-honed razor blade. An etched imprint of these two regions is found (see Fig. 35) indicating that these regions were hotter than the intermediate region.

The presence of extreme conditions is further emphasized in the breakdown shown in Fig. 36a. This occurred in a capacitor with a very thick bottom electrode of copper evaporated onto a glass substrate to a depth of several microns, followed by a 2000 Å-layer of SiO, and finally a 1000 Å-layer of aluminum. (This configuration was chosen so that the capacitor could be examined for the distribution of silicon after breakdown using an x-ray microprobe. The thick bottom layer of copper shielded the silicon-containing glass substrate from the electron beam of the microprobe.) Figure 36b contains a plot of surface height as a function of distance along a diameter of the breakdown of Fig. 36a. The central region is permanently deformed to a depth many times the dielectric thickness. Around this central region is a mound of material also many times the thickness of the dielectric. The resulting effect is the same as when a high velocity projectile strikes a material which deforms as a fluid.[22] This evidence of a very high pressure and high temperature region localized at the center of the breakdown gives further support to the hypothesis of a high pressure plasma in this region during breakdown.

It has been shown in Section III.B that the central section of a breakdown tends to be of constant size even when the outside diameter increases accompanying increases in the capacitor plate area. In attempting to understand the

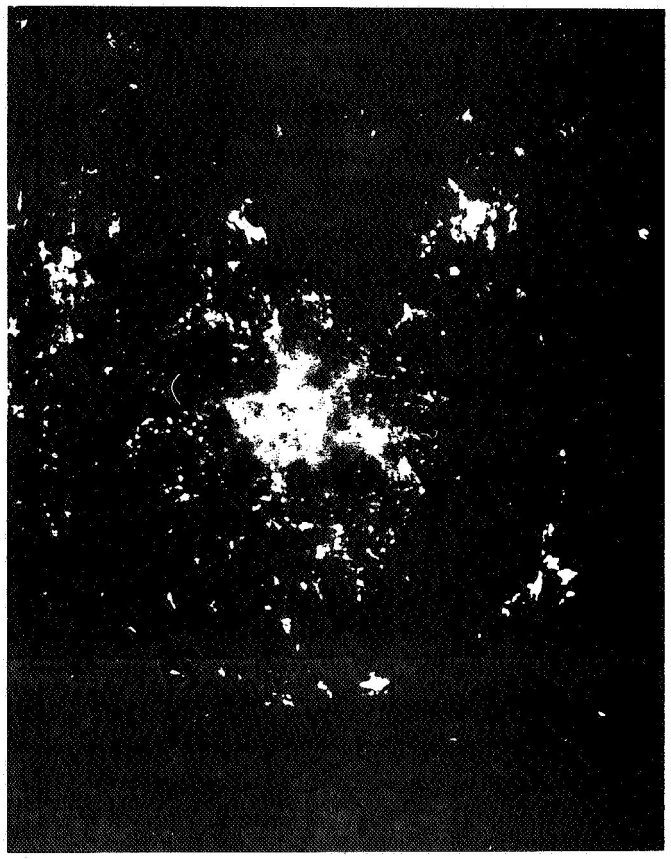

Fig. 35. Etch pattern left on glass substrate after breakdown in an Al-SiO-Al capacitor. The capacitor material has been scraped away using a well-honed razor blade.

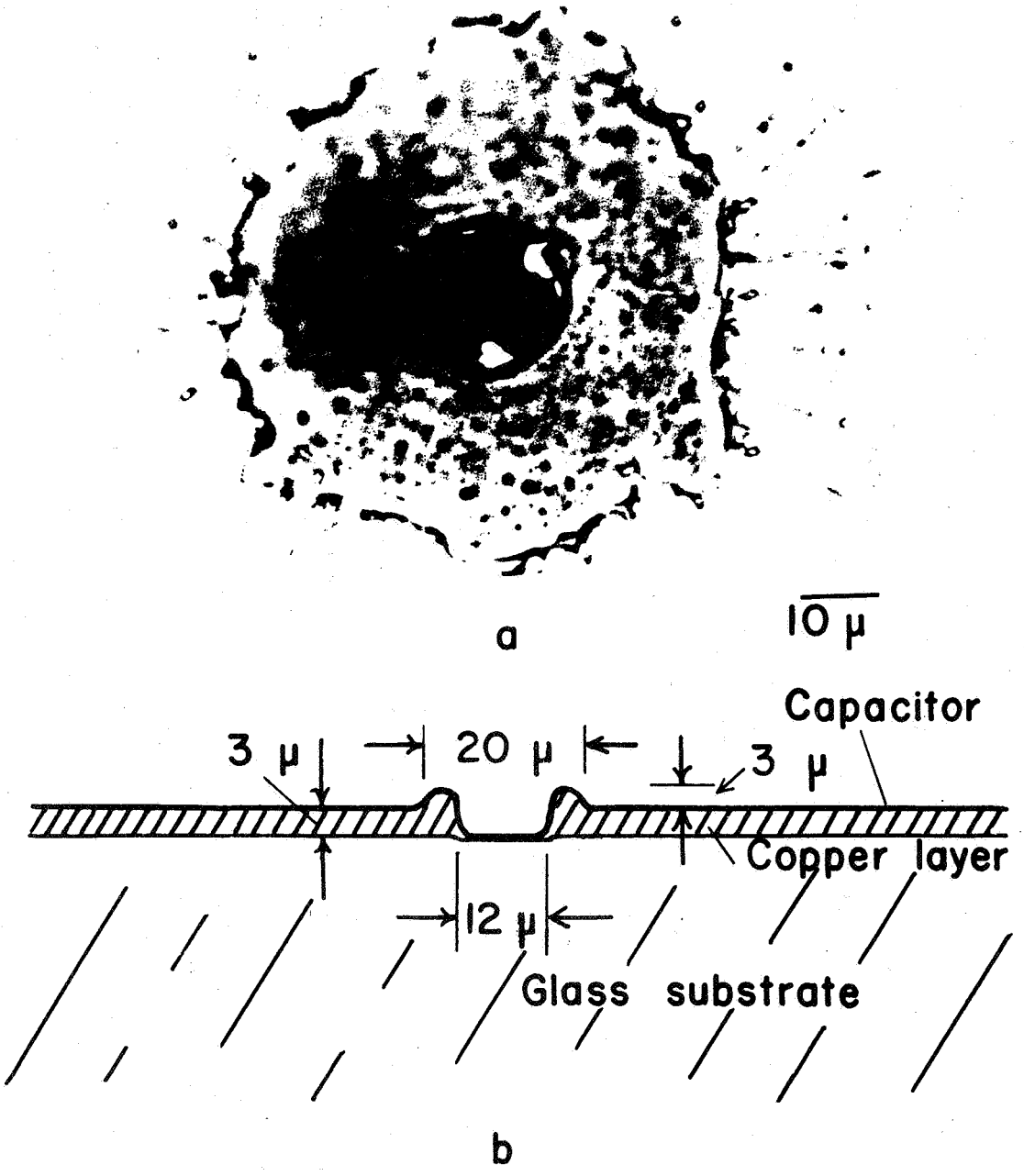

Fig. 36. Breakdown in a Cu-SiO-Al capacitor having a thick lower electrode of copper (about 3 microns). (a) Breakdown site. (b) Topograph of a section through the breakdown along a diameter.

configuration of breakdown patterns, it is necessary to account for the intermediate and outer edge configurations. As the high density plasma expands from the central region it travels over the surface of the capacitor and both heats and erodes the upper electrode. Heating should increase the local conductance, while erosion might well cut off the direct conducting path along the electrode surface to the central plasma-filled hole. Conduction could still occur through the expanding plasma and its contact region at the top electrode, but at higher resistance. It is difficult to say whether the blast can cause a thick layer of electrode material to pile up and form the edge of the breakdown, or if this edge is formed in some other fashion. It seems that the radial symmetry of some breakdowns which have to develop in the geometric shadow of previous breakdowns (see Fig. 37) is consistent with a blast effect. However, the unusual heating that occurs at the edge suggests secondary plasma effects occur in this region.

Figure 38 shows some breakdowns of a widely different nature. Each successive ring represents a new breakdown. Thus the breakdowns do not originate at a point, but rather along the edge of the previous breakdown. The uniformity in the thickness of the successive breakdown rings indicates that each breakdown nucleates almost simultaneously along the edge of the previous breakdown. It should be noted that there is still an aspect of competition involved for many concentric ring patterns develop simultaneously as the capacitor is subjected repeatedly to ramps. The pictures in Figs. 38a and 38b are of breakdowns in Al-CaF_2-Al capacitors. Klein, Gafni, and David[8] show similar ones for Al-SiO-Al capacitors (we have also seen them in Al-SiO-Al capacitors, but not frequently and not so well-developed as in the Al-CaF_2-Al capacitors). Figure 38b shows the pattern etched into the glass substrate when the capacitor has been scraped away after breakdown tests. The etched regions are believed to be the sites of

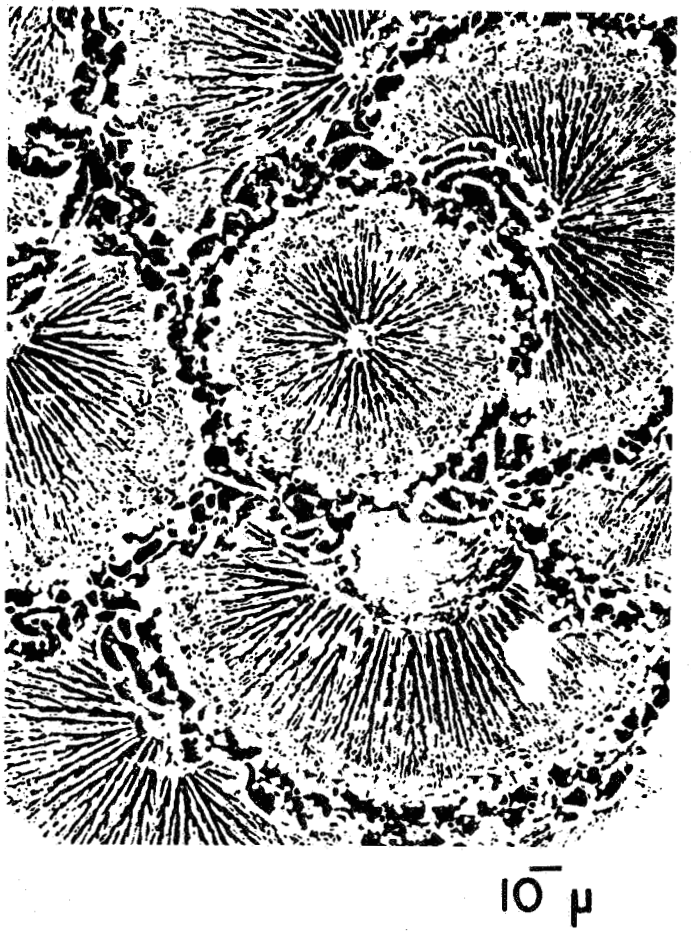

Fig. 37. Repeated breakdowns in Al-SiO-Al illustrating the radial symmetry of the breakdowns. Each "flower" represents a breakdown.

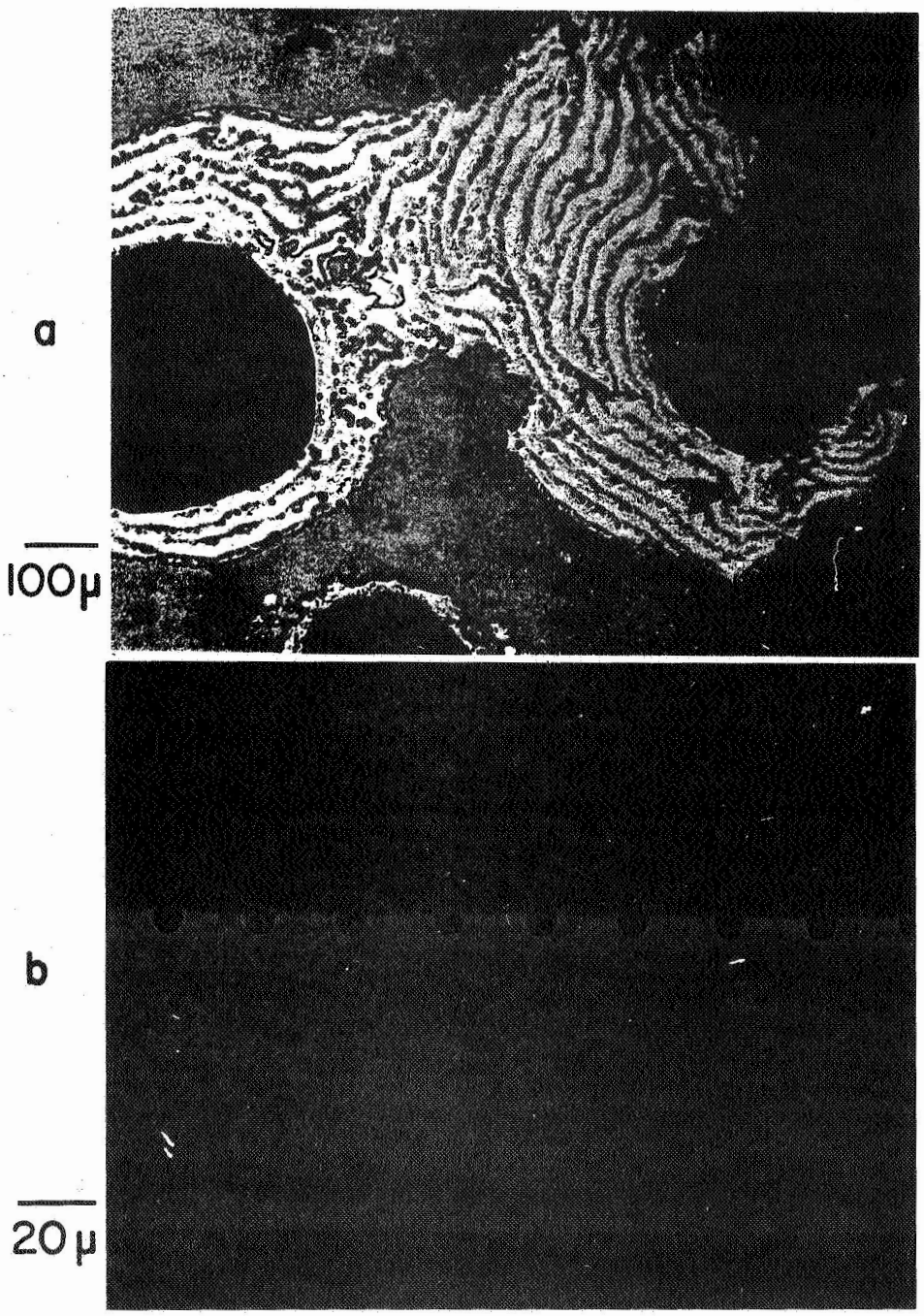

Fig. 38. Concentric breakdowns in Al-CaF_2-Al capacitors. Each ring is due to a single breakdown produced using a ramp applied voltage. (a) Concentric breakdowns seen with reflected light. (b) Etch patterns left on the glass substrate by concentric breakdowns.

local plasma action. Concentric breakdowns have not been observed in the other materials of this study.

2. X-ray diffraction.

X-ray diffraction of the crystalline materials CaF_2, MgF_2, and CeO_2 after deposition of the films yields the characteristic powder patterns with no indications of special orientation effects. However, the specimens are prepared for diffraction by scraping the films from the substrates. This means each particle is in the form of a small flat chip. If there were strong preferred orientation, it would probably show because the chips would tend to be parallel in the sample. There is a broadening of the lines indicating small grains. However, no quantitative evaluations have been made to date of the grain size. Crystalline silicon was found as a breakdown residual in Al-SiO-Al capacitors.[3] No other unusual residuals have been found in the other materials, but extensive tests seeking these have not been made.

3. X-ray microprobe.

Capacitors with a very thick bottom layer of copper (3-5 microns), an SiO layer of several thousand angstroms, and a top aluminum layer of about a thousand angstroms were broken down and examined with an x-ray microprobe. An attempt was made to locate the small regions that were identified in the electron microscope as nucleation centers for breakdowns.[3] However, the beam diameter of the probe is about 1 micron and the circle of confusion is probably twice this, so it is not surprising that the beam could not distinguish inhomogeneities of 0.5 microns diameter when these were not chemically different from the surrounding material. In the breakdown regions some inhomogeneity was found. Higher concentrations of aluminum corresponded with the shape of folded-back portions of the upper electrode. There was also an enhancement of silicon at the centers and edges of the breakdowns. The higher silicon concentration near

the edge is not believed to correspond to a folding back of SiO (which could conceivably be attached to the aluminum) since this enhancement is more circular and does not duplicate the ragged edges of the folded-back aluminum.

The electron microprobe did not give much information in the limited time it was used. Perhaps a more extensive program would have yielded fresh insights on the ultimate distribution of the capacitor constituents after breakdown.

IV. THEORY OF THE FIELD DISTRIBUTION WITHIN THE DIELECTRIC

An understanding of the onset of breakdown depends on a knowledge of the field distribution through the dielectric prior to breakdown. O'Dwyer [23] has attempted to construct a one-dimensional model that includes field or Schottky emission at the cathode, the condition of current continuity, a system of traps that gives rise to space charge, and a conductivity condition for the bulk current that contains parameters descriptive of the breakdown process. O'Dwyer indicates there is a space charge distribution and hence the field in the dielectric is inhomogeneous. He does not give the field distribution or the space charge distribution explicitly. O'Dwyer further emphasizes the inhomogeneity of the electric field in his recent treatment of the conditions for the onset of breakdown.[13]

As will be demonstrated shortly, there is an inhomogeneity within the dielectric whenever localized processes go at different rates for the same field. Thus, if the current depends both on electrode emission and bulk conduction characteristics, there is bound to be an inhomogeneous field and, hence, a space charge within the dielectric. If the space charge consisted of a sheet of positive charge, having a charge per unit area of $+\tau$ located near the cathode, then the field in the region between the cathode and the charge sheet would be increased by the amount $\tau/2\varepsilon$, while the field between the anode and the charge sheet would decrease by the same amount. Thus field emission at the cathode would become relatively more favorable than without the space charge, while the bulk-limited current would be decreased relative to its value without the space charge. Thus the space charge provides the balancing structure to maintain constant current.

The treatment that follows falls into two distinct parts. The first employs the condition of current continutity and examines the degree of inhomogeneity of field required if the injected current at the cathode is to equal the bulk-limited current. (This analysis is the work of P. J. Hayes.) The second part examines the field inhomogeneity that arises when the current is negligibly small,

yet there is some mobility of carriers. This might be the case in thick specimens having ionic conduction. (The second part is the work of J. L. Smith.)

A. FIELD INHOMOGENEITY DUE TO COMBINED ELECTRODE AND BULK PROCESSES.

1. Review

Some properties of both prebreakdown and breakdown conduction are suggestive of a spatially inhomogeneous field distribution through the dielectric. In many dielectrics prebreakdown dc voltage-current-temperature characteristics are not accurately described by any of the "well understood" conduction mechanisms: Fowler-Nordheim emission, Schottky emission, Poole-Frenkel effect, or space charge limited conduction. In measurements on many capacitors (SiO and CeO_2) the temperature-current characteristics at constant voltage are more readily interpreted in terms of the above mechanisms than are the current-voltage characteristics at constant temperature. Thus in SiO and CeO_2 a characteristic activation energy is found for nearly all capacitors, yet the voltage-current characteristics may or may not be described by any of the above mechanisms.

Using a triode arrangement (cathode-grid-plate), Hickmott[24] has observed a concentration of the field at the cathode in SiO films of about 600 Å thickness. The grid was 150 Å from the cathode. The high field region developed upon repetitive voltage sweeps. Practically all of the voltage drop was near the cathode and the field at the cathode was at least four times the ratio of the applied voltage to the dielectric thickness. This gives a lower bound for the field close to the cathode. Above a given voltage the current decreased (in a negative resistance fashion) simultaneously with an increase in the field in the cathode region.

Boer, Hansch, and Kummel[25,26] have directly observed field inhomogeneities in CdS single crystals of 1-2 mm thickness. They found that the wavelength of the visible light absorption edge was dependent upon the size of the dc electric field. Using transmitted light with a wavelength at this threshold of transmission they viewed the region between electrodes while applying voltages. With voltage

of sufficient magnitude a darkened region appeared which moved toward the cathode upon further increase in voltage. At a distance very close to the cathode the darkened region generally stabilized. Boer[26] and Adirowitsch[27] interpreted the darkened region as one of high field strength relative to the adjacent areas. The field on the cathode side of the darkening was thought to be greater than that on the anode side. The stopping of the darkened region in front of the cathode was interpreted to occur when the field at the cathode is sufficiently high so that tunnelling current from the cathode equals the bulk generated current. It was pointed out that the darkened region generally appears at voltages about one order of magnitude below the breakdown voltage.

O'Dwyer has investigated the continuity of current through dielectrics in prebreakdown[23] and breakdown-onset[13] conditions. He assumes the cathode-dielectric barrier is somewhere around 1 eV. In the breakdown-onset study, the field at the cathode, for the thicker films, could be over an order of magnitude greater than the field at the anode. For thinner films the field variation was not so great. A recent study by Waxman[28] shows the metal-dielectric barrier for Al-SiO is 2.7 $\pm$ 0.1 eV and for Au-SiO is 3.3 $\pm$ 0.1 eV. If these values are assumed as barriers, treatments of current continuity similar to O'Dwyer's would lead to even greater field inhomogeneity in the dielectric.

Several experimental aspects of breakdown are also indicative of field inhomogeneities. (The conduction mechanisms during breakdown are probably different from the prebreakdown mechanisms.) The value of V_{min} is found to be polarity sensitive, but reproducible in a given capacitor. However, it is not possible to predict for a new capacitor the magnitude or the sense of the polarity effect.[3] Both the existence of V_{min} and its polarity sensitivity suggest field inhomogeneities. Also the sensitivity of V_{max} to the rise time and the history of the capacitor is probably related to the development of critical fields within the capacitor.

2. Field Inhomogeneity Required for Continuity of the Injected and Bulk Currents

Prebreakdown current densities when the applied voltage is between 1 and 10 volts are generally of the order of 0.1 to 100 $\mu A/cm^2$. Assuming Waxman's experimental results for the cathode-dielectric barrier (ϕ_1 about 3 eV for Al-SiO and Au-SiO), it is of interest to calculate the tunnel current and Schottky current versus field. Tunnel current density is given by [29]

$$J_t = 3.34 \frac{F^2}{\phi_1} \exp\left(-6.90 \times 10^7 \frac{\phi_1^{3/2}}{F}\right) \quad (1)$$

and Schottky current density by [30]

$$J_s = (2.4 \times 10^7) T^2 \exp\left(-1.16 \times 10^4 \frac{\phi_1}{T} + 1.875 \frac{F^{1/2}}{T}\right), \quad (2)$$

where the current densities are in $\mu A/cm^2$, F is in V/cm, ϕ_1 is in eV, and T is in ^oK. A relative dielectric constant of 5.5 has been assumed and the transmission coefficient for electrons[31] at the peak of the barrier is taken as 0.2. A plot of J_t and J_s versus field and temperature is shown in Fig. 39. Very high fields, in the range of 10^7 V/cm, are necessary to produce current densities of 0.1 to 100 $\mu A/cm^2$. Also, for these current densities the tunnelling mechanism dominates by about 30 orders of magnitude. A field of 10^7 V/cm is one to three orders of magnitude greater than the value of $\frac{\text{voltage}}{\text{thickness}}$ required to produce these currents experimentally. If variations in the transmission coefficient and contact area of the cathode are permitted, these represent only small perturbations of the field because of the tremendous field dependence of J_t.

Furthermore, because of the strong field dependence, only a small change in the field would account for the whole range of currents measured from liquid nitrogen temperature to 100^oC and between 1 and 10 volts. Even near breakdown voltages, the prebreakdown current densities are only in the ma/cm^2 range, again

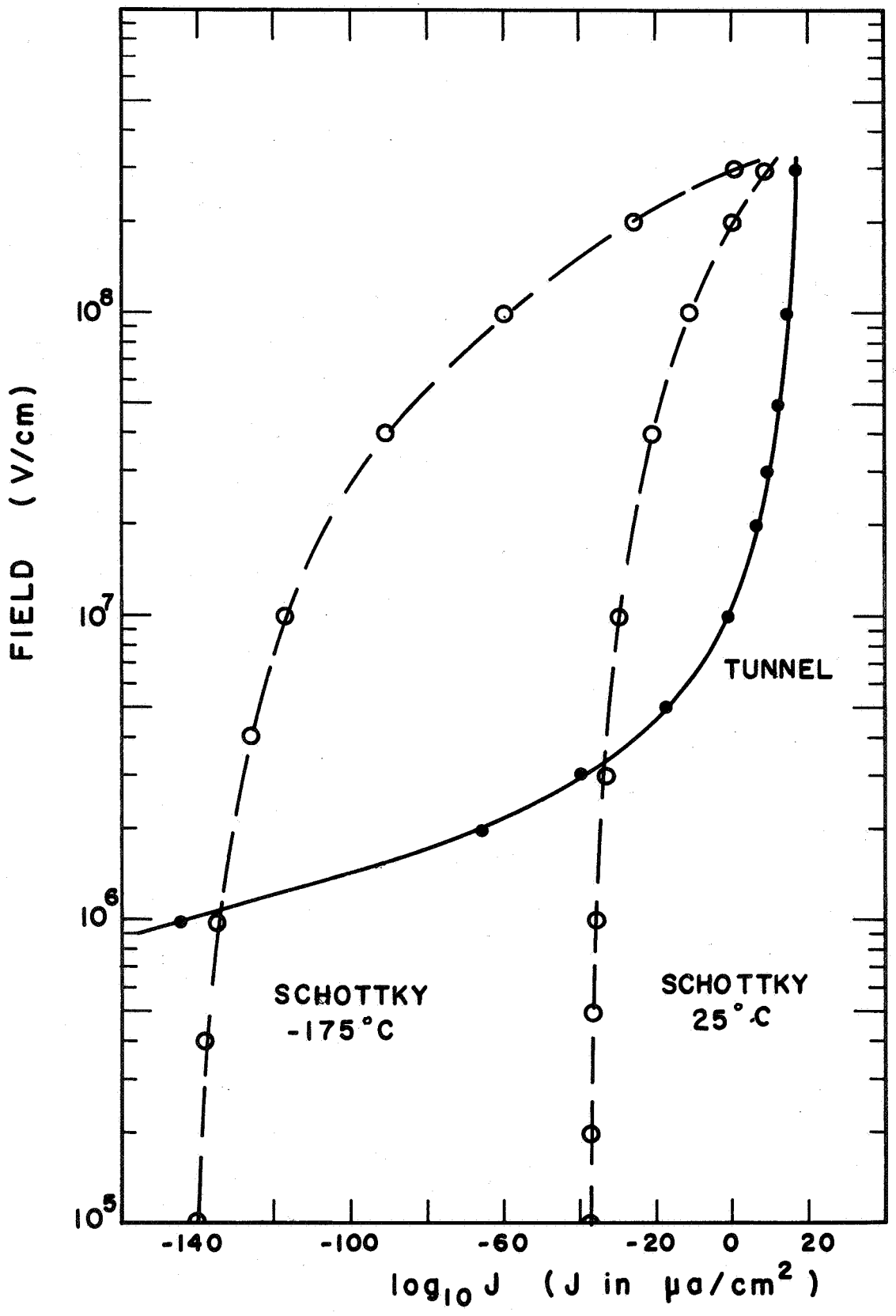

Fig. 39. Comparison of tunnel and Schottky current densities for a barrier of 3 eV.

accounted for by a small change in the field in J_t. Thus, assuming currents are evenly distributed over the area of the capacitor and the metal dielectric barrier is 3 eV, it appears that throughout a broad range of conduction a high field of about 10^7 V/cm is necessary at the cathode. (If ϕ_1 is chosen to be 1.5 eV, similar results hold with a high of 4×10^6 V/cm at the cathode.)

The above discussion applies specifically to a steady state condition. The development of a high field near the cathode would probably require a finite time. If the breakdown voltage is measured as the rate of rise of the ramp is increased (while choosing the circuit time constant small compared to the ramp rise time), it should be possible to determine the time to develop the cathode field.

SiO and CeO_2 capacitors exhibit a strong temperature dependence in pre-breakdown conduction. The activation energies ϕ_2 are approximately 0.5 eV and 0.3 eV, respectively. Such energies may be due to trapping levels or to relatively deep donor levels in the forbidden gap. Thermal excitation from these levels is negligible below about -100°C. Further thermal effects are due to smaller activation energy. The field and temperature dependence of the bulk current density J_b produced by excitation of trapped electrons is given by the Poole-Frenkel equation[32]

$$J_b = AF\exp\left(-1.16 \times 10^4 \frac{\phi_2}{T} + 3.75 \frac{F^{\frac{1}{2}}}{T}\right), \qquad (3)$$

where J_b is in $\mu A/cm^2$, F is in V/cm, T is in °K, and ϕ_2 is the energy in eV of the trap below the conduction band of the dielectric. A relative dielectric constant of 5.5 has been used. This equation will be used in a computation of bulk field versus cathode field with the condition of continuity of current. With a properly chosed value of A, a constant characteristic of the dielectric material, J_b will be in the order of magnitude of the experimentally observed current densities even though it does not describe accurately the observed voltage-current-temperature data. (If space-charge-limited conduction[33] is assumed instead of the Poole-Frenkel type, both fields and currents are qualitatively as described in Eq. (3).)

For trap depths of 0.3 and 0.5 eV there is negligibly small trap-to-conduction band tunnelling except at very low temperatures.[32]

The bulk current density J_b is more field dependent than the Schottky current density J_s. However, on the scale of Fig. 39, it appears similar but shifted toward higher currents. The magnitude of J_b depends upon the multiplicative constant A in Eq. (3). With A=0.42 μA/V-cm, ϕ_1 = 3.0 eV or 1.5 eV, and ϕ_2 = 0.5 eV, and the requirement that $J_b = J_t$, the curves of Fig. 40 are generated. As is expected, the bulk field F_b increases over several orders of magnitude while the cathode-dielectric interface field F_t increases only slightly. The value of A in Eq. (3) was chosen assuming the applied voltage gave rise to a uniform field within the dielectric. If a field enhancement occurs at the cathode as suggested, then the bulk field is smaller and the value of A should be increased to satisfy experimental data. With a higher value of A, the curves of Fig. 40 are shifted upward toward higher values of the cathode field.

The -125°C curves in Fig. 40 should represent the lowest extreme of bulk generated current even though actual experimental temperatures ranged as low as -193°C. The experimental temperature dependence of current density is significantly decreased below about -100°C. In dielectrics which have very little temperature dependence the cathode-interface fields should be of the shape of the 25°C curve in Fig. 40. The vertical location would depend on ϕ.

Dependence of the cathode-interface field on ϕ_1 is illustrated in Fig. 40. The dependence on ϕ_2 is much weaker than the ϕ_1 dependence. However, variations in either for various capacitors would result in vertical shifts in the curves of Fig. 40.

The ratios of the fields F_t/F_b decreases as both fields increase. Thus at lower voltages almost all the voltage drop is across the cathode-interface. But at higher voltages the voltage drop across the bulk increases with little increase in voltage drop at the cathode-interface. Such an effect should result in

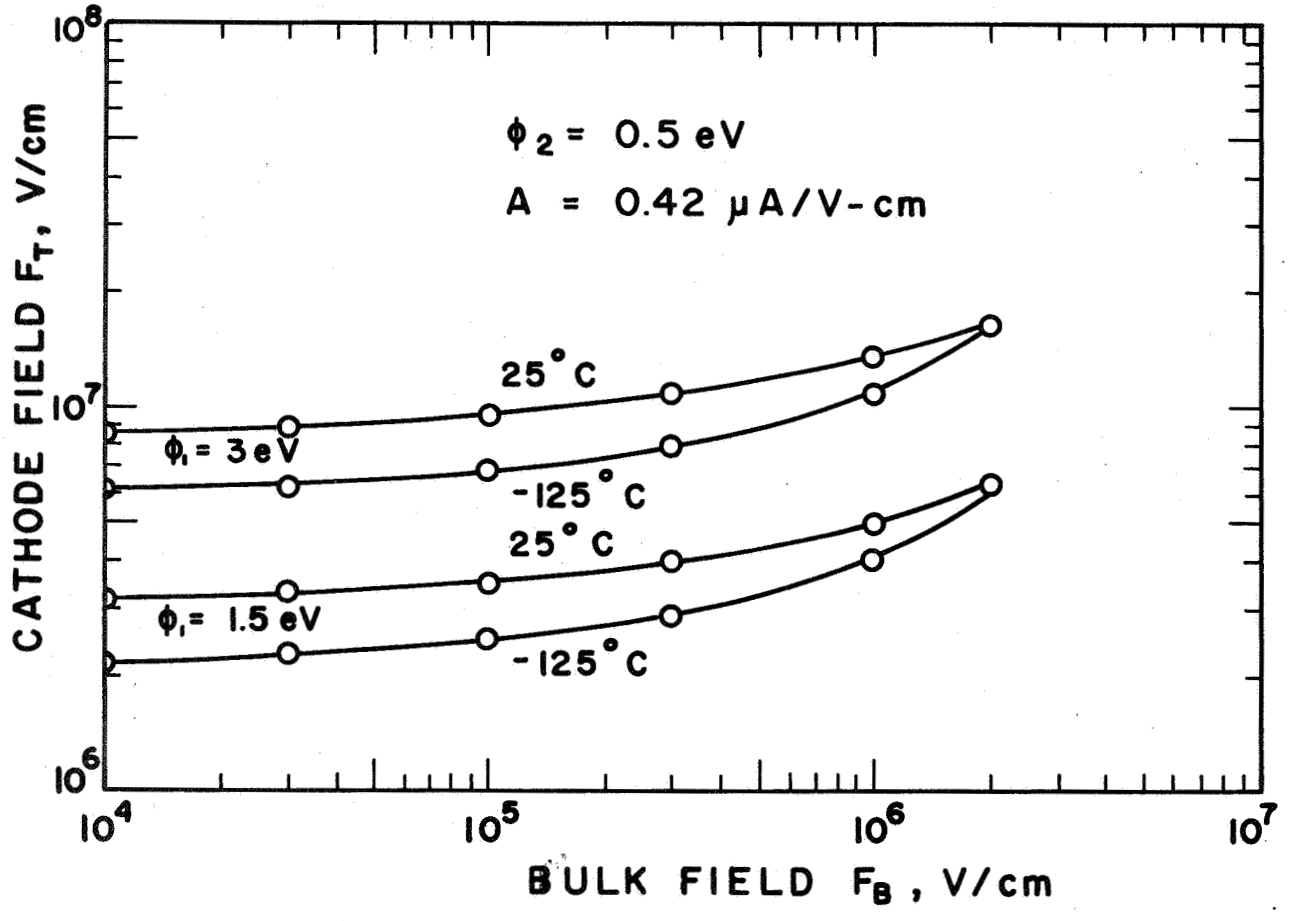

Fig. 40. Cathode field vs bulk field when current density is constant showing the effects of temperature and cathode barrier height ϕ_1.

an apparent bulk limited voltage-current characteristic with more field dependence than the Poole-Frenkel equation but approaching it at higher voltages. In CeO_2 capacitors the field dependence is stronger than that of the Poole-Frenkel.

3. Discussion of Inhomogeneous Fields and Breakdown

Some general features of breakdown are now discussed with respect to a possible criterion that strong cathode fields are necessary for breakdown.

The temperature dependence would be expected to vary with the principal conduction mechanism in the bulk. For thermal excitation by the Poole-Frenkel mechanism the curves of Fig. 40 show that to obtain a given field at the cathode, higher bulk fields must be applied for lower temperatures. Thus, if a critical field at the cathode is necessary for breakdown, the experimentally measured breakdown voltage will increase as the temperature decreases. The temperature dependence will be much smaller near the right side of the graph (Fig.40) and even disappear at the extreme right side where the trapping barriers are nearly reduced to zero by the bulk field.

Conduction during breakdown may be completely different from prebreakdown conduction. However, a high field at the cathode could explain the existence of V_{min}. Assuming the breakdown has been initiated, it continues until the field at the cathode falls to a minimum value necessary to sustain the breakdown. Because of the concentration of the field within a small region X_o near the cathode this will appear experimentally as a constant voltage rather than as a constant field. Depending on the dielectric-metal interfaces the high field region X_o, though quite small relative to the dielectric thickness d, may vary with polarity and also from one capacitor to another. Thus the voltage V_{min} could vary with polarity and from one capacitor to another but would be constant for a given polarity of a given capacitor.[3] If V_{min} were simply a voltage required to produce ionization in the dielectric (to sustain the breakdown) it should be constant for a given material and should show no polarity effects, contrary to observation.

"Dark Spots" were found in Al-SiO-Al capacitors at which breakdowns nucleated.[3] If the dark regions are regions of higher conductivity then fields at the cathode in this region would be greater than that in other areas. Thus if a high field at the cathode is necessary for breakdown, the breakdowns would begin at the dark regions.

Variations in the metal-dielectric interface would occur from one deposition to another and with polarity. These variations would produce different values of the metal-dielectric barrier ϕ_1. The "critical" field at the cathode would thus vary and produce different breakdown voltages and different average field strengths (voltage/thickness) for a given dielectric thickness.

Finally, the development of inhomogeneous fields would exhibit some time dependency since the existence of such fields implies spatial variations in the charge density. With faster voltage sweeps the cathode "critical" field would have a shorter time to develop and the breakdown voltage would appear to be higher. This is generally observed experimentally.[2]

B. CHARGE DISTRIBUTION AND FIELD INHOMOGENEITY OF A NEUTRAL ISOLATED INSULATOR

1. General Theory

This treatment seeks to find the equilibrium electric field and charge distributions in a slab of insulating material located in a uniform electric field. The insulator is assumed to contain slightly mobile carriers that are thermally activated in the presence of an applied field. Polarization effects are not considered. The case to be examined assumes:

i. The insulator is an isotropic slab of thickness D that contains charge carriers of only one type (negative) with sufficient mobility to move in response to an applied field.

ii. The carriers move in a periodic potential arising from an array of bonding or trapping sites.

iii. Thermal excitation is required before the carriers are mobile.

iv. No external charge injection takes place and total charge neutrality is maintained.

Systems fulfilling the above criteria include alkali halides which contain on the order of 10^{17} ion-vacancy pairs per cm^3 at room temperature.[34] The positive ions are assumed so much more mobile than the negative ions that the latter can be regarded as stationary. Motion of a positive ion occurs when a positive ion and an adjacent positive ion vacancy interchange. This can occur repeatedly with different ions and vacancies provided the requisite activation energy is supplied. Transport of charge can be followed by keeping track of the relatively few positive ion vacancies instead of the more numerous positive ions. Each positive ion vacancy behaves the same as a positive ion, but with opposite charge. In the treatment that follows the carriers are these vacancies, i.e., negative charges with the dynamic properties of positive ions.

The present work differs from that done previously through the boundary condition given in Statement iv above. The method is similar to that of references 16 and 35-37.

Figure 1 depicts the potential energy seen by a negative carrier of charge -q in the absence of an applied field (solid line) and in the presence of an applied field E (broken line). A and B, adjacent equilibrium sites, are a distance a apart and are separated by a barrier of height Φ. Sites A shall represent a plane of sites perpendicular to an applied electric field at position x_A. The volume of a site is defined as the crystal volume divided by the number of sites within that volume. In addition, let

N_A = number of negative carriers per unit volume at sites A

N_B = number of negative carriers per unit volume at sites B

ν = vibration frequency of a carrier when in an equilibrium site.

The probability per unit time of a negative charge crossing the barrier of height

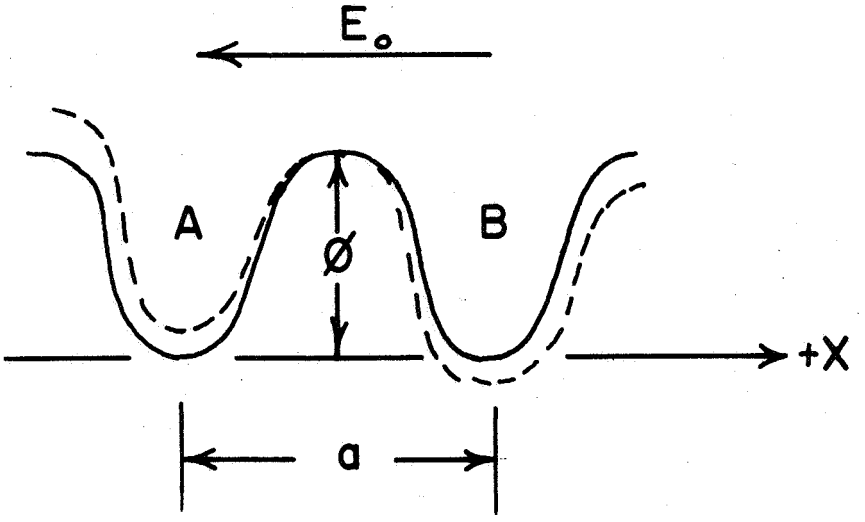

Fig. 41. Potential energy of negative ions. Solid line represents the potential energy in the absence of a field and the dotted line represents the potential energy in the presence of a field E_o. A and B are adjacent equilibrium sites, a distance a apart, with a separating barrier of height ϕ.

ϕ when the system is at a temperature T is [16,35,37]

$$p = \nu e^{-\phi/kT} \quad . \tag{1}$$

The applied field causes electrons in sites A to see a barrier $(\phi - \frac{qaE}{2})$ on the right. Those in site B see a barrier of height $(\phi + \frac{qaE}{2})$ on the left. The equilibrium condition requires that the current to the right equals the current to the left. Thus,

$$N_A \nu e^{-(\phi - \frac{qaE}{2})/kT} = N_B \nu e^{-(\phi + \frac{qaE}{2})/kT}$$

and hence

$$N_A = N_B e^{-qaE/kT} \quad . \tag{2}$$

Thus

$$N_B - N_A = N_B(1 - e^{-qaE/kT}). \tag{3}$$

In the above E and q are positive numbers. Equation (3) can be expanded in a series giving

$$N_B - N_A = N_B \left[\frac{qaE}{kT} - \frac{1}{2}\left(\frac{qaE}{kT}\right)^2 + \ldots\right] . \tag{4}$$

Equation (4) can be converted to a function of position by introducing the variables x and N(x) such that $N(x_i)$ is equal to N_i for all values of i:

$$N(x + \Delta x) - N(x) = N(x + \Delta x)\left[\frac{qE}{kT}\Delta x - \frac{1}{2}\left(\frac{qE}{kT}\right)^2 \Delta x^2 + \cdots .\right] \tag{5}$$

In the limit as $\Delta x \to 0$, Equation (5) becomes

$$dN = N(x)\frac{qE(x)}{kT}\, dx \ , \tag{6}$$

where higher order terms in dx have been dropped.

Use Poisson's equation to relate the electric field to the charge density:

$$\nabla \cdot \vec{E} = \frac{\rho}{\varepsilon}$$

$$\frac{dE}{dx} = \frac{q}{\varepsilon} \; [N(x) - M], \tag{7}$$

where M is the density of positive charges, which are immobile. (Note that the electric field is in the negative x-direction.)

Differentiate Equation (6), then combine Equations (6) and (7).

$$\frac{d}{dx} \left(\frac{1}{N} \frac{dN}{dx}\right) = \frac{q^2}{\varepsilon kT} \; [N(x) - M] \tag{8}$$

To solve this differential equation, let $y = \ln N(x)$. Then

$$\frac{dy}{dx} = \frac{1}{N} \frac{dN}{dx}$$

and

$$\frac{d^2y}{dx^2} = \frac{q^2}{\varepsilon kT} \; [e^y - M] \; . \tag{9}$$

If the further substitution $p = \frac{dy}{dx}$ is made, then

$$\frac{d^2y}{dx} = \frac{dp}{dx} = \frac{dp}{dy} \; \frac{dy}{dx} = \frac{ydp}{dy}$$

$$\frac{ydp}{dy} = \frac{q^2}{\varepsilon kT} \; [e^y - M]$$

$$dp = \frac{q^2}{\varepsilon kT} \; \left[\frac{e^y - M}{y} \right] dy \tag{10}$$

Upon integrating, returning to the original variables, and using the boundary conditions

$$x = 0, \quad N = N_o$$

$$x = 0, \quad \frac{dN}{dx} = N_o \frac{qE_o}{kT} \quad , \tag{11}$$

where x = 0 is the low potential edge of the insulator, the result is

$$x = \int_{N_o}^{N} \frac{dN^1}{N^1 \left[\frac{2q^2}{\varepsilon kT} (N^1 - N_o - M \ln \frac{N^1}{N_o}) + (\frac{qE_o}{kT})^2\right]^{\frac{1}{2}}} \tag{12}$$

2. Low Field Approximation

Equation (12) is so complex that it has to integrate numerically. To do so requires assignment of plausible values for N_o and E_o. To obtain insight on this assignment and on the entire solution, the applied field and the resulting disturbance in the charge distribution will be assumed small. Then Equation (6) can be simplified by replacing N(x) by M, i.e.,

$$\frac{dN}{dx} \approx M \frac{qE(x)}{kT} \quad . \tag{13}$$

Equation (8) becomes

$$\frac{d^2N}{dx^2} = \frac{Mq^2}{\varepsilon kT} [N(x) - M].$$

This is a linear second order equation with the solution

$$N = M + C_1 \cosh \alpha x + C_2 \sinh \alpha x, \tag{14}$$

where

$$\alpha^2 = \frac{Mq^2}{\varepsilon kT} \text{ , and } C_1 \text{ and } C_2 \text{ are constants.}$$

The boundary conditions are:

$$\text{At } x=0, \quad \frac{dN}{dx} = \frac{Mq}{kT} E_o \tag{15a}$$

$$\int_o^D N dx = M \int_o^D dx \ , \tag{15b}$$

where the insulator slab has a thickness D. Equation (15b) is a charge neutrality condition. After using these conditions, we have

$$N = M + \frac{MqE_o}{\alpha kT} \sinh \alpha x - \frac{MqE_o}{\alpha kT} \tanh \frac{\alpha D}{2} \cosh \alpha x \ . \tag{16}$$

If $M = 10^{17}/cm^3$, $T = 300^oK$, $\varepsilon = \varepsilon_o$ and $D = 10^{-4}cm$, then $\alpha \approx 10^8/m$ and $\alpha D \approx 100$. Thus $\tanh \frac{\alpha D}{2}$ is very nearly unity, so we can write

$$N \approx M + \frac{MqE_o}{\alpha kT} [\sinh \alpha x - \cosh \alpha x] = M - \frac{MqE_o}{\alpha kT} e^{-\alpha x} \tag{17}$$

$$\text{At } x = 0, \quad N = N_o = M - \frac{MqE_o}{\alpha kT} \ . \tag{18}$$

Since $M - N_o$ is supposedly small compared to M, take $M - N_o = 0.1\ M$ and compute E_o. This gives $E_o \approx 2.5 \times 10^3$ V/cm, which may be taken as an upper limit for the low field approximation.

The charge density at x = D is found from Equation (16) to be

$$N(D) = M + \frac{MqE_o}{\alpha kT} \ . \tag{19}$$

The field at any position is found by integrating Equation (7) using Equation (16).

$$E = E_o + \frac{Mq^2E_o}{\alpha^2 \varepsilon kT} [\cosh \alpha x - \tanh \frac{\alpha D}{2} \sinh \alpha x - 1] \ . \tag{20}$$

At both x = 0 and x = D, Equation (20) gives $E = E_o$.

Thus there is a net positive charge in the region about x = 0 and a net negative charge at the region about x = D. The electric field is higher at the two ends than it is in the central region. The ratio of the minimum field (which occurs at x = D/2) to the maximum field E_o is very nearly

$$\frac{E(D/2)}{E_o} \simeq 1 - \frac{Mq^2}{\alpha^2 \epsilon kT} \simeq 0 ,$$

where we have used α^2 as defined in Equation (14).

Figures 41a and 41b illustrate the net charge density and the electric field variations. The charge layers are almost completely contained within a distance of D/20 from the two surfaces.

3. Discussion

If Equation (6) were used instead of the low field approximation of Equation (13), the qualitative nature of the solution would probably be unaltered.

The field distribution has several noteworthy features.

a. The internal field never exceeds the applied field.

b. The internal field is the same as the applied field at both surfaces and it falls off rapidly with distance from the surfaces.

c. The field is very nearly zero in the central portion (as is expected of an ordinary conductor in electrostatics).

d. Polarization effects would probably influence the field only slightly since the field is virtually zero throughout all but the transition layers.

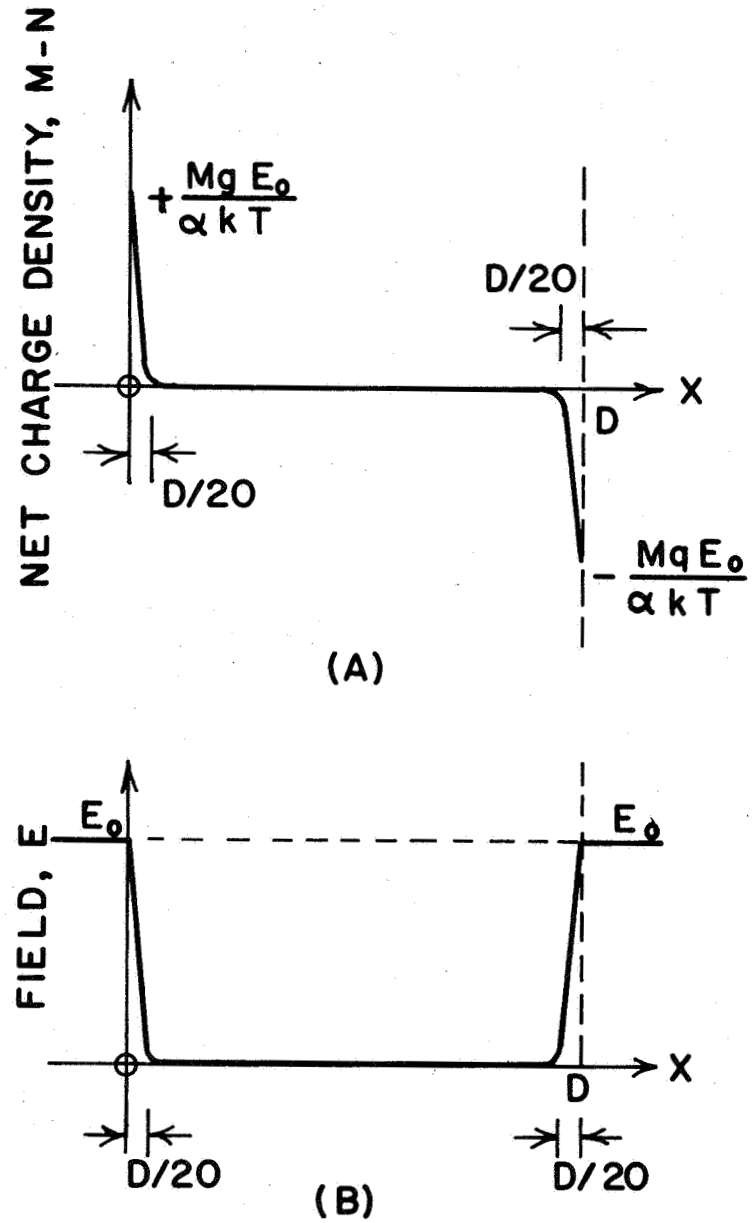

Fig. 41. (a) Net charge distribution (M-N) due to the applied field E_o. (b) Field configuration in the dielectric.

V. COMPARISON OF BREAKDOWN DATA WITH THEORY

In this section the breakdown measurements are discussed in terms of theories for the onset of breakdown. The treatments considered are those of Forlani and Minnaja[15], O'Dwyer[13], and Klein and Gafni[9]. The first two are microscopic in their approach. Each is based on the electron avalanche ideas developed by von Hippel, Fröhlich, Seitz, Callen, and Franz (see the monographs by O'Dwyer[38] and Whitehead[39] for an account of these earlier papers). The treatment of Klein and Gafni is phenomenological. It assumes that breakdown is a purely thermal condition produced when the Joule heating exceeds the rate at which thermal energy can be conducted from the breakdown site. After considering each of the above individually, a critique will be made on breakdown theories in general.

A. THEORY OF FORLANI AND MINNAJA

The basic features in the theoretical argument of Forlani and Minnaja are:

i. The dielectric is an ionic crystal.

ii. Electrons are "free" in the conduction band.

iii. The number of electrons in the conduction band can be enhanced by ionization from the valence band. This ionization can occur only after electrons already in the conduction band have absorbed from the field an energy greater than E_{gap}, the energy separating the valence and conduction bands.

iv. Electrons transfer energy to the crystalline lattice by means of an interaction with the optical phonon spectrum. The optical phonons are connected with ionic vibrations where adjacent ions of different species move 180^{o} out of phase.

v. Tunnel injection is assumed to occur at the cathode.

vi. The critical condition for breakdown is for the current density to reach,

"at some point internal to the dielectric thickness, a certain current j_b peculiar to the considered dielectric."

The predictions obtained are:

i. The breakdown field (defined as the applied voltage divided by the dielectric thickness w) varies as $w^{-\frac{1}{2}}$.

ii. The breakdown field is independent of temperature.

In Figures 23 and 24 are straight lines with slopes of $-\frac{1}{2}$ showing that these give a good representation of the thickness dependence of the breakdown field in CaF_2, CeO_2, SiO and MgF_2. The data on CeF_3 and Teflon are too sparse to allow conclusions.

The temperature dependence in different materials of the breakdown field is shown in Fig. 22. Here SiO and MgF_2 exhibit no temperature dependence, while CaF_2, CeF_3 and CeO_2 show systematic decreases in breakdown field as temperature increases. Temperature data have not yet been taken on Teflon.

Thus, the theory of Forlani and Minnaja has to be modified if it is to give the proper temperature dependence. Further, the applicability of the theory to non-ionic crystals needs some examination. The predictions of the theory hold well for an ionic crystal (MgF_2) and a glassy material (SiO). However, even though CeF_3, CeO_2 and CaF_2 are primarily ionic, they do not have the temperature dependence predicted. As indicated in Section IV.A, a temperature dependence can arise either from the injection mechanism, the bulk conduction mechanism, or both.

B. THEORY OF O'DWYER

O'Dwyer points out that the avalanche mechanism, as elaborated by Seitz[40], requires many generations (Seitz estimates 40 for a specimen one cm thick when the breakdown field is about 10^6 V/cm) and hence implies a current density that increases as the avalanche progresses. Accompanying this, however, is a residual space charge that would lead to internal fields of the order of 10^{11} V/cm if the

avalanche were to proceed as described by Seitz. This can be avoided if a current continuity condition is added. The continuity condition forces a redistribution of the space charge left in the avalanching. (Since time is required for this redistribution, it forms a basis for understanding why the breakdown threshold depends upon the rate of application of voltage.) O'Dwyer assumes electrons in the conduction band are free and develops an expression for the ionization rate. This is combined with the current continuity condition, Poisson's equation, and the assumption of field injection at the cathode. He concludes the cathode field is greater than the field in the remainder of the dielectric. Breakdown is taken to occur when a small change in the applied field implies an enormous change in the current. This occurs at a well-defined applied voltage for a given thickness. O'Dwyer denotes the average field in the dielectric at breakdown by the symbol $\bar{F}_b$ (equivalent to F_{max}) and then defines two parameters, H and λ, such that H has the dimensions of an electric field and λ the dimensions of a length. He plots $H/\bar{F}_b$ vs $\log \frac{w}{\lambda}$, where w is the dielectric thickness. This is a universal curve in terms of the material parameters H and λ. The length λ is descriptive of the distance between ionizing collisions and it is given by $\lambda = \frac{\bar{\mu}\sqrt{2mI}}{e}$, where $\bar{\mu}$ is the mobility of the electrons, m the electron mass, I the energy gap between the valence and conduction bands, and e the electron mass.

O'Dwyer's universal breakdown curve is replotted in Fig. 42 in the form $\log \bar{F}_b/H$ vs $\log u$, where $u = w/\lambda$. If the graph paper is chosen so that the distance per cycle is the same for both the experimental curve and the theoretical curve, then the values of H and of λ can be determined by first aligning the coordinate axes of the two curves so they are parallel, then by making suitable translations parallel to the coordinate axes until a best fit is reached between the experimental data and some portion of O'Dwyer's theoretical curve. The scale correspondences can then be read directly (a pin hole may be made extending through

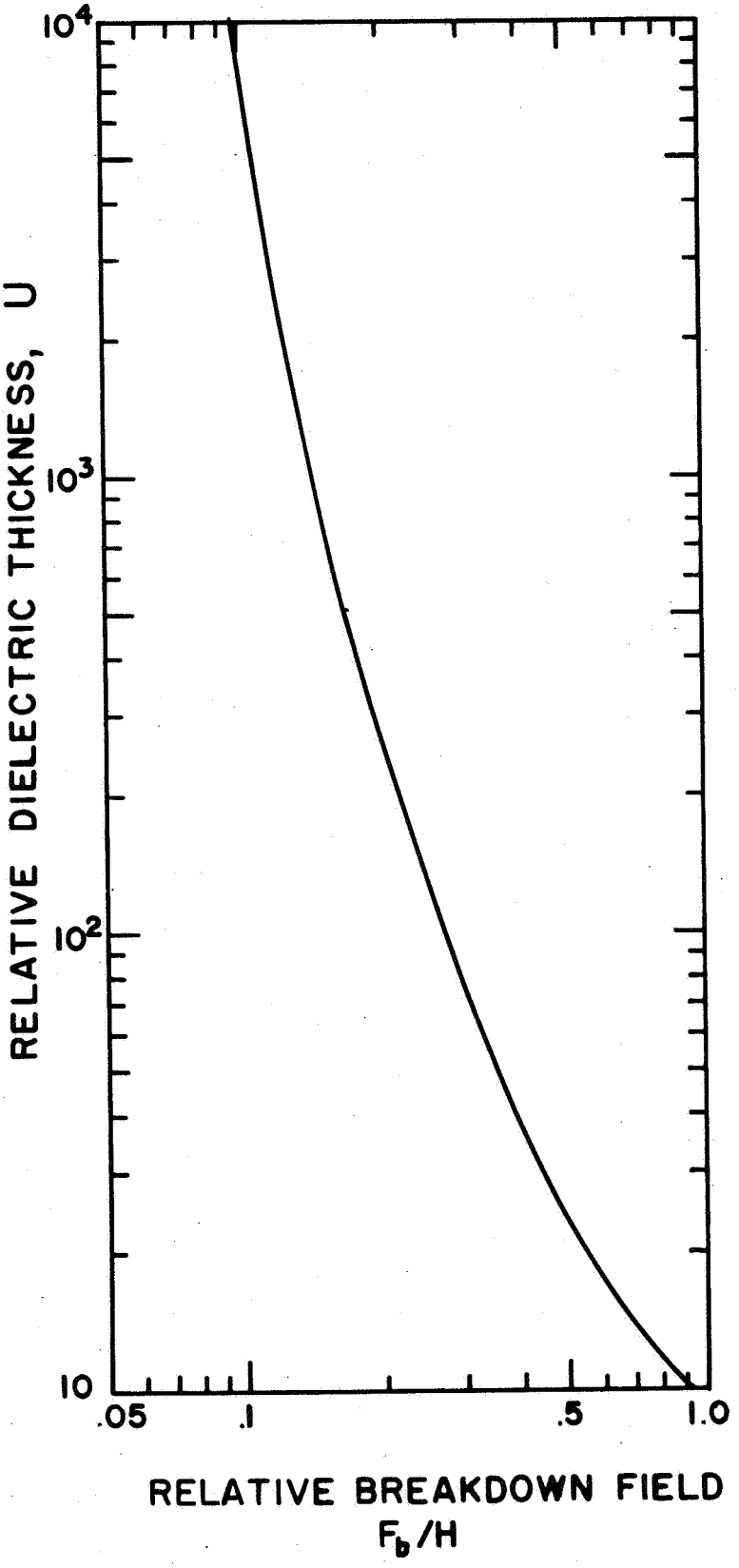

Fig. 42. O'Dwyer's universal breakdown curve.

the two graphs and then the coordinates of the pin hole read from both graphs). The ordinates give the couplet $\bar{F}_b$, $\bar{F}_b/H$ and the abscissae give w, w/λ. The ratio of the first two determines H and the ratio of the second two determines λ.

Upon attempting to fit O'Dwyer's universal curve as expressed in Fig. 42 with the experimental data of Figs. 23, 24, and 25, it is found that the scatter in the data makes it very difficult to judge a best fit. Since the straight lines drawn for making a comparison with the theory of Forlani and Minnaja give a fairly good representation of the data, these lines are used to obtain the values of H and λ given in Table 6. These values are uncertain by about a factor of 2. Also shown in Table 6 is an approximate of the mobility of $\bar{\mu}$, where $\bar{\mu} = e\lambda/\sqrt{2mI}$, as indicated above.

The universal curve of O'Dwyer did not seem to give as good a fit to the experimental data as did the $w^{-\frac{1}{2}}$ relation of Forlani and Minnaja.

O'Dwyer states that the value of $\bar{F}_b$ should be independent of temperature if u has a value about 10. On the other hand, when u is about 10^4, the temperature dependence is given approximately by

$$\bar{F}_b \propto \left(1 + \frac{2}{e^{\hbar\omega/kT} - 1}\right), \qquad (1)$$

where the angular frequency ω is connected with the longitudinal optical modes. From Table 6 it is seen that u is 10^2 or less for SiO_2, CaF_2, MgF_2 and CeO_2. Experimentally, SiO and MgF_2 have breakdown fields that are independent of temperature, which is consistent with the predictions of O'Dwyer. However, the breakdown fields in CaF_2, CeF_3, and CeO_2 (see Fig. 22) decrease monotonically with temperature, while Eq. (1) predicts a monotonic increase in breakdown field with temperature.

O'Dwyer's theory has appeal because it gives perspective for the dependence of the breakdown voltage on the rate of rise of the applied voltage. He gives a method for evaluating the internal field, which is non-uniform because of the

Table 6. Parameters of O'Dwyer's Theory evaluated by comparing experimental breakdown field-thickness data with O'Dwyer's universal curve.

Material	λ (Å)	H (V/cm)	$\bar{\mu}\left(\frac{cm^2}{V\text{-}sec}\right)$
SiO	100	2.3×10^6	10
MgF_2	130	1.4×10^6	13
CaF_2	140	4.6×10^6	14
CeO_2	60	3.3×10^6	6

space charge set up to maintain the condition of current continuity. The field at the cathode is enhanced by about an order of magnitude over his bulk field, but the transition is gradual. The calculations of Section IV.A suggest that a more realistic model of the bulk conductivity might alter this distribution further so that there is a far stronger field near the cathode.

C. THEORY OF KLEIN AND GAFNI.

Klein and Gafni use the phenomenological equation expressing the balance between Joule heating and thermal conduction. When the Joule heat is too great so the thermal conduction cannot remove energy fast enough, then breakdown occurs. Klein and Gafni apply this theory to their "maximum voltage" breakdowns (see Section I) in SiO. However, as they carefully point out, they do not usually measure the breakdown voltage directly because their entire capacitor is thereby destroyed. They measure a point on their voltage-current characteristic beyond which the current increases and the voltage decreases. They map out a definite part of this negative resistance region and then turn off the applied voltage before destruction occurs. Thus their experimental data on breakdown voltages are really non-breakdown measurements on the dc characteristics.

The Joule heating is computed using the experimentally determined V-I-T characteristics. Klein and Gafni obtain the relation

$$\sigma = \sigma_o \exp [a(T-T_o) + bF], \qquad (2)$$

where σ is the conductivity, $\underline{a}$ and $\underline{b}$ are constants, T is the temperature of the dielectric, T_o is the ambient temperature and σ_o is a function of the geometry and the ambient temperature ($\sigma_o = Ae^{aT_o}$, where $\underline{A}$ is a constant). The basic energy balance equation used is

$$\sigma F^2 A_b w = \Gamma(T - T_o), \qquad (3)$$

where A_b is the area of the breakdown, w is the dielectric thickness, and Γ is the heat conductance. Klein and Gafni combine Eq. (2) and (3) and then differentiate

the resulting equation with respect to T to find the critical condition on the temperature. This is (calling the critical temperature T_m)

$$T_m - T_o = 1/a \ . \qquad (4)$$

When this is substituted back into the original equation, the value of field determined by the equation is referred to as the breakdown field. The values of $T_m - T_o$ range from about 25 to 50°C.

The thickness dependence that Klein and Gafni find is shown in Fig. 43a and the temperature dependence is shown in Fig. 43b. In each case good agreement is shown between theory and experiment. At the same time, it should be noted that the breakdown-thickness data do not fit either the $w^{-\frac{1}{2}}$ relation of Forlani and Minnaja or the theoretical curve of O'Dwyer.

Both the thickness and the temperature dependence data of Klein and Gafni differ from that summarized in Figs. 24 and 27 (see the SiO data).

Sze[12] has used the approach of Klein and Gafni in describing breakdowns in Si_3N_4 capacitors. He uses Eq. (IV.A.3) to describe the current density as a function of applied field and temperature. With this and the method above, he obtains good agreement between his theoretical predictions and experimental results on breakdown field vs. temperature. He does not give data on breakdown field as a function of thickness. The temperature difference between ambient and the critical value T_m is about 15°.

The temperature dependence of F_{max} for CeO_2 and CaF_2 (see Fig. 22) is qualitatively like that of Sze. The prebreakdown conduction in CeO_2 is similar to that in Si_3N_4 in its temperature dependence, but the prebreakdown conduction in CaF_2 is very different and is only slightly temperature dependent. Further, SiO has about the same type of temperature dependence as Si_3N_4 in its prebreakdown behavior, but it has different temperature dependence in its breakdown behavior (see Figs. 22 and 43).

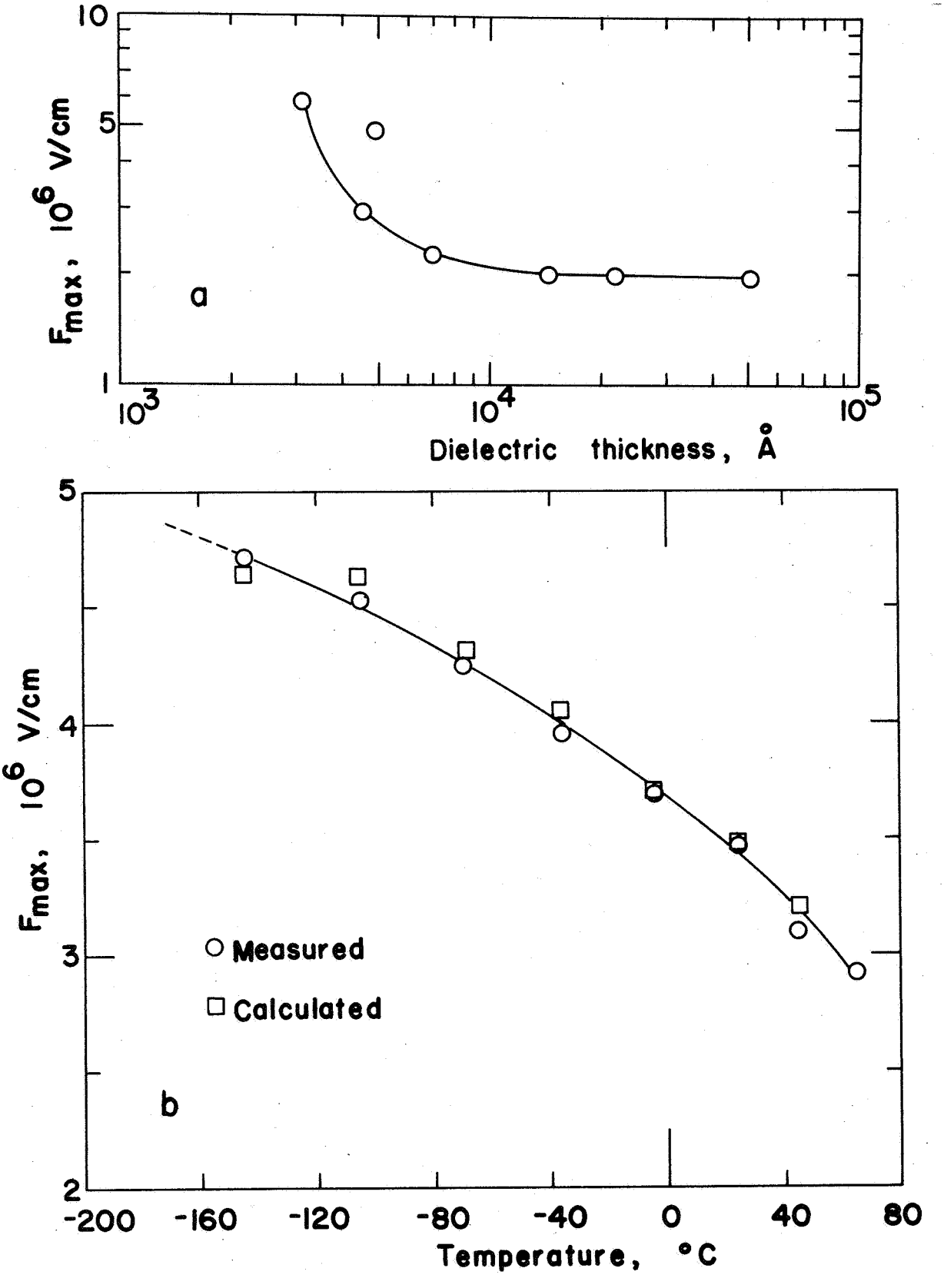

Fig. 43. Maximum voltage breakdown data of Klein and Gafni for SiO. (a) F_{max} vs dielectric thickness. (b) F_{max} vs temperature. In each case F_{max} is obtained from prebreakdown V-I-T characteristics.

The approach of Klein and Gafni can be tried on MgF_2. Here the temperature dependence in the conductivity is so small that it can be regarded as nil. Then Eq. (3) would give breakdown when the temperature reaches the point where either the electrodes or the dielectric melt or decompose. This is at a temperature in the order of 1000°K. Thus Eq. (3) predicts a well-defined decrease in F_{max} according to the relation

$$F_{max} = \sqrt{\frac{\Gamma}{\sigma A_b w} (T_m - T_o)} . \qquad (5)$$

The data of Fig. 22 show this is not obeyed.

D. CRITIQUE

None of the theoretical treatments considered describe all of the materials studied. The experimental evidence is strong that prebreakdown conductance cannot generally be related to breakdown thresholds. Neither is there any clean-cut relationship between dielectric constants and breakdown thresholds. This is surprising, but the breakdown field in CeO_2 is about the same as in SiO, whereas the real part of the dielectric constant in CeO_2 is several hundred (see Fig. 13) while it is only 6 in SiO. If F_{max} is used to compute a local field[40], the local field is enhanced because of the polarization by the amount $\vec{P}/3\epsilon_o$, where P is the polarization field. Thus, the local field in CeO_2 is about 50 times stronger than the local field in SiO so one might expect F_{max} for the two materials to differ correspondingly.

The experimental work on breakdown indicates that breakdown fields are about the same in bulk specimens (see the extensive data in Whitehead's book) as they are in thin films. This raises questions about any avalanche mechanism. One way to include avalanches would be to require avalanches to be highly localized, so that each one originates and runs its course to destruction within a path of, say, 100 to 1000 Å.

The values of $(T - T_o)$ found by both Klein and Gafni and Sze are from 10 to 50^oC, which seems too small to reach a critical condition. In the extensive tests on SiO described in references 1-3, essentially no temperature dependence of F_{max} was found when the ambient temperature was altered by 300^oC.

The heat conduction relation used by Klein and Gafni is also hard to understand. They present a curve showing that the value of Γ is not constant with temperature, but its temperature dependence is far stronger than a linear variation. Hence the law of heat conduction should show a temperature dependence stronger than T^2.

The use of Klein and Gafni's "maximum voltage" breakdowns wherein the breakdown voltage is measured without the occurrence of breakdown leaves undetermined the actual breakdown voltage. Hence, "breakdown" thickness and temperature data are subject to serious question. It has been pointed out that the current densities of Klein and Gafni in their "maximum voltage breakdowns" are 10 to 100 times as large as those familiar to the authors. Perhaps this is an areal effect not understood. The capacitors of Klein and Gafni were generally 0.2 cm^2 in plate area. As indicated in the areal study of Section III.A.2.d, there is a genuine rise in F_{max} in capacitors of area less than 1 cm^2. It is possible these small capacitors had prebreakdown current densities comparable to those of Klein and Gafni since measurements of prebreakdown currents were only made on larger capacitors.

The observation of high breakdown voltage accompanying small-area capacitors is not explained by any of the theories considered.

The theories of breakdown conduction have attempted only one portion of the problem of breakdown conduction, namely, the prediction of the breakdown threshold as a function of temperature and thickness of the dielectric. In the microscopic treatments the assumption is that the system is homogeneous and the electrode-

dielectric interface can be described simply. Yet the breakdown voltage can be strongly sensitive to the polarity of the applied voltage[1-3]. Most treatments regard the field in the dielectric to be almost uniform, but the work of O'Dwyer and that in Section IV.A emphasize the importance of having an inhomogeneous field.

The problem of conduction during breakdown has not been given serious attention by theorists, although it may be easier to solve than the problem of the onset of breakdown. It is this problem that will be considered further in the next section.

VI. MODEL FOR BREAKDOWN CONDUCTION

Experimental results indicate there are three phases of the problem of describing breakdown conduction:

i. Transition from prebreakdown conduction to breakdown conduction.

ii. Breakdown conduction.

iii. Termination of breakdown conduction.

The first phase has been discussed in Section V. However, the results described in Section III indicate a re-examination is appropriate. Hence, all three phases will be discussed below.

A. TRANSITION FROM PREBREAKDOWN CONDUCTION TO BREAKDOWN CONDUCTION

The basic experimental results bearing on this transition are:

i. The magnitude of the breakdown field, for a given dielectric geometry is about the same for all of the materials studied. The materials studied were structurally quite different, ranging from glassy to crystalline to polymer. The breakdown threshold F_{max}, for the different materials, was only mildly temperature dependent.

ii. No correlation existed between the temperature dependence of F_{max} and the prebreakdown voltage-current-temperature characteristics. Similarly, F_{max} was not found to be related to the complex dielectric constants or to their temperature dependence. Thus the state of prebreakdown dc and ac conduction seems immaterial in determining the behavior of F_{max}.

iii. The transition from prebreakdown conduction to breakdown conduction is very abrupt. It occurs in a time less than 10 nanoseconds. It is estimated that the conductivity at the breakdown site changes by a factor of about 10^{10} during these 10 nanoseconds. The resistance after the transition is about 30 ohms. The resistance remains constant at this value until the capacitor voltage

has fallen close to V_{min}.

iv. The light emitted during breakdown has a line spectrum characteristic of the free ions and atoms of both electrodes and of the dielectric. This light is emitted from the very beginning of the breakdown process, i.e., light emission begins when the voltage waveform indicates breakdown begins.

v. Most breakdowns originate at a center. The region close to this center attains both a high temperature and a high pressure during breakdown.

The theoretical considerations of Sections IV and V indicate that the development of a non-uniform field within the dielectric is probably basic to understanding the onset of breakdown.

In the breakdown study of Al-SiO-Al capacitors[3], the basic idea offered to explain the onset of breakdown was the field-dissociation of the molecules. This presumably provided the electrons that modified the conductivity so much. It was assumed that the constancy of the resistance of the capacitor during breakdown and the rapid transition from prebreakdown to breakdown conduction required a mechanism for the lateral spread of the active conducting region in the transition time of less than 10 nanoseconds. A stepwise process was hypothesized to accomplish this. In the description that follows, low value of resistance and its constancy are explained in a different fashion.

A description of the onset of breakdown that is believed consistent with the experimental results will now be given. Upon application of a voltage there is some leakage current and possibly some ion migration. The requirement of current continuity implies that a space charge will be built up near the cathode (assuming electronic conduction). The field in the cathode region may be 100 times the bulk field (see Section IV.A). However, this ratio decreases with increasing voltage. To explain the rapid transition from prebreakdown conduction there must be a mechanism such as impact ionization avalanche or field dissociation in the

high field region by which dissociation starts in the central breakdown region. This dissociation must change the solid into a dense plasma (if it is to account for the light emission observed) that is a good conductor. If the dissociation is due to a high cathode field, the high field region is pushed toward the positive electrode as the conducting plasma is formed. Within the 10 nanoseconds the material in the central portion between the electrodes has been converted into a highly dense plasma. The plasma, which is in contact with the electrodes in this central area, vaporizes them. All of this happens before the plasma has had a chance to expand appreciably.

B. BREAKDOWN CONDUCTION

If the plasma is the principal conduction path during breakdown, it is somewhat surprising that the breakdown resistance changes so little as the plasma expands. However, it should be noted that the highly dense plasma at the beginning of breakdown probably has a much smaller electronic mobility than is found in the more rarified plasma later on. For conduction, charges must be taken from one electrode and go through the plasma to the other electrode. Thus as the plasma expands, it becomes more conducting and, at the same time, there is a longer path between electrodes. These will tend to keep the conductivity constant.

As the plasma travels outward, it passes over the surface of the top electrode causing erosion and heating in both the electrode and the dielectric beneath it. If the conductivity of the dielectric is temperature sensitive, then this region will conduct more strongly than previously, but not nearly as strongly as the plasma. The dissipation of energy along the capacitor surface should rapidly remove energy from the expanding plasma. The light emission waveforms show that there is continued generation of excited ions and neutrals within the plasma throughout the breakdown conduction interval.

One of the puzzling questions with regard to breakdown is the geometric configuration and size of the breakdown. In the areal study of Section III.A.2.d, it was found that the size of the central region remained almost constant as the plate area of the capacitor (and hence the energy available during breakdown) increased. Also the resistance during breakdown was nearly constant except for the smallest case, suggesting that the resistance is determined primarily by this central region. For small plate area capacitors there is essentially only a central region. As the plate area increases the outer diameter increases, at first quite rapidly, but for areas greater than 2 cm^2 the increase is much more gradual. The amount of light given off is also greater for the larger area capacitors. This suggests that the plasma is more highly ionized when the plate area is larger. The outer edge of the breakdown may occur when the pressure wave breaks contact with the capacitor surface. Such a break should occur because the hemispherical wave would not experience strong dissipative forces except along the surface of the capacitor. Thus the velocity of the shock front along the surface would drop rapidly while the wave heading into the atmosphere (or the vacuum) would maintain a relatively high velocity. At the place where contact was broken, there is probably an unusual amount of turbulence and hence considerable heat transfer. This is the region where etch patterns on the substrate indicate an unusually high temperature.

Another factor that is of importance in determining the resistance during breakdown is the "spreading" resistance in the electrodes as the charge on the electrodes funnels into the plasma shorting site. For aluminum electrodes 1000 Å thick, this probably is about 5 ohms. Most of this resistance is localized close to the plasma short, hence is considerable extra heating in this region. Probably some of the damage pattern is connected with this heating.

In some breakdowns the resistance increases abruptly when the voltage has fallen, say, to three-fourths of the way to V_{min}. This may be an increase of a factor of 10 to 100 in the resistance. The light output seems to continue during this period, so some plasma is being generated. Possibly the erosion effects have completely cut off the central region from the electrodes and the central plasma has lost all electrode contact. At the edge of the breakdown, there may be secondary plasma formation (edges frequently serve as nucleation centers for subsequent breakdowns) which produces the thermal etch effect and the complex edge patterns sometimes observed.

C. TERMINATION OF BREAKDOWN CONDUCTION

The termination of breakdown is best approached through the properties observed for V_{min}. These are:

i. There exists a threshold V_{min} for all materials studied.

ii. V_{min} is polarity sensitive.

iii. V_{min} has a value of 10 to 20 volts for almost all capacitors (regardless of the dielectric) studied.

iv. V_{min} is not temperature dependent.

v. V_{min} is not thickness dependent.

The above properties suggest strongly that V_{min} is connected with the minimum voltage required to sustain the plasma. The situation seems to be about the same as in a gaseous discharge. There the field close to the cathode is very high and the field in the positive column region is low. The discharge is maintained so long as the applied voltage can continue to produce ionization in the region near the cathode. Thus the discharge is quenched at a voltage that is almost independent of the electrode separation (almost all of the voltage drop being close to the cathode regardless of the electrode separation).

Because of the polarity effects on V_{min}, it seems that the nature of the electrode-plasma interface must be important. The difference in V_{min} with polarity may be as much as ten volts, although it is usually less than this.

VII. CONCLUSIONS

Breakdown properties of SiO, MgF_2, CaF_2, CeF_3, CeO_2, and Teflon have been measured for thin films in the range from 1000 Å to 15000 Å. All of the materials have a characteristic breakdown field which varies only slightly with temperature and with film thickness. A field of 10^6 V/cm is representative. All of the materials exhibit a voltage threshold for the cessation of breakdown in the range of 10 to 20 volts for most capacitors. This voltage is independent of temperature and of dielectric thickness.

On comparing the magnitude of the field for the onset of breakdown among the different materials with the measured prebreakdown V-I-T characteristics and the complex dielectric constant-temperature characteristics, it is concluded that the magnitude of the breakdown field is not a function of these prebreakdown phenomena. Moreover, the temperature and thickness dependences of the threshold field for the onset of breakdown do not depend upon prebreakdown conduction.

None of the theoretical treatments considered were found to be completely satisfactory. Predictions of Forlani and Minnaja on the thickness dependence of the threshold for the onset of breakdown were in good agreement with experiment. However, this theory did not adequately describe the temperature dependence of the threshold field.

The measurements of the characteristics of single breakdowns wherein the voltage waveforms are correlated with the light intensity waveforms of individual spectral lines during breakdown are believed to provide a new perspective to the understanding of breakdown conduction. Based upon these, the optical micrography and the electrical measurements, a model of the many aspects of breakdown has been proposed. This represents an advance on a model previously suggested by the

authors. The central feature in this model is the transition in a time of less than 10 nanoseconds from the prebreakdown conducting state to a breakdown conducting state. In this time a region about 10 microns in diameter is converted from a solid into a conducting plasma. This conducting plasma is responsible for the low resistance during breakdown, for the light emission during breakdown, and for the final quenching of the breakdown.

Although the primary emphasis in this paper has been upon the breakdown problem, much of the data on prebreakdown conduction is of interest and is not available in the literature.

VIII. PLANS FOR FURTHER STUDY

The general program of work described in this report is being continued at present. Work in progress includes:

i. Theoretical treatment of prebreakdown and breakdown conduction.

ii. Additional measurements on the materials of this study to fill gaps in the data.

iii. Study of the prebreakdown and breakdown conduction in the alkali fluorides. These have been chosen because much theoretical work and related experimental work has been done on these materials (including thin-film prebreakdown studies and breakdown studies of bulk samples). The theories of breakdown originated by von Hippel and by Fröhlich (and exemplified by the treatments of O'Dwyer and Forlani and Minnaja) are expressed in terms of ionic crystals like the alkali fluorides.

iv. Construction of an rf-sputtering unit so that Teflon, glasses, and other temperature-sensitive materials can be fabricated in thin films.

Work that is planned for the near future includes:

i. Further electron microscopy. This will use the new Phillips EM300 electron microscope recently brought to the Auburn University campus. Both replication studies to determine the topography of evaporated films and in situ electrical measurements of capacitors are planned. If rf-sputtering yields good films of ferroelectric materials, these will be studied in situ.

ii. Study of the prebreakdown conduction effects that lead to erratic behavior in the current.

iii. X-ray diffraction analysis of crystalline films using modern Fourier techniques to distinguish crystallite size and cell distortion effects.

PERSONNEL

The following persons, all of whom are affiliated with the Physics Department of Auburn University, have contributed to this project.

1. Paul P. Budenstein, Associate Professor (Project Director)
2. Paul J. Hayes, Graduate Student
3. James Lynn Smith, Graduate Student
4. Wallace B. Smith, Graduate Student

In addition to the above, the following undergraduates have served as laboratory technicians during the investigations:

Harold Ketterer

Michael G. Faulkner

James Heptinstall

James Zealy

Richard Bradshaw

Dwayne McCay

Samuel Pettijohn

During the summer of 1967, Paul J. Hayes worked as a research participant at the Marshall Space Flight Center. There he continued the work of this project and did the rf-sputtering of Teflon films. He was able to have some of the films examined with the x-ray microprobe at the Propulsion and Vehicle Engineering Laboratory. We are indebted to R. A. Poor and Gordon Marsh for their aid in this examination.

We are also indebted to Dr. Roy Bicklehaupt of the Southern Research Institute for his x-ray microprobe survey of one of our capacitors.

REFERENCES

1. P. P. Budenstein and P. J. Hayes, Final Report, NAS8-11279 (1966).

2. P. J. Hayes, Supplement to Final Report, NAS8-11279 (1966).

3. P. P. Budenstein and P. J. Hayes, J. Appl. Phys. 38, 2837 (1967).

4. P. J. Hayes, "Experimental Study of Thin Film Dielectrics: Vacuum Deposited SiO, CeO_2; RF-Sputtered Teflon," Technical Memorandum, George C. Marshall Space Flight Center, Huntsville, Alabama (1967).

5. J. L. Smith, P. J. Hayes, and P. P. Budenstein, "Breakdown Thresholds in Thin Film Capacitors," Meeting of the Southeastern Section of the American Physical Society, Clemson University, November 2-4, 1967.

6. P. P. Budenstein and W. B. Smith, "Time Resolved Spectrum of Light Emitted During Destructive Breakdown of Al-SiO-Al Capacitors," Meeting of the Southeastern Section of the American Physical Society, Clemson University, November 2-4, 1967.

7. R. W. Hoffman, "Mechanical Properties of Deposited Films," Physics of Thin Films, Volume 3, Academic Press, Inc., Edited by Georg Hass and R. E. Thun, Academic Press, New York (1965).

8. N. Klein, H. Gafni, and H. J. David, "Mechanism of dc electrical breakdown in thin silicon oxide films," Symposium on the Physics of Failure in Electronics, Chicago, Sept. 29-Oct. 1, 1964.

9. N. Klein and H. Gafni, "The maximum dielectric strength of thin silicon oxide films," IEEE Trans. on Electron Devices, ED-13, 281 (1966).

10. N. Klein and N. Levanon, "ac Electrical Breakdown in Thin Silicon Oxide Films," J. Appl. Phys. 38, 3721 (1967).

11. N. Klein and Z. Lisak, Proc. IEEE 54, 979 (1966).

12. S. M. Sze, "Current Transport and Maximum Dielectric Strength of Silicon Nitride Films," J. Appl. Phys. 38, 2951 (1967).

13. J. J. O'Dwyer, "The theory of avalanche breakdown in solid dielectrics," J. Phys. Chem. Solids 28, Pergamon Press, 1137 (1967).

14. F. Seitz, Phys. Rev. 76, 1376 (1949).

15. F. Forlani and N. Minnaja, Phys. Stat. Solidi 4, 311 (1964).

16. A. J. Dekker, Solid State Physics, Prentice-Hall, Inc., Englewood Cliffs, N.J., 153 (1957).

17. J. T. Johansen, J. Appl. Phys. 37, 499 (1966).

18. C.A. Neugebauer, "Structural disorder phenomena in thin metal films," Physics of Thin Films, Vol. 2, 10 (1964).

19. Karl Henisch, Electroluminescence, Pergamon Press, New York, 17 (1962).

20. T. W. Hickmott, J. Appl. Phys. 36, 1885 (1964; J. Appl Phys. 37, 4380 (1966); J. Electrochem. Soc. 113, 1223 (1966).

21. W. Heitler, The Quantum Theory of Radiation, Oxford University Press, 107 (1936).

22. O. G. Engel, J. Appl. Phys. 38, 3935 (1967).

23. J. J. O'Dwyer, J. Appl. Phys. 37, 599 (1966).

24. T. W. Hickmott, J. Appl. Phys. 35, 2679 (1964).

25. K. W. Böer, H. J. Hänsch, U. Kümmel, Z. Physik 155, 170 (1959).

26. K. W. Böer, Z. Physik 155, 184 (1949).

27. E. I. Adirowitsch, Z. Physik 155, 195 (1959).

28. A. Waxman, J. Appl. Phys. 38, 4763 (1967).

29. J. G. Simmons, J. Appl. Phys. 34, 1793 (1963).

30. T. E. Hartman, J. C. Blair, and R. Bauer, J. Appl. Phys. 37, 2468 (1966).

31. R. B. Leighton, Principles of Modern Physics, McGraw-Hill Book Company, Inc., New York, 156 (1959).

32. C. A. Mead, Phys. Rev. 128, 2088 (1962).

33. M. A. Lampert, Rept. Prog. Phys 27, 329 (1964); Phys. Rev. 125, 126 (1962); RCA Rev. 20, 682 (1959); ___ and A. Rose, Phys. Rev. 121, 26 (1961); A. Rose, Phys. Rev. 97, 1538 (1955).

34. C. Weaver, Advances in Physics 11, 102 (1962).

35. N. F. Mott and R. W. Gurney, Electronic Processes in Ionic Crystals, Oxford University Press, 40 (1940).

36. K. Hauffe and B. Illschner, Z. Elektrochem. 58, 478 (1954).

37. A. T. Fromhold, Jr. and E. L. Cook. J. Appl. Phys. 38, 1546 (1967).

38. J. J. O'Dwyer, The Theory of Dielectric Breakdown in Solids (Oxford University Press, London, 1964).

39. S. Whitehead, Dielectric Breakdown in Solids, (Oxford University Press, London, 1951).

40. W. K. H. Panofsky and Melba Phillips, Classical Electricity and Magnetism (Addison-Wesley Publishing Company, Inc., Reading, Massachusetts, 1962), 38.